Susanne Maria Fischer, BSc.

Towards Redox-Active Polymers: Synthesis and Characterisation of Monomers and Coordination Compounds with Quinone Moieties

MASTER'S THESIS

to achieve the university degree of

Master of Science

Master's degree programme: Chemistry

submitted to

Graz University of Technology

Supervisor

Assoc.Prof. Dipl.-Ing. Dr.techn. Christian Slugovc

Institute for Chemistry and Technology of Materials

Graz, October 2019

AFFIDAVIT

I declare that I have authored this thesis independently, that I have not used other than the declared sources/resources, and that I have explicitly indicated all material which has been quoted either literally or by content from the sources used. The text document uploaded to TUGRAZonline is identical to the present master‘s thesis.

Date

Signature

The important thing is to never stop questioning.

Albert Einstein

Abstract

Redox-active polymeric materials have been heavily researched in particular towards their use in organic polymer-based batteries because the polymeric nature of the active material prevents dissolution of the redox-active moieties into the electrolyte. Polymeric materials containing metal ions, such as coordination polymers, metal-organic frameworks or cross-linked metal complexes, provide additional redox centres while being inherently insoluble. Amongst performance indicators such as cyclability or capacity, a straight forward and thus low cost synthetic route towards the polymeric active materials is essential for a potential commercial success.

In this work, high yielding synthetic procedures towards redox-active monomers and their polymerisability via Ring-opening Metathesis Polymerisation (ROMP) starting from well priced building block chemicals such as 1,4-benzoquinone and cyclopentadiene are disclosed. To study the influence of the redox state of the monomer on the polymerisation behaviour, tetrahydro-1,4-methanonaphtalene-5,8-dione (**1**), its isomer dihydro-1,4-methanonaphthalene-5,8-diol (**2**) and its oxidized product dihydro-1,4-methanonaphtalene-5,8-dione (**3**) are synthesized and investigated in ROMP. While **1** and **2** are polymerizable under certain conditions, **3** does not show any conversion. The same behaviour is observed for the homologous anthracene and tetracene derivatives clearly indicating that the oxidized monomers cannot be used in ROMP. Furthermore, direct functionalisation of **1** and **3** via an Aza-Michael addition of pyrazoles and imidazoles does not work because the nucleophiles act as bases and promote the thermodynamically favoured aromatisation to **2**. Thus, an alternative synthetic sequence is elaborated to synthesize functionalized monomers. These monomers can be used as ligands for the syntheses of nickel complexes containing redox-active quinones and a norbornene moiety which can potentially be cross-linked or functionalized. Finally, three new coordination polymers with copper, zinc and manganese as metal ions and (±)*endo,exo*-5-norbornene-2,3-dicarboxylic acid as linker are synthesized and characterised.

Kurzfassung

Redoxaktive Polymere werden hinsichtlich ihrer Verwendung in organischen Batterien intensiv erforscht, da sie das Auflösen der redoxaktiven Einheiten im Elektrolyten verhindern. Polymere, die Metallionen enthalten, wie Koordinationspolymere, metallorganische Gerüstverbindungen oder vernetzte Metallkomplexe, bieten zusätzliche Redoxzentren und sind außerdem in herkömmlichen Elektrolyten weniger löslich. Unter Leistungsindikatoren wie der Zyklisierbarkeit oder der Kapazität einer Batterie, ist auch eine einfache und somit kostengünstige Synthese der aktiven Materialien für einen potentiellen wirtschaftlichen Erfolg entscheidend.

In dieser Arbeit wird die Synthese von redox-aktiven Monomeren ausgehend von preisgünstigen Chemikalien wie 1,4-Benzochinon und Cyclopentadien in hoher Ausbeute dargestellt und deren Polymerisierbarkeit in der Ringöffnenden Metathese Polymerisation (ROMP) untersucht. Um den Einfluss des Oxidationsgrades des Monomers auf das Polymerisationsverhalten zu untersuchen, wurden Tetrahydro-1,2-methanonaphtalin-5,8-dion (**1**), dessen Isomer Dihydro-1,4-methanonaphtalin-5,8-diol (**2**) und sein oxidiertes Analogon Dihydro-1,4-methanonaphtalin-5,8-dion (**3**) synthetisiert und deren Verhalten in ROMP untersucht. Während **1** und **2** unter bestimmten Bedingungen polymerisierbar sind, zeigt die Polymerisation von **3** keinen Umsatz. Das gleiche Verhalten wird für die homologen Anthracen- und Tetracenderivate beobachtet, was eindeutig zeigt, dass die oxidierten Monomere für ROMP ungeeignet sind. Darüber hinaus, funktioniert die direkte Funktionalisierung von **1** und **3** über eine Aza-Michael-Addition von Pyrazolen und Imidazolen nicht, da die Nucleophile ebenfalls als Basen agieren und die thermodynamisch bevorzugte Aromatisierung zu **2** fördern. Daher wird in dieser Arbeit eine alternative Synthesesequenz zur Herstellung von so funktionalisierten Monomeren ausgearbeitet. Diese Monomere können als Liganden für die Synthese von Nickelkomplexen verwendet werden, die redoxaktive Chinone und eine Norborneneinheit enthalten, die möglicherweise vernetzt oder funktionalisiert werden kann. Schließlich werden drei neue Koordinationspolymere, die Kupfer, Zink oder Mangan als Metallionen und 5-Norbornen-*endo*-*ex*o-2,3-dicarbonsäure als Linker enthalten, synthetisiert und charakterisiert.

Danksagung

An dieser Stelle möchte ich mich bei den Menschen bedanken, ohne die die Anfertigung dieser Masterarbeit nicht möglich gewesen wäre.

Vielen Dank an Christian Slugovc für die ausgezeichnete Betreuung. Danke für die zahlreichen Ideengebungen und Hilfestellungen sowie die vielen Möglichkeiten, die ich in dieser Arbeitsgruppe erhalten habe. Vielen Dank, dass ich Teile dieser Arbeit in Form eines Posters bereits auf einer wissenschaftlichen Konferenz in Barcelona präsentieren durfte.

Des Weiteren möchte ich mich bei der gesamten Arbeitsgruppe für die lockere und angenehme Atmosphäre und die spannenden Diskussionen bedanken. Insbesondere möchte ich mich bei Katharina Kodolitsch bedanken, in der ich nicht nur eine großartige Arbeitskollegin, sondern auch eine Freundin gefunden habe. Ein großer Dank gilt auch Petra Hofstadler für ihre Hilfsbereitschaft und die zahlreichen Tipps im Labor und bezüglich organisatorischer Angelegenheiten.

Danke an Petra Kaschnitz, Josefine Hobisch und Raffaele Ricco für die Durchführung von Messungen. Danke an Daniel Boese für die Bereitstellung der Ressourcen für die Durchführung von quantenchemischen Berechnungen, die ich ohne Einschränkungen während meiner gesamten Masterarbeit nutzen durfte.

Vielen Dank an Nadja Lenkova, die ich im Rahmen ihrer Bachelorarbeit betreuen durfte, für die Durchführung von zahlreichen Synthesen (Produkte 4, 5, 6a, 6b, 8 und poly4), die in dieser Arbeit beschrieben werden. Dadurch hat sich die Zeit, die ich für meine Masterarbeit benötigt habe, stark verkürzt.

Ich möchte mich auch bei meiner Familie bedanken, die mir immer alles ermöglicht hat. Ohne ihre finanzielle und mentale Unterstützung wäre ich jetzt nicht da wo ich bin. Danke an meine Eltern und meinen Bruder Stefan für alles was sie für mich tun und dass sie immer an mich glauben.

Zu allerletzt möchte ich mich bei meinem Freund Andi für die vielen fachlichen Diskussionen und seine Unterstützung in jeder Lebenslage bedanken.

Table of Contents

1 Introduction

These days, most battery systems are based on the Li-ion technology because it provides outstandingly high power densities and good cyclability. Despite these advantages, conventional Li-ion batteries cannot satisfy all the demands that will be imposed in the future, i.e. flexibility, environmental compatibility, sustainable production from renewable resources, fast charging, good cycle life and efficient processing.[1]

These requirements can potentially be met by replacing metal-based active components in electrodes with organic ones. Many redox-active compounds are suitable for battery applications since the basic requirement is a reversible electrochemical redox reaction. Quinones, however, are a substance class that is of special interest due to their ability of storing two electrons per molecule resulting in excellent charge-to-mass ratios and high capacities. Compared to metal-based batteries, the redox potential can be tailored more easily via the introduction of functional groups. Nevertheless, the application of small molecule quinones in commercial devices is limited by their solubility in battery electrolytes which leads to poor cycling stability and self-discharge of the battery.[1,2]

The dissolution of active material into the electrolyte can be circumvented by making it inherently insoluble through polymerisation. There are several polymerisation methods suitable for the synthesis of redox-active polymers as electrode materials, including ring-opening metathesis polymerisation (ROMP) which has been reported a few times in literature.[3–5] Another strategy of preventing dissolution of active material into the electrolyte is the fabrication of insoluble coordination polymers (CPs) which are polymeric coordination compounds with high porosities making them suitable for the intercalation of redox active species.[6]

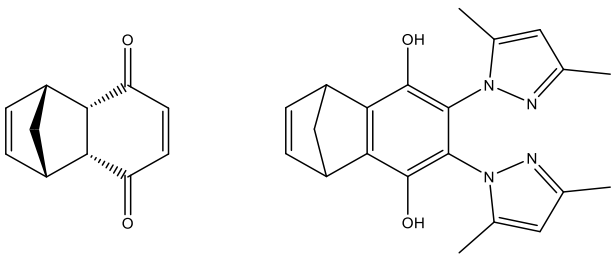

Figure 1 Compounds under investigation: left: monomer for the preparation of redox-active polymers, right: ligand for the formation of metal complexes or potentially porous CPs

In this work, precursors for quinone based electrode materials will be synthesized (Figure 1).

On the one hand, synthesis and functionalisation of monomers based on tetrahydro-1,4-methanonaphthalene-5,8-dione in high yields are presented. Subsequently, the suitability of ring-opening metathesis polymerisation (ROMP) for the fabrication of quinone based redox-active polymers will be examined.

On the other hand, quinone derived ligands capable of coordinating to metal ions should be synthesized and reacted with various metal salts to trigger the formation of metal complexes or coordination polymers that are potentially applicable as electrode materials.

2 Theoretical Background

2.1 Polymer-Based Batteries

Polymer-based batteries are energy storage systems containing organic components as active materials in electrodes. Like metal-based batteries, they consist of two electrodes placed in an ion-conducting electrolyte separated by a porous ion-permeable membrane.[1]

Polymer-based batteries have several advantages over conventional metal-based ones. Their electrochemical behaviour is based on simple redox reactions which lead to high rate performances and long life cycles. They can be disposed more easily due to the absence of toxic components. Furthermore, the mechanical flexibility of polymers allows straightforward and cheap manufacturing techniques.[2]

However, commercial success is still hampered not only because of demanding synthesis conditions and high costs of these materials, but also worse battery stability and self-discharge.[2]

A schematic of the charging and discharging processes is displayed in Figure 2. An all-organic battery consists of one electrode made of a p-type material which is oxidized during charging to form cations and one n-type material which is reduced during charging to form anions. These charges are compensated by electrolyte ions. Charging is thus limited by complete oxidation of the cathode material, complete reduction of the anode material or consumption of the electrolyte salt. During discharging, electrons are transported from the anode to the cathode via an external load leading to migration of the counter ions from the polymer matrix into the electrolyte.[1]

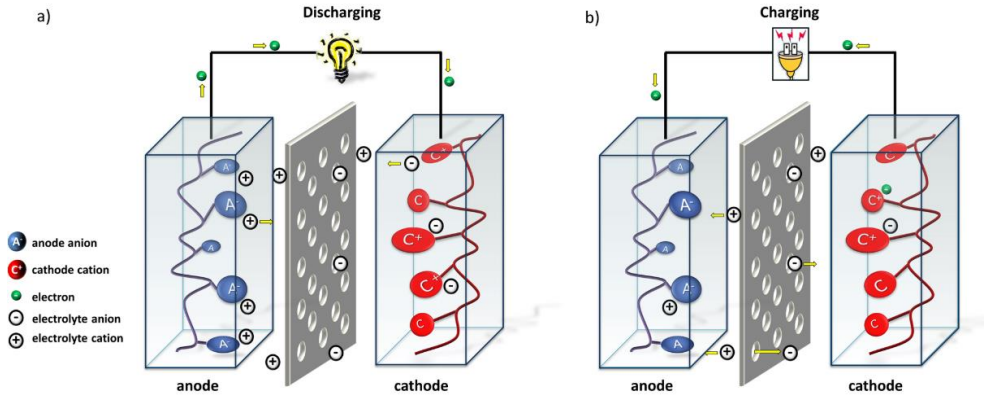

Figure 2 All-organic battery based on redox-active polymers during a) discharging and b) charging, picture from[1]

New materials are usually not tested in an all-organic battery but a in a metal-organic battery to guarantee comparability to conventional systems. In this case, a metal (usually lithium) is used as anode and both p- and n-type materials can be tested as cathodes.[1]

Despite the active material, which is discussed in more detail in the next paragraph, the electrodes consist of several other components, i.e. conductive additives, binders and current collectors. Conduc-

tive additives (mostly carbon-based ones) are necessary because the active material is usually an intrinsically non- or low-conductive polymer that cannot transport the electrons from the redox-active units to the current collector and vice versa. Binders like PTFE or PVdF increase the contact area between the current collector and the carbon-polymer composite and provide mechanical stabilization. As current collectors, aluminium foil for the positive and copper for the negative electrode are used similar to Li-ion based batteries.[1]

The electrolyte consists of a solvent and a conductive salt whose function is to transport the ions between the electrodes which is crucial for the charge balance at the redox-active groups of the active material. The solvent must be stable in the potential window of the battery and has to be chemically inert to all battery components. Besides, it has to dissolve sufficient amount of conductive salt. Among the solvents that are used most commonly are carbonates (e.g. propylene carbonate, ethylene carbonate, dimethyl carbonate), organic ethers (e.g. 1,2-dimethoxyethane, 1,3-dioxolane) or other organic solvents like acetonitrile. A conductive salt is added to increase ion conductivity and to compensate charges formed upon the redox processes at the electrodes. If lithium is used as anode, the salt's cation has to match the metal while for all-organic batteries tetrabutylammonium (TBA) salts are commonly used as well. A range of anions can be utilized (i.e. tetrafluoroborates, perchlorates and bis(trifluoromethane)-sulfonimide (TFSi)).[1]

2.2 Quinones as Active Compounds in Energy Storage Materials

In principle, all organic compounds that feature reversible redox reactions can be used in an organic battery. Among those that are investigated intensively are conjugated polymers[7], stable radicals[8], organosulfur[9] and carbonyl compounds[10]. Quinones which belong to the class of carbonyl compounds are one of the most promising substance classes for the application as active materials in batteries because they have high theoretical capacities due to their ability of storing two electrons per molecule and excellent redox reversibility.[11] For example, the simplest quinone, 1,4-benzoquinone, has a specific capacity of 496 mAh/g at a redox potential of 2.8V vs Li/Li^{+}[12] which is exceeding traditional inorganic cathode materials like $LiCo_2O_4$ (3.9 V vs Li/Li^{+}, ~140 mAh/g)[13] by far. Moreover, the redox potential of quinones can be tailored more easily compared to metal-based batteries via functionalisation (i.e. alkylation, arylation, amination or sulfenylation).[14]

Besides that, they are low cost and sustainable since they are a respiratory product of bacteria that can be extracted from biomass, potentially making batteries environmentally friendly someday.[15,16]

The electrochemical behaviour of quinones is strongly influenced by the electrolyte (Scheme 1). In aqueous solution, they undergo a reversible two-electron reduction coupled with a proton transfer. The reduction potential is strongly dependent on the pH of the solution. In aprotic media, two independent cathodic waves corresponding to the two successive one-electron transfer steps to semiquinone ($Q^{\cdot-}$)

and the quinone dianion (Q^{2-}) can be observed.[17] The formation of an aromatic system contributes to the stabilization of the reduced species because the negative charge can be dispersed.

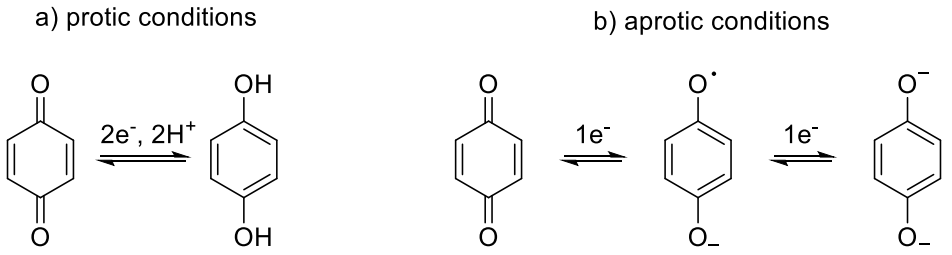

Scheme 1 Electrochemical behaviour of p-benzoquinone in different media, a) protic conditions: $2e^-$ reduction to hydroquinone, b) aprotic conditions: one-electron reduction to semiquinone and the quinone dianion

2.2.1 Polymerisation

Although single molecule quinones can undergo reversible multi-electron transfer reactions, they cannot be used as active material in electrodes due to their solubility in most electrolytes. One way to tackle this problem is making the material inherently insoluble through polymerisation which provides additional advantages like improved stability, better processability and easier device fabrication.[18,19]

The resulting redox-active polymers can be divided into two groups, i.e. conjugated and non-conjugated polymers (Figure 3). Conjugated polymers have band structures similar to semiconductors because of the overlap of adjacent π-orbitals caused by an alternative bonding structure of single and double bonds. These materials can be made electrically conductive via doping through charging which creates anions and cations that are delocalized along the polymer backbone. Thus, the charged redox centres strongly influence each other which leads to a dependency of the redox potential on the doping level and subsequently the charging level of the battery. This huge disadvantage made researcher's focus shift to non-conjugated polymers which are polymers where a non-conductive backbone bears electroactive groups which leads to stable redox-potentials.[1,19] Most quinone based redox-active polymers belong to this group.

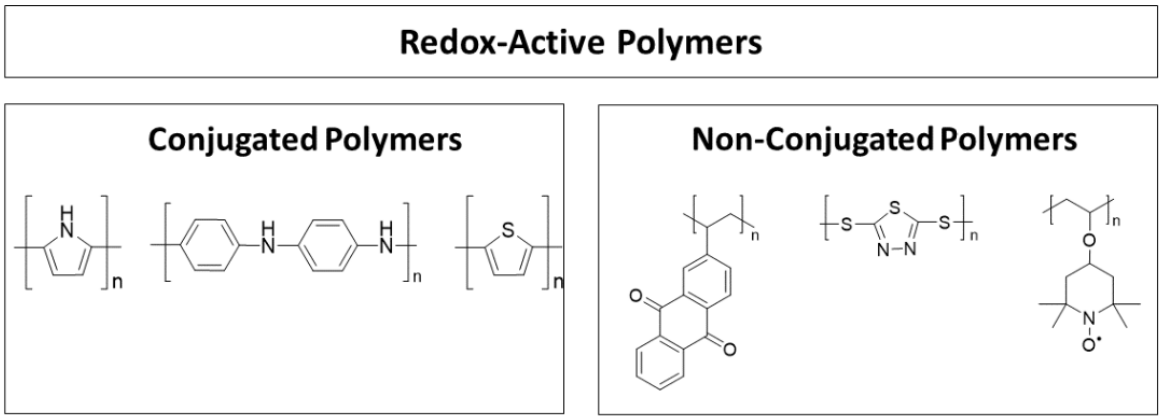

Figure 3 Classification of redox active polymers into conjugated polymers and non-conjugated polymers with representative examples of each class; from left to right: poly(pyrrole), poly(aniline), poly(thiophene), poly(anthraquinonenorbornene), poly(thiathrenenorbornene) and poly(2,2,6,6-tetramethylpiperidinyloxy-4-yl vinylether)

For the synthesis of non-conjugated polymers, a polymerizable functionality has to be introduced to the redox-active molecule which is then polymerised mostly through polycondensation, oxidative polymerisation or free radical polymerisation.[19] These methods provide easy access to cheap polymers but the ability to control the structure of the electroactive polymer is limited.[19,20] Controlled polymerisations like ring-opening metathesis polymerisation (ROMP) could be an alternative or at least an addition to traditional polymerisation methods for the fabrication of electrode materials.

The use of ring-opening metathesis polymerisation for the controlled synthesis of electroactive polymers has already been proposed in 1992.[20] This method allows to control the length and nature of blocks in co-polymers, to introduce unique end-groups and to produce a polymer with low polydispersity.[20]

In literature various examples of ROMP derived redox-active polymers that have been tested in batteries are described (Figure 4). The synthesis of these polymers, however, either requires multiple steps or expensive starting materials making these procedures unattractive to industry. In this work, we address this problem and prepare a redox-active polymer that is synthesized from cheap and readily available starting materials, i.e. benzoquinone and cyclopentadiene in the simplest case.

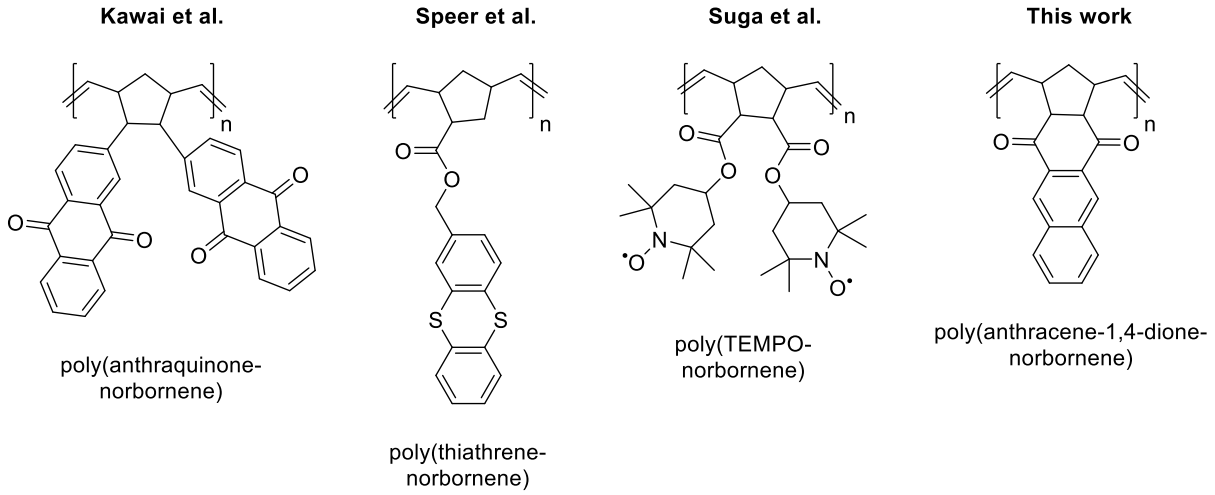

Figure 4 Comparison of structures of ROMP derived redox-active polymers that have been tested in battery applications (Kawai et al.[4], Speer et al. [5],Suga et al.[3]) and our work

2.2.2 Metal Complexes, Coordination Polymers (CPs) and Metal-Organic Frameworks (MOFs)

Besides quinone polymers, metal complexes or coordination polymers containing quinone ligands can be synthesized to limit solubility of active material into the electrolyte.

Transition metal complexes have already been investigated as potential electrode materials in Li-metal redox-flow batteries. They provide additional structural stability compared to organic redox species while the potential depends on the choice of the redox active metal because it acts as the charge transfer centre.[21,22] The potential can be tuned via the introduction of different ligands that are either innocent which means that they do not participate in the redox reaction or non-innocent (e.g. quinones) which can store charges themselves.[22]

In order to keep the electrochemical behaviour of the quinone ligand intact, a metal must not coordinate to the quinone via the oxygen atoms. Thus, the double bond has to be functionalized to generate additional coordination sites for metal ions. For this reason, pyrazole heterocycles that provide two nitrogen atoms capable of coordinating to metals were added to the quinone moiety.

The terms coordination polymer (CP) and metal-organic framework (MOF) are colloquially used similarly although the IUPAC definitions[23] distinguish between them. A CP is “a compound with repeating coordination entities extending in 1,2 or 3 dimensions” whereas a MOF is “a coordination network with organic ligands containing potential voids”. The definition of a coordination network includes the multidimensionality of the compounds - therefore, a MOF cannot be a 1D chain polymer.[23,24]

However, both CPs and MOFs are useful for energy storage applications due to their inherent insolubility in most electrolytes. Since the redox processes of conventional Li-ion batteries are based on intercalation mechanisms, MOFs are potential candidates for the fabrication of electrode materials due

to their high porosity allowing reversible insertion of metal ions. The pore size of these compounds can be tuned via the choice of the linker also enabling the insertion of larger redox-active species.[25]

For example, a quinone based coordination polymer that can be used as positive electrode was synthesized by Xiang et al.[6] Upon charging and discharging, the Li ions can be inserted reversibly at the positions of the oxygen when the carbonyl groups are reduced (Scheme 2). Besides, the CPs provides additional stability.

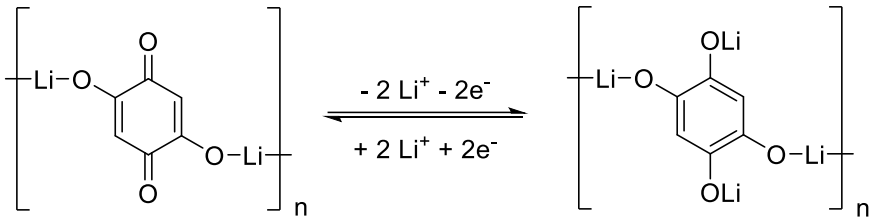

Scheme 2 Reversible Li-ion insertion into a 1D coordination polymer, proposed by Xiang et al.[6]

3 Results and Discussion

3.1 Synthesis of Redox-Active Monomers

The target of this work was to prepare polymers possessing redox active groups, in this case 1,4-benzoquinone, appended to their non-conductive polymer backbones.[19] Since ring-opening metathesis polymerisation (ROMP) should be performed, synthesis started from the simplest redox-active monomer, 1,4,4a,8a-Tetrahydro-1,4-methanonaphthalene-5,8-dione (**1**). To study the influence of extending the conjugation on the redox potential and the properties of the polymer, the anthracene and tetracene[I] derivatives were investigated as well. These monomers can be oxidized chemically (or electrochemically) and can then undergo a redox reaction to the corresponding hydroquinone derivatives in protic solvents as displayed in Scheme 3.[17]

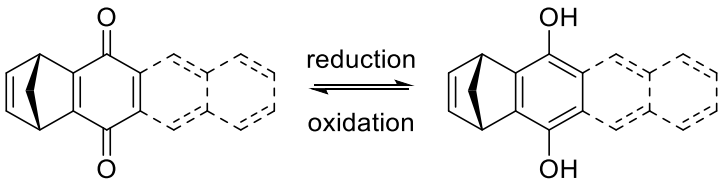

Scheme 3 Overview of redox reaction for methanonaphthalene, -anthracene (one aromatic ring) and -tetracene (two aromatic rings) derivatives

The reaction sequences can be divided into three parts, all consisting of the same reaction steps. An overview of reactions performed for the first group, the methanonaphthalene derivatives, is displayed in Scheme 4.

[I] The tetracene derivative was prepared by Melina Much. It was purified via column chromatography with toluene as eluent (Rf=0.11) and used in all further steps.

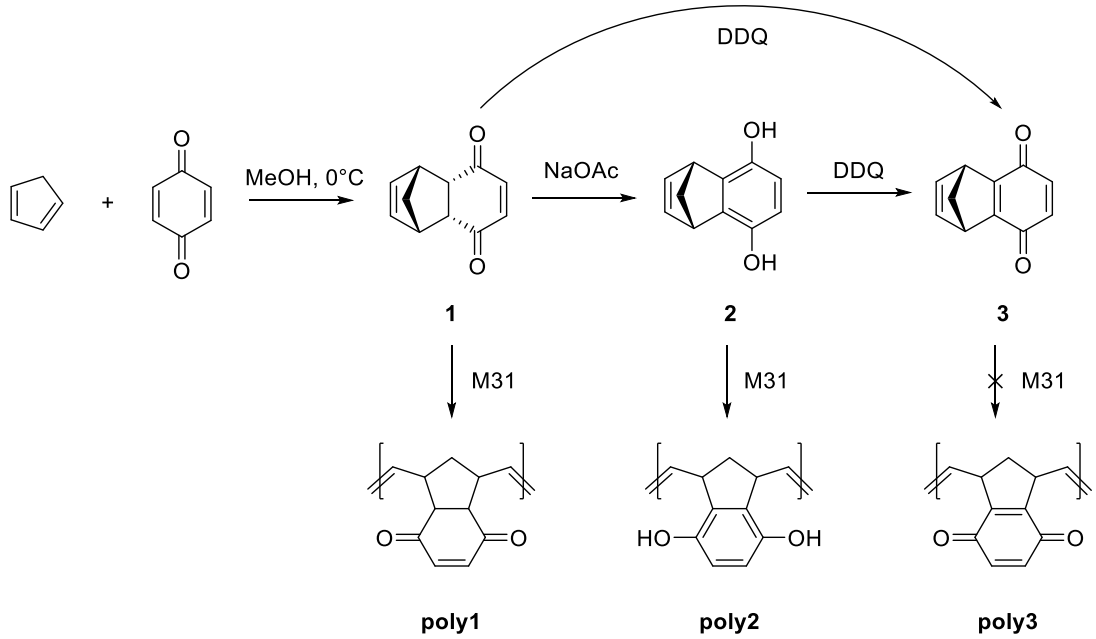

Scheme 4 Overview of reactions of methanonaphthalene derivatives

The addition of one aromatic ring leads to the anthracene derivatives whose reactions are displayed in Scheme 5.

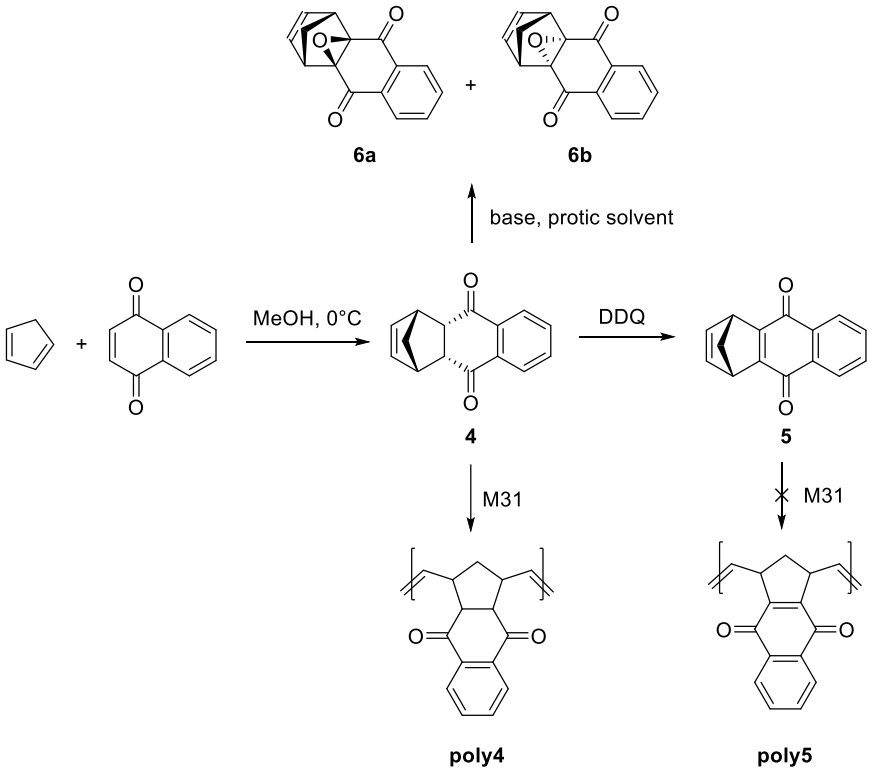

Scheme 5 Overview of reactions for the anthracene derivatives

Lastly, the tetracene derivatives with an additional benzene ring were investigated. Again, an overview of the performed reactions is displayed in Scheme 6.

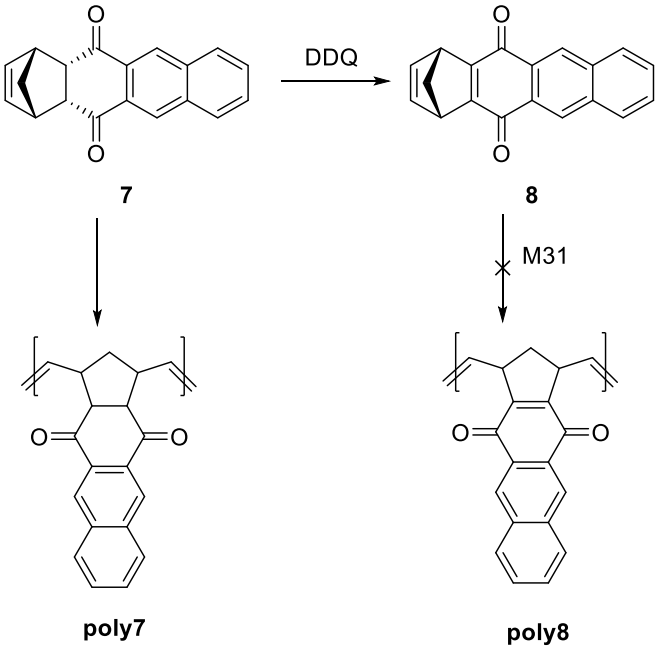

Scheme 6 Overview of reactions for the tetracene derivatives

3.1.1 Diels-Alder Addition

The reaction sequences of the methanonaphthalene- and the anthracene derivatives both commence with a Diels-Alder addition. This reaction is a [2+4]-cycloaddition of a diene (cyclopentadiene) and an electron-poor dienophile (1,4-benzoquinone or 1,4-naphtoquinone) that typically leads to the formation of two stereoisomers, the *endo* and the *exo* form (Scheme 7).[26] According to DFT calculations, the *endo* isomer is thermodynamically slightly favoured (Table 1). Boltzmann's equation says that a difference of 0.364 kcal/mol for **1** corresponds to a product distribution of 64.9 % of the *endo* and 35.1 % of the *exo* isomer.

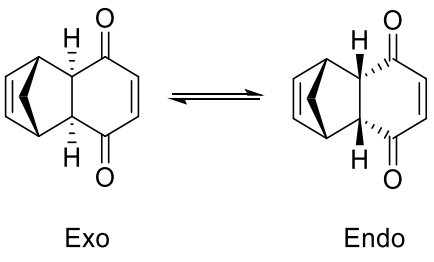

Scheme 7 *Endo* vs. *Exo* isomer of **1**

Table 1 Comparison of Gibbs free energy (ΔG) of exo and endo isomers of **1**,**4** and **7**

Compound	**ΔG (*Exo*-*Endo*) [kcal/mol]**[II]
1	0.364
4	0.361
7	0.228

However, ^{1}H NMR spectroscopy revealed that the product ratio between the *endo* and the *exo* isomer is 98:2 indicated by the integrals of the protons of the double bond at 6.06 ppm (*endo* isomer) and 6.18 ppm (*exo* isomer). This observation is in contrast to computational suggestions but can be explained by the low level of theory that has been applied in the calculations being apparently not able to describe the system properly.

Tormena and co-workers[26] investigated the reaction of 1,4-benzoquinone and cyclopentadiene on a high level of theory (CBS-Q) figuring out that indeed the *endo* isomer is thermodynamically and kinetically favoured by 1.1 kcal/mol, corresponding to a product ratio of 87:13 (*endo*:*exo*). The thermodynamic stability can be explained by attractive delocalization which is favoured in the *endo* adduct, compensating its increased steric interactions. They found that the same transition state leads to the *endo* and the *exo* adduct but it is energetically favoured for the *endo* adduct by 1.8 kcal/mol which explains its kinetic preference.

Experimentally, the Diels-Alder reaction to compound **1** was performed in methanol at 0°C. Cyclopentadiene was freshly distilled, and 1,4-benzoquinone was sublimed to minimize the formation of by-products. 1,4-benzoquinone was used in a slight excess (1.02 equivalents) to avoid the formation of the doubly substituted side product (Scheme 8). The unreacted quinone can then be easily removed via the addition of water and subsequent steam distillation with a rotary evaporator. The pure product was obtained in 83% yield as a dark yellow solid. The ^{1}H and ^{13}C NMR spectra are consistent with those published in literature.[26,27]

The doubly substituted by-product, displayed in Scheme 8, is formed if an excess of cyclopentadiene is used during the reaction. It can be converted to the monosubstituted product upon applying temperatures of 60°C or higher and sodium acetate in methanol. **1** is formed as intermediate which further reacts to its isomer **2**. The reaction is slow, as only 20% of **2** can be detected after 24 hours of stirring.

[II] Calculated using def2-SVPD basis set and PBE+D3 functional, fully optimizing the structures, RRHO approximation was applied for temperature effects at 25°C and zero-point energies

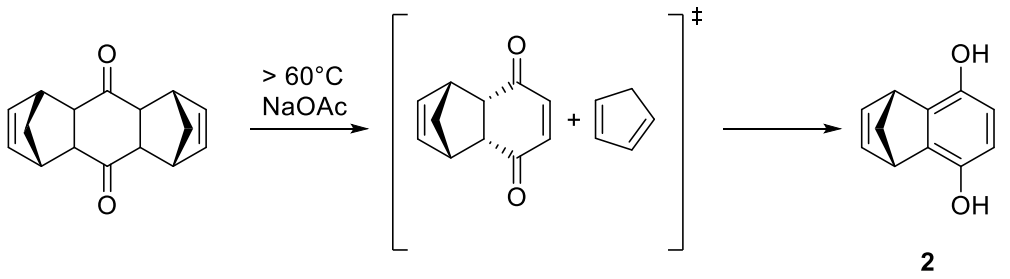

Scheme 8 Reaction of the doubly substituted **1** to **2**

Apparently, the Diels-Alder adduct **1** is not stable under UV light because a range of new peaks can be detected in the ^{1}H-NMR spectrum after two months of storage as a solid with exposure to light. A multiplet at 2.02-1.86 corresponding to two protons and singlets at 2.68, 2.79, 2.90 and 3.15, each integrating for two protons, appear. These NMR data are consistent with those of Cookson's dione,[28] a rearrangement product first described in 1964,[29] formed upon irradiation of **1** with various UV wave lengths. Thus, product **1** should be stored under exclusion of light.

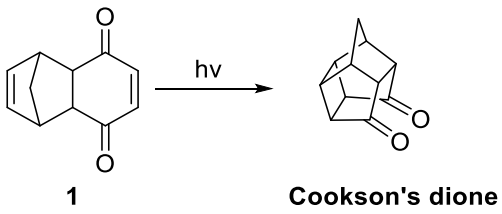

Scheme 9 Formation of Cookson's dione upon UV irradiation of **1**

The reaction of naphthoquinone and cyclopentadiene to **4** was performed similarly. Zhang et al. reported the direct synthesis of the corresponding aromatic product of **7** when using ethanol as solvent.[30] However, our experiments yielded exclusively product **4** upon performing the reaction in ethanol or methylene chloride. Again, cyclopentadiene was freshly distilled and added in excess (1.44 equiv.) to a solution of 1,4-naphtoquinone to ensure complete addition. Reaction was performed at 0°C and stirred overnight. The crude product was washed with ligroin to get rid of dicyclopentadiene which was formed as a side product. The product was obtained as beige solid in 78% yield. Subsequent ^{1}H-NMR measurements in $CDCl_3$ revealed multiplets for the aromatic protons at 8.00-7.98 and 7.68-7.65 ppm. The protons of the norbornene double bond resonate at 5.95 ppm while the rest of the norbornene moiety gives rise to singlets at 3.63 and 3.43 ppm. The methylene group can be assigned to a multiplet at 1.51 ppm. The integral ratio is 2:2:2:2:2:2. The ^{13}C-NMR spectrum reveals signals at 197.83, 135.62, 135.89, 134.14, 126.91, 49.59 and 49.29 ppm.

3.1.2 Aromatisation vs. Epoxidation

Aromatisation

Interestingly, **1** and **2** are structural isomers and not tautomers. This means that the latter is not formed spontaneously but its formation requires a distinct isomerisation reaction as indicated in Scheme 10.

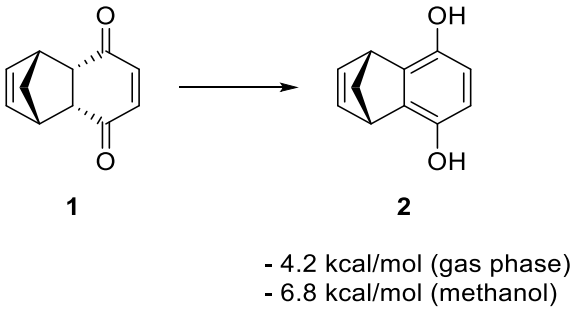

Scheme 10 Aromatisation of **1** and relative stabilities obtained by DFT calculations

DFT calculations suggest that the aromatic product is more stable in the gas phase (-4.2 kcal/mol) as well as in methanol (- 6.8 kcal/mol).[III] These calculations are in line with chemical intuition suggesting that the formation of an aromatic systems leads to increased stability. A transition state search of this reaction showed that the phenolic proton of **2** does not come from the backbone of **1** but has to be provided by a protic solvent molecule, like methanol or water.

The intramolecular pathway, displayed in Figure 5, occurs via two separated proton transfer steps. The first one is the rate-determining step of the reaction, because it has the highest activation barrier (64.5 kcal/mol) which can be assigned to the break of a C-H bond and the formation of an O-H bond happening coincidently. The formed intermediate is 10.9 kcal/mol higher in energy due to the loss of planarity of the quinone ring. The second proton transfer step again occurs via a simultaneous break of a C-H bond and formation of an O-H bond with an activation barrier of 54.7 kcal/mol ($E_A=E_{Ts2}-E_{Im}$). Product **2** is 4.2 kcal/mol lower in energy compared to the educt which can be assigned to the formation of a planar, aromatic system.

[III] Calculated using def2-SVPD basis set and PBE+D3 functional, fully optimizing the structures, RRHO approximation was applied for temperature effects at 25°C and zero-point energies, COSMO for solvent effects

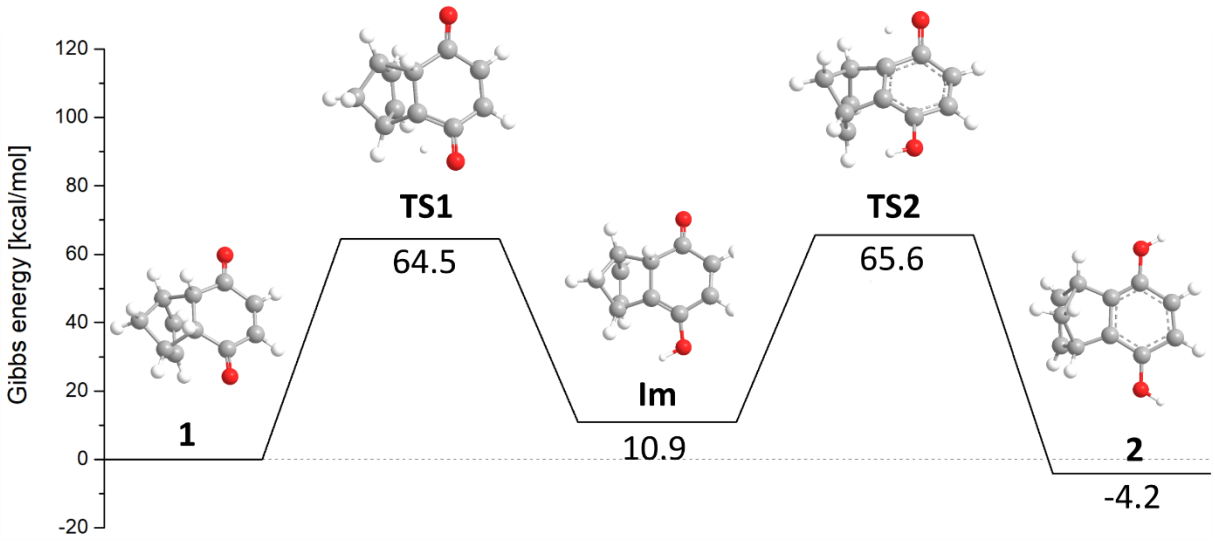

Figure 5 Intramolecular pathway for the reaction of **1** to **2**, calculated with def2-TZVPPD/B3-LYP D3

However, this reaction mechanism is energetically not feasible, even at elevated temperatures, because the activation barriers for both proton transfer steps are too high in energy.

The activation energy of the rate-determining step can be correlated with the rate constant through the Eyring equation[31] where k_b is Boltzmann's constant, T is the temperature, h is Planck's constant, ΔG corresponds to the activation barrier and R is the ideal gas constant.

$$k = \frac{k_B \cdot T}{h} e^{-\Delta G/RT}$$

A barrier of 64.5 kcal/mol corresponds to a conversion rate of $1.27*10^{-16}$ mol/day at 25°C or $3.75*10^{-12}$ mol/day at 70°C which is too low to be even observable.

An intermolecular reaction pathway where two methanol molecules provide protons and act as H+ shuttle is presented in Figure 6. Again, the first proton transfer step is rate-determining and has an activation barrier of 37.6 kcal/mol. Interestingly, the intermediate and **2** are higher in energy compared to the intramolecular pathway.

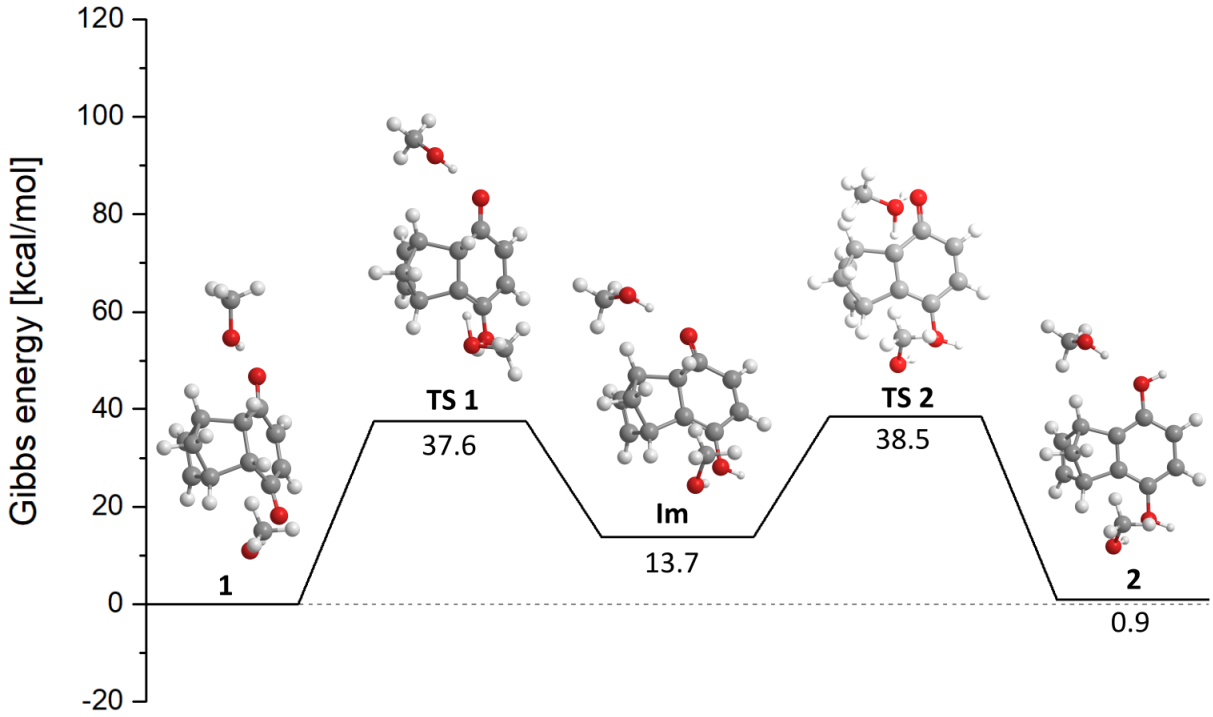

Figure 6 Intermolecular pathway for the reaction of **1** to **2**, calculated with def2-TZVPPD/B3-LYP D3

The calculated barrier is energetically feasible which is also supported by experimental observations as 10% conversion of **1** to **2** could be observed after 24 hours of stirring in refluxing methanol. Besides, formation of the *exo* product of **1** and a dark brown to black precipitate, probably the corresponding quinhydrone (Figure 7), could be detected.

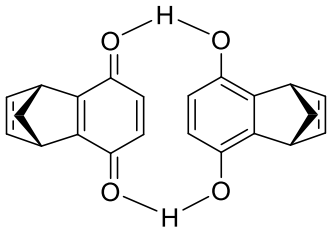

Figure 7 Postulated quinhydrone dimer formed upon thermal treatment of **1**

In literature, various conditions to obtain the aromatic product are known.[32–34] Their common feature is the addition of a base that triggers the formation of the desired product. It can be expected that the activation barrier for a base-catalysed aromatisation are much lower because conversion occurs within hours. Experimentally, aluminium oxide and sodium acetate were tested as bases and both considered suitable for the reaction.

For the first procedure, **1** was dissolved in ethyl acetate and an excess of basic aluminium oxide was added. The reaction mixture was vigorously stirred overnight at reflux temperature under nitrogen atmosphere to avoid formation of quinhydrone by-products. Aluminium oxide was filtered off and washed several times with ethyl acetate and methanol. The washing process reduced the yield to 60.8 %

because the product strongly stuck on the aluminium oxide surface. The solvents were then removed under reduced pressure whereupon a sticky oil formed which could be crystallized through the addition of chloroform and subsequent ultrasonification.

For the second procedure, 3.00 equivalents of sodium acetate were added to a solution of **1** in methanol. The clear solution was stirred overnight at reflux temperature whereupon it gradually turned light-brown. The solvent was evaporated under reduced pressure and the solid was washed with tetrahydrofuran to separate off sodium acetate, which is insoluble in this solvent. The filtrate was evaporated to dryness yielding 78% of crude product which was then recrystallized from chloroform. This method gives a higher yield, as the separation step from the base can be done more efficiently but the expended effort is higher.

The pure product was obtained as a white powder which was characterised via NMR spectroscopy in $CDCl_3$ (poorly soluble) and DMSO-d_6. Compared to **1**, all signals in the ^{1}H NMR spectrum in $CDCl_3$ are shifted downfield indicative for the formation of an aromatic ring. The protons of the double bond of the quinone moiety resonate at 6.80 compared to 6.56 ppm and those of the double bond of the norbornene moiety are shifted from 6.06 to 6.35 ppm. The phenolic protons give rise to a broad singlet at 4.30 ppm. The peak of the bridge protons has disappeared whereas the other protons of the norbornene moiety resonate at 4.08 ppm. **2** is stable at ambient atmosphere, even after months of storage in solution and as solid.

Epoxidation

For the aromatisation of **4**, the same reaction conditions as for the aromatisation of **1** were applied, namely sodium acetate was used as a base and reaction was performed in refluxing methanol under nitrogen atmosphere.

Interestingly, the aromatic product was not formed but a mixture of products could be detected in the ^{1}H NMR spectrum whereof **5** (47.8%), **6a** (39.7%) and **6b** (12.5%) could be identified. The ratio of products changed upon storage in solution since after one month a product ratio of 24.7% (**5**), 59.1% (**6a**), 16.2% (**6b**) could be detected, indicating that the epoxides are formed from the oxidized monomer **5**.

Numata and co-workers[35] reported the formation of the aromatised product via two methods in a patent. The first one is the base-catalysed aromatisation with sodium hydroxide and a solvent mixture of dimethyl acetamide and water (1:1). Sodium hydroxide is a much stronger base with a pK_A value of 15.7, compared to sodium acetate (pK_A=4.76)[36] which could be too weak to abstract a proton from **4** which is necessary for the formation of the aromatic product. Compound **4** is perfectly soluble in this solvent mixture, contrary to methanol and water which were used previously. After dissolution, the reaction mixture was stirred for 5 hours at 75-80°C. Then, the mixture was acidified to a pH of 4-5

whereupon a brown precipitate formed which was analysed via ^{1}H NMR spectroscopy. The aromatic product could not be detected, but again **5** (46.9%), **6a** (45.2%) and **6b** (7.9%) were formed. Besides, traces of at least a third species were observed which could probably be a light-induced isomerisation product of **6b** which would also explain the low amount of **6b** that was formed in the reaction.

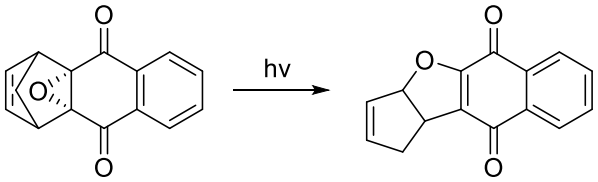

6b

Scheme 11 Reaction product of **6b**, caused by light-induced isomerisation[37]

Product **5** is characterised by two multiplets at 8.07-7.93 ppm and at 7.72-7.70 ppm, each integrating for two aromatic protons, two singlets at 6.90 (two protons) and 4.25 ppm (two protons) and a multiplet at 2.37-2.34 ppm (two protons). The aromatic protons of **6a** are characterised by the same signals in the aromatic region, namely at 8.09-7.93 and 7.72-7.70. Besides, singlets at 6.60 and 3.60, each integrating for two protons and a multiplet at 1.64-1.81 are characteristic for the endo epoxide. The *exo* epoxide's (**6b**) aromatic protons also give rise to multiplets in the region of 7.9-7.4 ppm (two protons) and 7.43 ppm (two protons). Additionally, two singlets at 6.17 and 3.76 and a multiplet at 1.64-1.81 ppm can be attributed to **6b**. NMR data are depicted in Figure 8 and are consistent with those published in literature.[38]

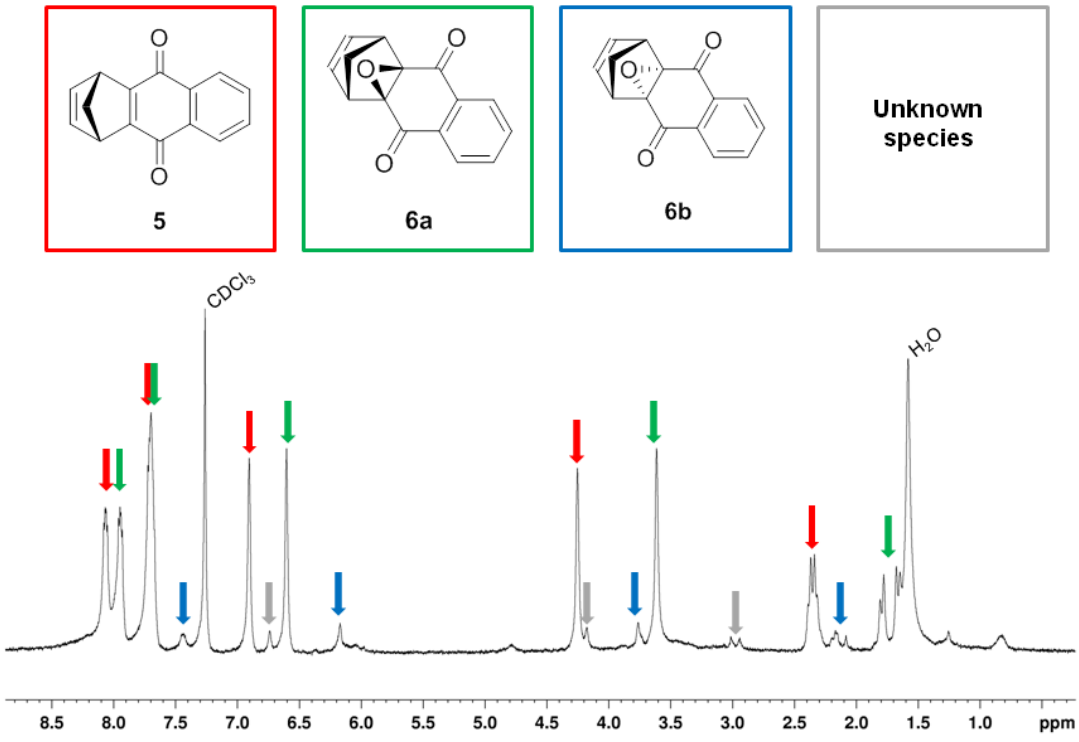

Figure 8 ^{1}H NMR spectrum of **5**,**6a** and **6b** obtained after treatment of **4** with sodium hydroxide

The second method that has been reported for the formation of the aromatic product of **4** is acid promoted aromatisation.[35] Therefore, reaction was performed in dimethylacetamide/water and hydrochloric acid. This reaction proceeded significantly more slowly because a stirring time of 48 hours had been necessary before a precipitate was formed. ^{1}H NMR spectroscopy revealed that this precipitate contained the products **5** (20.5%), **6a** (66.9%) and **6b** (12.56%). The prolonged stirring time shifts the equilibrium from the oxidation product to the *endo* epoxide indicative that **6a** is formed from **5**. Besides, many unidentifiable by-products could be detected in the ^{1}H NMR spectrum.

It was found that the oxidized product **5** is also formed without the addition of a catalyst upon stirring of **4** in dimethyl acetamide and water (1:1) for 16 hours at 80°C whereas only traces of the epoxides and other products could be detected.

The aromatic product seems to be unstable since no NMR data have been published in literature and it is described only as intermediate formed through the addition of a strong base like NaH and subsequent trapping by methyl iodide to form a stable aromatic product.[39]

Contrary, formation of epoxides from **4** is known to proceed under various conditions.[37–40] Mixtures of **6a** and **6b** have been detected upon treatment of **4** with sodium hydroxide in aqueous methanolic solution at ambient atmosphere or aqueous hydrogen peroxide in strongly alkaline conditions. The main product is in each case the thermodynamically more stable epoxide **6a,**[39] as the *endo* face of **5** is more

susceptible to an attack. The mechanism is supposed to proceed via semiquinone radicals and hydroperoxide anion species which are formed through the presence of oxygen in alkaline medium.[40]

Treatment of the π-extended product **7** with methanol and sodium acetate resulted in a vast mixture of products, of which **8** could be identified. The formation of epoxide species is likely but could not be confirmed.

3.1.3 Oxidation

Compounds **1**, **2**, **4** and **7** were subsequently oxidized to yield **3**, **5** and **8**, respectively. The oxidation was performed with various oxidants including 2,3-dichloro-5,6-dicyano-1,4-benzoquinone (DDQ), ceric ammonium nitrate (CAN) and hydrogen peroxide (Figure 9). DDQ used in stochiometric amounts proved to be most suitable. With its high redox potential ($2e^-/2H^+$) of 0.887 V vs. NHE[41] (compared to 0.643 V of 1,4-benzoquinone) it is a commonly used oxidant for a range of organic molecules.[42]

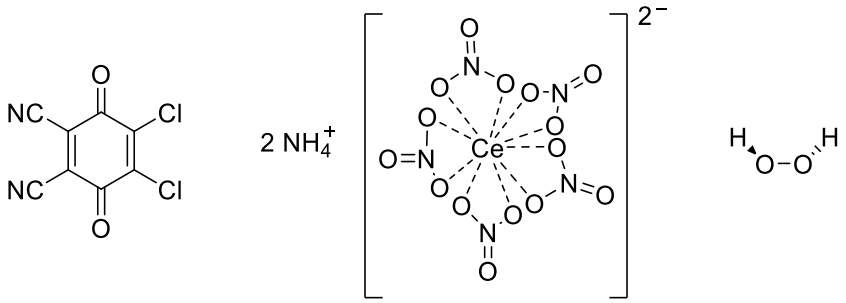

Figure 9 Applied oxidants for oxidation of **1**, **2**, **4** and **7**

Since the oxidation of **1** and **2** lead to the same product, it was tested if the reactions proceed equally well. Thus, the aromatic product **2** was first reacted with 1.0 equiv. of DDQ in 1,4-dioxane. The resulting by-product, the reduced form of DDQ (DDQ-HQ) is insoluble in this solvent and was filtered off after completion of the reaction. The product can be further purified via column chromatography with cyclohexane and ethyl acetate (3:1) as eluent.

Product **2** could also successfully be oxidized with 2.0 equivalents of ceric ammonium nitrate, $(NH_4)_2Ce(NO_3)_6$, within two hours of stirring in a solvent mixture of acetonitrile and water. Although the reaction time is shorter, this method is inferior as the work-up procedure consumes more time and the yield is worse (54.5% vs. 95.6%). The poorer yield can be explained by the solubility of product **3** in water which limits the yield when using liquid-liquid extraction with water and diethyl ether because the product is not selectively transferred to the organic phase. In contrast to DDQ oxidation

where the by-product can be simply filtered off, CAN oxidation requires liquid-liquid extraction to yield a pure product.

1 can also be oxidized with 1.2 equiv. of DDQ and p-toluenesulfonic acid as catalyst (0.1 equiv.). The reaction proceeds more slowly as stirring overnight is necessary for complete conversion compared to the 4 hours as in the case of the oxidation of **2**. DDQ is removed via liquid-liquid extraction with water and ethyl acetate before the product is again purified via column chromatography. The product was characterised via NMR spectroscopy where singlets at 6.85 and 6.56 ppm corresponding to the CH=CH protons of the quinone and the norbornene moiety, respectively, could be detected. A singlet at 4.10 ppm which can be assigned to the bridge protons of the norbornene moiety and a multiplet at 2.30-2.26 ppm corresponding to the CH_2 group were further observed. Compared to **1** and **2**, all signals are shifted downfield indicative for a reduced electron density. ^{13}C NMR spectroscopy was used to ensure that DDQ is absent in the product since this reagent does not have any protons which can be detected in the ^{1}H NMR spectrum. The product is characterised by peaks at 184.15, 160.85, 142.65, 135.85, 73.97 and 48.53 ppm and can be considered as NMR pure. The yield of the reaction of **1** to **3** and of **2** to **3** differs significantly. While the first procedure yields 69.5% of the product, the second one yields 95.6 % when using aluminium oxide as base. This is due to the solubility of **3** in water which reduces the yield when liquid-liquid extraction is used.

4 was oxidized similarly with 1.2 equiv. of DDQ as oxidant and p-toluenesulfonic acid as catalyst. The same work-up procedure that was used for **3** was applied. Additional purification can be achieved via column chromatography with cyclohexane and ethyl acetate (5:1) as eluents. Again, all signals of the ^{1}H-NMR spectrum are shifted downfield, indicative for successful oxidation and NMR data are consistent with those published in literature.[39]

The oxidation of **7** was done according to Zhao and co-workers' procedure with DDQ as oxidant and p-toluenesulfonic acid as catalyst.[43] The product had to be purified via column chromatography with toluene as eluent since the impure educt, still containing approximately 10% of quinizarin, was used. Thus, the yield of pure product was only 43.1%. ^{1}H and ^{13}C NMR spectra can be found in the appendix and are consistent with those published in literature.[43]

The oxidations of **1**, **3** and **7** were also attempted with hydrogen peroxide and ferric chloride as catalyst. However, this procedure did not prove to be effective as only traces of the desired product could be observed in the ^{1}H NMR spectrum. Derikvand and co-workers[44] described the oxidation of hydroquinones to benzoquinones with silver oxide (Ag_2O) and hydrogen peroxide as oxidant. This procedure was not tested in our investigations but would be a reasonable alternative worth considering.

Photosensitivity of oxidized products 3, 5 and 8

The oxidized products **3**, **5** and **8** are not stable under irradiation with visible light as solids and in solution. Solutions of **3**, **5** and **8** were stored in chloroform at daylight and investigated for a month in the ^{1}H NMR spectrum. Gradually, new peaks appear which increase in intensity and an insoluble white precipitate, which could not be further analysed, formed. The ^{1}H NMR spectrum of **5** and the corresponding photo dione **5p** is exemplarily shown in Figure 11 and is in line with literature data.[45] It can be concluded that a metastable quadricyclane structure, containing a highly strained cyclobutane and two cyclopropane rings, has been formed (Scheme 12).

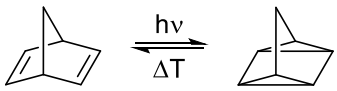

Scheme 12 Valence isomerisation of norbornadiene to quadricyclane

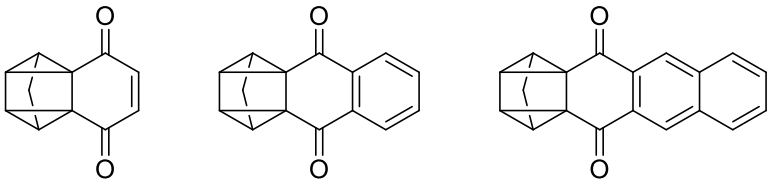

3p **5p** **8p**

Figure 10 Structures of the formed photo diones **3p**, **5p** and **8p**

Norbornadiene itself does not isomerise under visible light (> 300 nm) as it does not absorb in these wavelenghts.[46] Benzo- or naphtoquinone units shift the absorption to a range of 310-410 nm yielding photoproducts in almost quantitative yield after some time.[47] The more aromatic rings are present in the molecule structure, the faster occurs the conversion to the corresponding photo dione which is due to the increased absorbance of visible light. Back-isomerisation happens upon thermal treatment of quadricyclane (> 140°C) or irradiation which can be catalysed through metal ions.[46]

Upon storage of **5**, a new multiplet of the CH_2 protons at 2.42 ppm and two doublets at 2.99-2.98 and 3.14 corresponding to the CH protons of the quadricyclane moiety appear. The aromatic protons give rise to new multiplets at 8.27-8.24 ppm and 7.80-7.76 ppm. The integral ratio cannot be determined since the signals of compound **5** are superimposed. The ^{1}H NMR data are depicted in Figure 11.

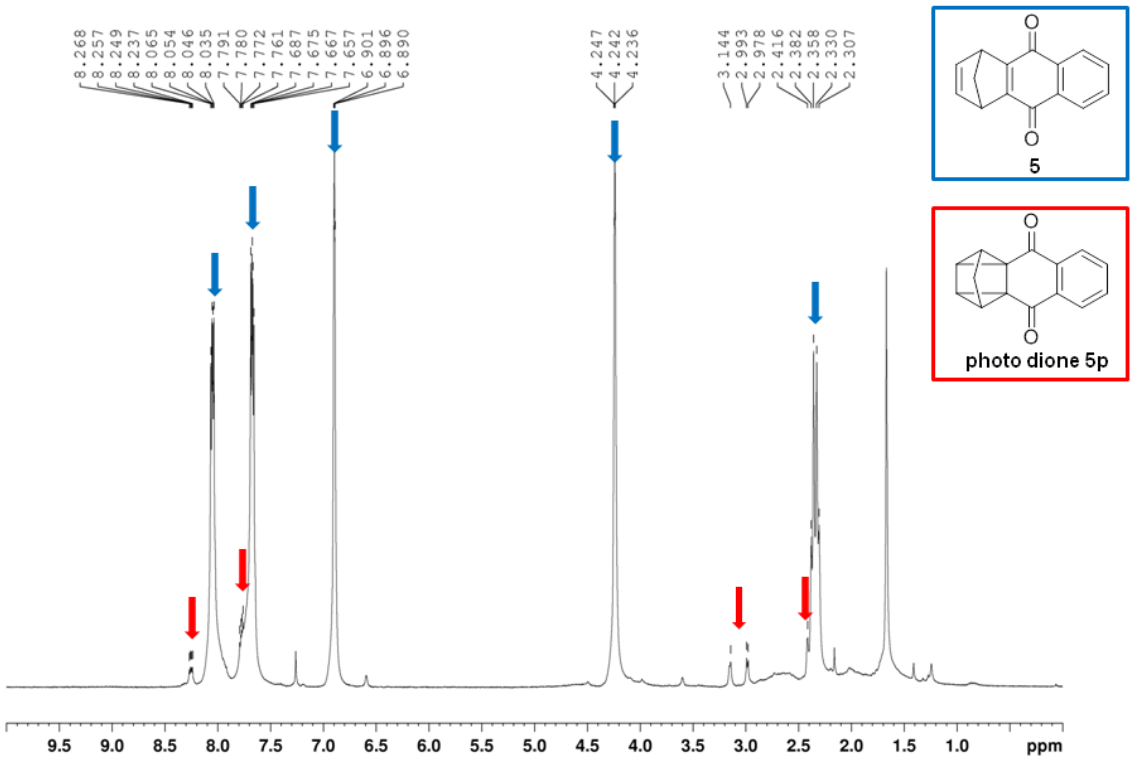

Figure 11 Comparison of ^{1}H NMR spectra of 5 and **photo dione 5p** after storage in chloroform at visible light

These newly formed peaks increase in intensity during storage. After one month of storage of **5** and **8** in solution in visible light, 6% of photo dione **5p** and 22% of photo dione **8p** have formed (Figure 10), clearly showing that an expanded aromatic system leads to faster conversion.

This reaction was also observed for **3** and **8** whose ^{1}H NMR data are displayed in the Appendix.

3.2 Functionalisation of Redox-Active Monomers

In the next steps, it was tried to introduce functionalities to the monomers to alter their redox potential and investigate their behaviour in ring-opening metathesis polymerisation. Moreover, functionalisation of the double bond generates additional coordination sites for metal ions. Thus, Aza-Michael additions of nitrogen containing heterocycles like pyrazoles or imidazoles to the double bond of 1,4-benzoquinone, as depicted in Scheme 13, were performed.

3.2.1 Functionalisation of 1,4-Benzoquinone

Functionalisation of 1,4-benzoquinone with N-containing heterocycles has been known in literature since 1972.[48–52] Pyrazole addition was first discovered by Gauss et al.[48] and further investigated by Ballesteros et al.[49] who proposed a mechanism consisting of an Aza-Michael addition followed by an oxidation and a second addition as displayed in Scheme 13.

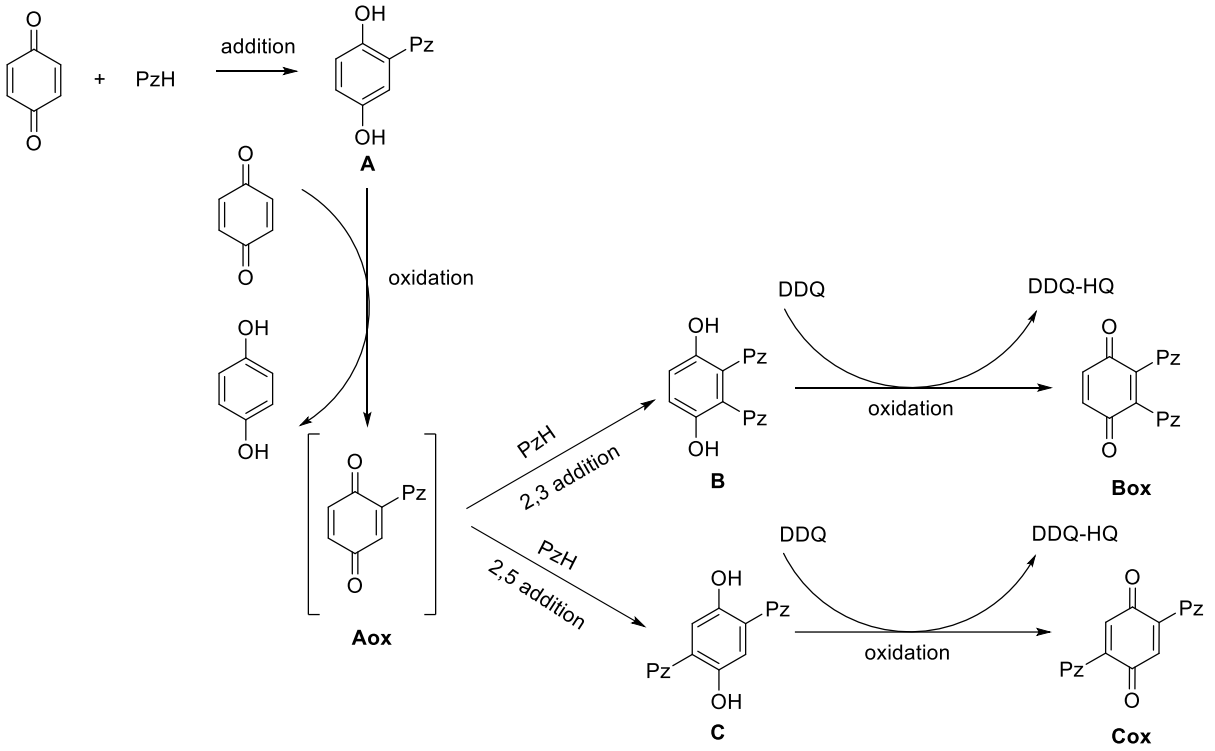

Scheme 13 Mechanism of pyrazole (PzH) addition to 1,4-benzoquinone, adapted from [49]

The reaction can lead to three different hydroquinone derivatives, the monosubstituted one (**A)** formed directly after the first Michael addition and two disubstituted ones (**B, C**) formed after an oxidation step. This oxidation step is slow because the monosubstituted hydroquinone adduct has an oxidation potential generally higher than 1,4-benzoquinone.

As soon as this oxidized intermediate (**Aox**) is formed, it is trapped by the attack of a second nucleophile leading to the disubstituted 2,3- and 2,5-adduct, whereby the 2,3-adduct is strongly favoured in

the reaction with pyrazoles (1H-pyrazole, 3,5-dimethylpyrazole, 4-chloro-3,5-dimethylpyrazole and 4-nitropyrazole). The oxidation potentials of the oxidized adduct as well as of the 1,4-benzoquinone educt are not high enough to further oxidize the disubstituted products.[49] Thus, trisubstituted products formed without the addition of an additional oxidant have not been described in literature yet.

The product ratio of **A** to **B** and **C** strongly depend on the choice of the nucleophile as well as the reaction time and not the ratio of nucleophile to quinone. Thus, the stronger the nucleophile, the higher the probability that the 2,3- and 2,5-adducts are formed as the oxidized intermediate can be attacked more efficiently.

This is especially true for 3,5-dimethylpyrazole (pK_A=15.0, Table 2) which selectively adds to 1,4-benzoquinone to form the 2,3-disubstituted product. The reaction has been described in literature before where the product could be isolated in 35% yield. Besides, 10% of 2-(3,5-dimethylpyrazole)hydroxyquinone and hydroquinone were found.[50]

In order to maximize yield of the desired 2,3-disubstituted product, we prolonged the reaction time from 1 hour to 16 hours promoting the oxidation of the monosubstituted product and subsequent Aza-Michael addition. The crude product was washed with diethyl ether as the hydroquinone side product is known to have excellent solubility in this solvent.[53] With this method, yield could be maximized to 82%. The product is insoluble in cyclohexane, ethyl acetate, methylene chloride, acetone, diethyl ether and water. Upon heating, it is slightly soluble in methanol, dimethyl sulfoxide and dimethyl formamide. Subsequent ^{1}H-NMR measurements in DMSO-d_6 revealed a broad singlet at 9.32 ppm corresponding to the phenolic protons and two sharp singlets at 6.95 and 5.68 ppm. The methyl groups of the pyrazole moiety give rise to a doublet at 2.01-1.94 ppm. The integral ratio of the signals is 2:2:2:12. IR bands are consistent with those published in literature.[54]

Preference of 2,3- over 2,5-adducts

The preferential formation of the 2,3- over the 2,5-adduct in the reaction of pyrazoles with 1,4-benzoquinone[49] is counterintuitive at first sight and the 2,3 isomer was proposed first based on elemental analysis only and the reasonable assumption that the less hindered isomer should be formed in this reaction.[55] This is also supported by DFT calculations suggesting that the 2,5 isomer is more stable by 3.73 kcal/mol. Thirty years later, Catalan and co-workers corrected the published structure on the basis of single crystal X-ray diffraction analysis revealing the selective formation of the 2,3-adduct.[50]

The general preference of the 2,3- over the 2,5-adduct has already been described in 1900 for cyano substituents[56] and Wallenfels et al.[57] proposed a mechanism explaining this observation, which is displayed in Scheme 14. After the first addition of a nucleophile, rearrangement of electrons occurs before the addition of the second nucleophile. However, if the nucleophile is not strong enough to attack the mono-substituted adduct, rearrangement to the 2-adduct (**A**) occurs.

The formation of the 2,3-adduct after a second attack is favoured because the double bonds remain in the conjugated system whereas aromaticity is lost in the course of the reaction to the 2,5-adduct. Finally, the 2,3-adduct is oxidized with a molecule of 1,4-benzoquinone forming the oxidized adduct and one equivalent of hydroquinone. Oxidation is strongly favoured in this case as an aromatic ring is formed indicating that the oxidation potential is significantly lower compared to compound **A**. However, it has also been proven that oxidation of **A** is possible with 1,4-benzoquinone.[58]

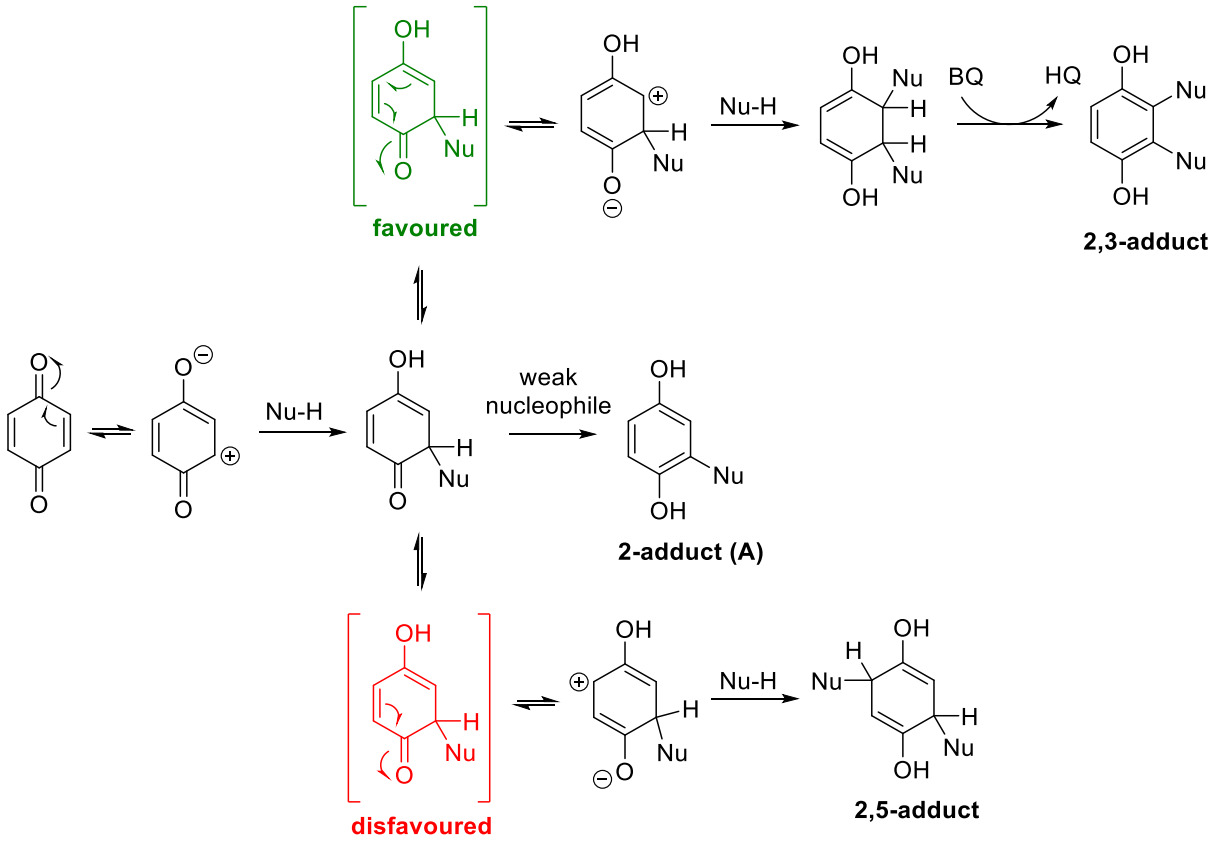

Scheme 14 Mechanism of nucleophile addition to 1,4-benzoquinone, adapted from [57]

Literature research revealed that in contrast to 3,5-dimethylpyrazole which selectively reacts to the 2,3-disubstituted product, pyrazole forms all three adducts **A** (57%)**, B** (29%) and **C** (14%).[49] Thus, it can be concluded that nucleophilicity is lower and that its 3-position must be partly deactivated via delocalization of electron density from the nitrogen lone pair over the quinone ring. As the 6-position is also deactivated via resonance interaction with the C=O, the attack occurs at the 5-position. This conclusion is true if the nucleophile lone pair can be delocalized into the quinone ring which is only possible if a planar geometry can be formed like for 1H-pyrazole, chloro or methoxy substituents (Scheme 15).[49]

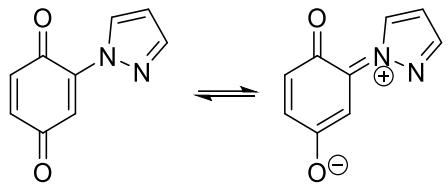

Scheme 15 Deactivation of 3-position towards nucleophilic attack via delocalization of electron density[49]

Besides 3,5-dimethylpyrazole, we also reacted 1H-imidazole and biimidazole with 1,4-benzoquinone. For 1H-imidazole, the reaction was conducted in 1,4-dioxane at room temperature and a stirring period of one hour according to a published procedure.[51] The crude ^{1}H-NMR spectrum showed signals of all three products **A**, **B** and **C** as well as of hydroquinone. This mixture was not worked-up as a combination of re-crystallization and column chromatography necessary for purification contrasts with our aim of a large-scale production of 2,3-adducts. However, literature research revealed that the product ratio is 31 % of **A**, 28% of **B** and 41% of **C**[51] indicating that 1H-imidazole is a stronger nucleophile than 1H pyrazole as the relative amount of **A** is lower compared to the reaction with 1H pyrazole indicating that a second attack is facilitated in the case of 1H-imidazole. It must be considered that product ratios can change with longer reaction times and that in this case, the reaction mixture was stirred for only one hour. Furthermore, the delocalization of electron density from the nitrogen lone-pair into the quinone ring is easier in the case of 1H-imidazole as the 3-position seems to be more deactivated promoting attack of the 5-position which leads to larger relative amounts of **C**.

Although biimidazole possesses high nucleophilicity, not even the monosubstituted adduct could be detected in the ^{1}H-NMR spectrum. This is probably due to the poor solubility of the nucleophile being only slightly soluble in hot dimethyl sulfoxide and dimethyl formamide.

Prediction of product ratios

Nucleophilicity can be correlated with basicity according to the Bronsted equation [59] which means that the more basic a substrate (higher pK_A), the better it performs as a nucleophile and the more likely is the formation of disubstituted products.

This correlation is supported upon regarding the high pK_A-values of 3,5-dimethylpyrazole reacting exclusively to the disubstituted 2,3-adduct. The formation of disubstituted adducts is due to its high nucleophilicity enabling attack of the monosubstituted product and the preference of 2,3 over 2,5 adducts due to its inability to push electrons into the aromatic system.

2-methylimidazole which also has high pk_A value reacts in the ratio of 10% of **A**, 85% of **B** and traces of **C**.[51] In this procedure, reaction was performed for only 4 hours at room temperature, which is probably too short and can explain the formation of 10% of **A**. Since only traces of the 2,5-adduct have been found, it can be concluded that the electrons of the nitrogen lone pair cannot be delocalized into the quinone ring.

If the 2,3- or 2,5 adduct are formed, one equivalent of hydroquinone can always be detected since it is a by-product when DDQ is applied as oxidant.

The structures of the monosubstituted adducts have been optimized with DFT-calculations to investigate planarity and predict if deactivation of the 3-position and associated formation of 2,5 adducts is likely to occur. The optimized structures of imidazole and 3,5-dimethylpyrazole substituted 1,4-benzoquinone can be seen in Figure 12. The results are summarized in Table 2.

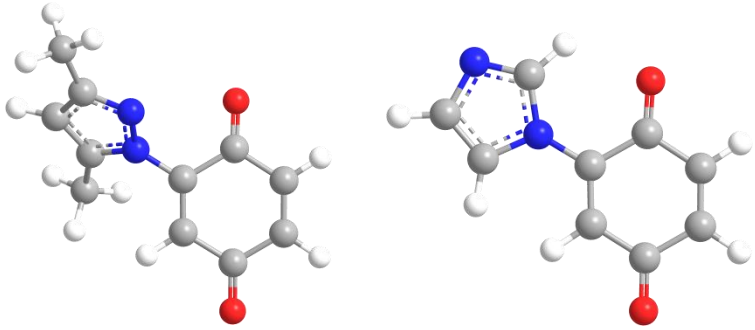

Figure 12 Comparison of structures for monosubstituted 1,4-benzoquinones; left: 3,5-dimethylpyrazole substituted, right: imidazole substituted 1,4-benzoquinone

Table 2 Comparison of pK_A values and geometries of selected nucleophiles

	2-phenyl-imidazole	**imidazole**	**pyrazole**	**3,5-dimethyl-pyrazole**	**2-methyl-imidazole**	**bi-imidazole**
structure	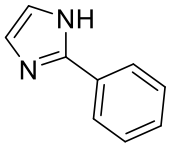			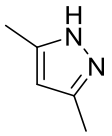	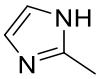	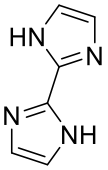
Planarity of the 2-adduct[IV]	yes	yes	yes	no	no	no
pK_A-value (experimental)	-	7.00/14.9[60]	2.50/14.2[61]	4.10/15.0[61]	7.85/15.1[60]	-
pK_A value (calculated)[V]	6.84/13.00	7.18/13.89	2.83/14.00	4.06/15.12	8.15/14.44	5.98/12.16
Product ratio A:B:C	no reaction	31:28:41[51]	57:29:14[49]	0:100:0	10:85:5	no reaction

[IV] Calculated using def2-TZVPPD basis set and B3-LYP+D3 functional, fully optimizing the structures, RRHO approximation was applied for temperature effects at 25°C and zero-point energies
[V] Calculated using Advanced Chemistry Development (ACD/Labs) Software V11.02 (© 1994-2019 ACD/Labs)

Oxidation of the 2,3-adducts

After formation of the disubstituted 2,3-(3,5-dimethylpyrazole)hydroquinone (**9**), it was oxidized with 2,3-dichloro-5,6-dicyano-1,4-benzoquinone (DDQ) to give 2,3-bis(3,5-dimethylpyrazole)-benzoquinone (**10**), as depicted in Scheme 16, according to a literature procedure.[49]

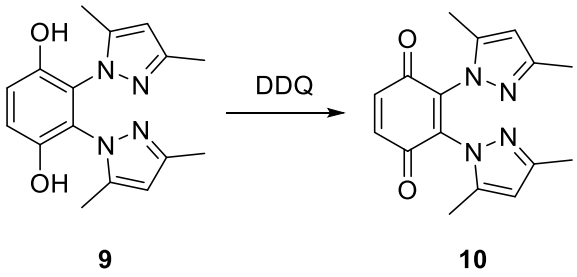

Scheme 16 Formation of **10** via oxidation of **9** with DDQ

9 was reacted with 1.0 equiv. of DDQ in 1,4-dioxane. After two hours of stirring, a precipitate formed (DDQ-HQ) which was filtered off. The solvent was evaporated, and the bright yellow solid was analysed via ^{1}H-, ^{13}C-NMR (in $CDCl_3$) and IR spectroscopy. The ^{1}H-NMR spectrum reveals two singlets at 6.95 and 5.82 ppm and two singlets at 2.07 and 1.94 ppm. The integral ratio is 2:2:3:3. ^{13}C-NMR shows signals at 182.1, 151.4, 143.1, 137.4, 135.8, 107.4, 13.4 and 11.2 ppm. Successful conversion is indicated by the absence of the signal for the OH groups and a strong carbonyl frequency at 1677 cm^{-1} in the IR spectrum (Figure 13). Aside from that, the broad band from 3200-2000 cm^{-1} corresponding to OH vibrations disappears.

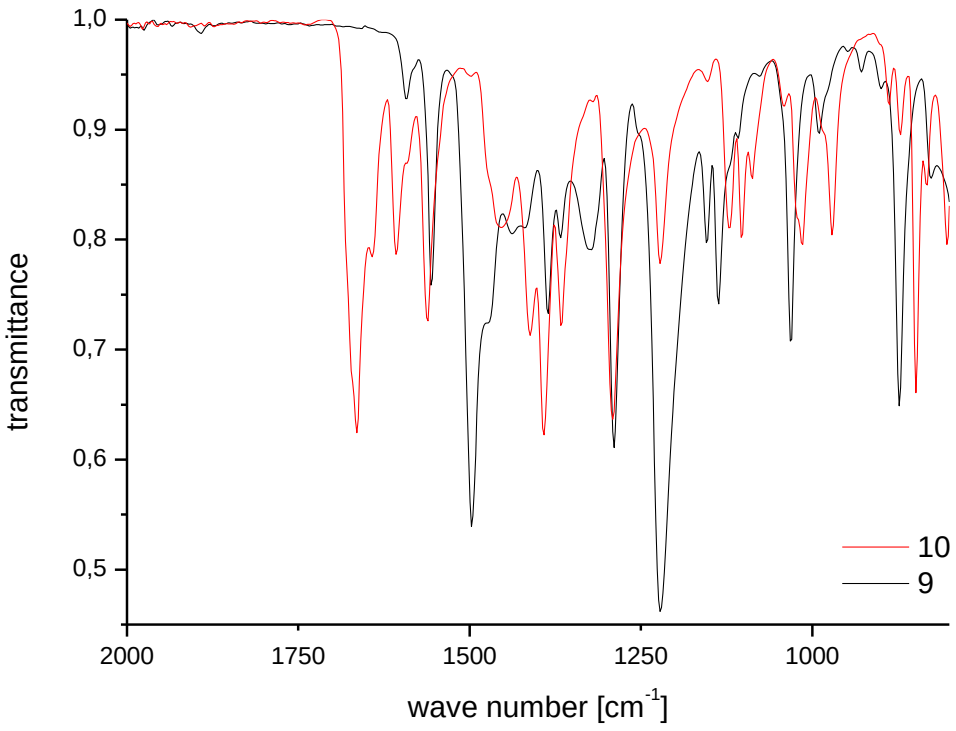

Figure 13 Comparison of ATR-FTIR spectra in the range of 2000-800 cm^{-1} of **9** and **10**

3.2.2 Functionalisation of 1,4-Naphtoquinone

Compared to the Aza-Michael addition to 1,4-benzoquinone, literature research showed that the addition to 1,4-naphtoquinone leads to the monosubstituted 2-adduct and the disubstituted 2,3-adducts as the 5-position is not accessible because of the presence of the aromatic ring.[51,58] Upon addition of pyrazoles (1H-pyrazole, 4-chloropyrazole, 3,5-dimethylpyrazole) to 1,4-naphtoquinone, only the monosubstituted adduct is described in literature.[48,58] Addition of imidazoles (1H-imidazole, 2-methylimidazole) leads selectively to the 2,3-adduct.[51] This is in line with pK_A values as imidazole heterocycles tend to have higher basicity compared to pyrazoles (Table 2). Since the nucleophile 3,5-dimethylpyrazole, which has the highest basicity, also reacts to the monosubstituted product it can be assumed that either 1,4-naphtoquinone is a significantly worse electrophile or that steric factors play a more important role compared to addition to 1,4-benzoquinone.

However, in our group we managed to prepare bis-2,3[pyrazolyl]-dihydroxynaphthalene after a prolonged stirring time of 48 hours as described in Josef Hödl's master thesis indicating that the nucleophilicity is high enough for a second attack.

3.2.3 Functionalisation of Naphthalene Derivatives

Since both 1,4-benzoquinone and 1,4-naphtoquinone can be functionalized with nitrogen-containing heterocycles, it was attempted to directly add nucleophiles to **1.**

The Aza-Michael addition was performed with different nucleophiles including pyrazole, 3,5-dimethylpyrazole, imidazole, phenyl imidazole, methyl imidazole and biimidazole as exemplarily shown in Scheme 17 with pyrazole.

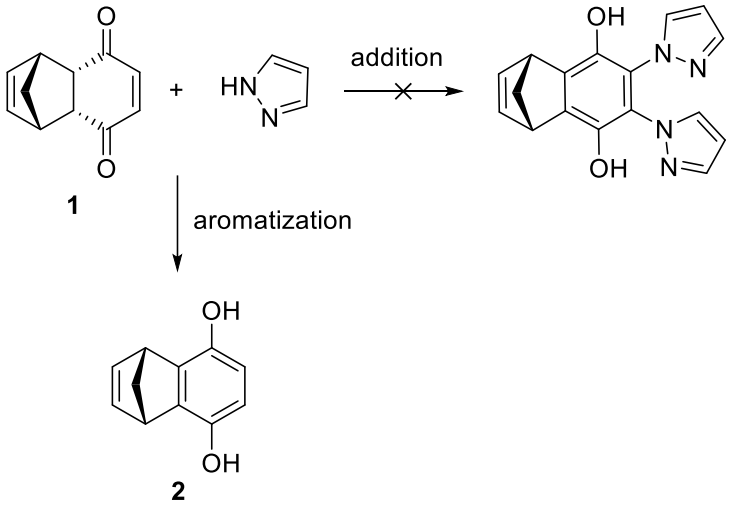

Scheme 17 Aza-Michael Addition of pyrazole to **1** vs. aromatisation of **1** to **2**.

Even after 24 hours of stirring in refluxing 1,4-dioxane, the formation of adducts (mono- or disubstituted) could not be observed. Instead, traces of the aromatic product **2** were detected suggesting that the N-containing heterocycles act as bases and promote aromatisation instead of nucleophilic attack of the double bond. It can be concluded that rearrangement of electrons to make the 3-position more susceptible towards nucleophilic attack (Scheme 14) is hindered because of the attachment of the norbornene moiety.

In a second attempt, the oxidized product **3** was employed in the reaction since the thermodynamically favoured aromatisation is not expected to happen. Nevertheless, reactions were also not satisfactory in this case because the formation of products could not be detected upon addition of phenyl-imidazole, imidazole and pyrazole to **3**. The exception was 3,5-dimethylpyrazole where 10% conversion could be observed after 24 hours of stirring at 115°C in 1,4-dioxane. This is probably due to the high nucleophilicity, but the general failure of this reaction cannot be explained.

Unable to prepare these compounds in high yield, a work-around procedure was elaborated which is depicted in Scheme 18.

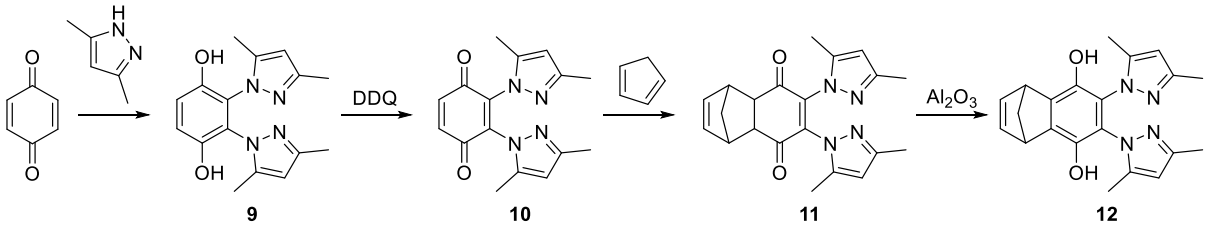

Scheme 18 Syntheses of product **9**, **10**, **11** and **12**

Synthesis was performed for 3,5-dimethylpyrazole as it is the only nucleophile reacting selectively to the 2,3-disubstituted product which is crucial since cyclopentadiene can only be added to an unsubstituted quinone double bond. For the formation of product **11**, **10** was dissolved in methanol and 1.0 equiv. of freshly distilled cyclopentadiene was added. The reaction mixture was stirred for 3.5 hours at 0°C whereupon the solution turned turbid. After evaporation of the solvent, the resulting dark yellow product was analysed via ^{1}H-, ^{13}C- and IR-spectroscopy. The ^{1}H-NMR spectrum in $CDCl_3$ shows singlets at 6.28, 5.80, 3.68 and 3.52 ppm each corresponding to two protons. The methyl groups give rise to a doublet at 2.05-2.00 ppm with a relative intensity of 12 protons. The methylene group of the norbornene moiety resonate at 1.64-1.52 ppm as a multiplet integrating for two protons.

The last step of this synthetic sequence completed with the aromatisation of **11** which was done via suspending **11** and an excess of aluminium oxide in ethyl acetate. The reaction mixture was vigorously stirred overnight. After completion of the reaction has been detected via thin-layer chromatography, the solid was filtered off and washed several times with ethyl acetate and methanol. This washing pro-

cess proved to be very difficult because product **12** strongly stuck to aluminium oxide reducing the yield of this step to 29%.

Subsequent characterisation was done via ^{1}H-, ^{13}C (in $CDCl_3$) and IR-spectroscopy. Successful conversion is indicated by the absence of the carbonyl frequency in the IR spectrum and a broad singlet at 7.84-7.60 ppm corresponding to the phenolic protons in the ^{1}H NMR spectrum. The compound further gives rise to a singlet at 6.83 ppm which can be assigned to the HC=CH protons of the norbornene moiety, a doublet at 5.84 that can be assigned to the CH protons of the pyrazole ring and a singlet at 4.25 ppm that can be assigned to the CH protons of norbornene. The broad singlet at 2.26 ppm can be attributed to both the CH_2 group of norbornene and two CH_3 groups of the pyrazole rings. Finally, the other CH_3 groups of the pyrazole resonate as a multiplet at 1.59-1.56. The integral ratio of the signals is 2:2:2:2:8:6 indicating successful conversion. Compared to compound **11**, the signals of **12** are shifted downfield corresponding to reduced electron density and the formation of an aromatic system that causes a -M effect and de-shielding. NMR spectra of **11** and **12** are displayed in Figure 14 and Figure 15, respectively.

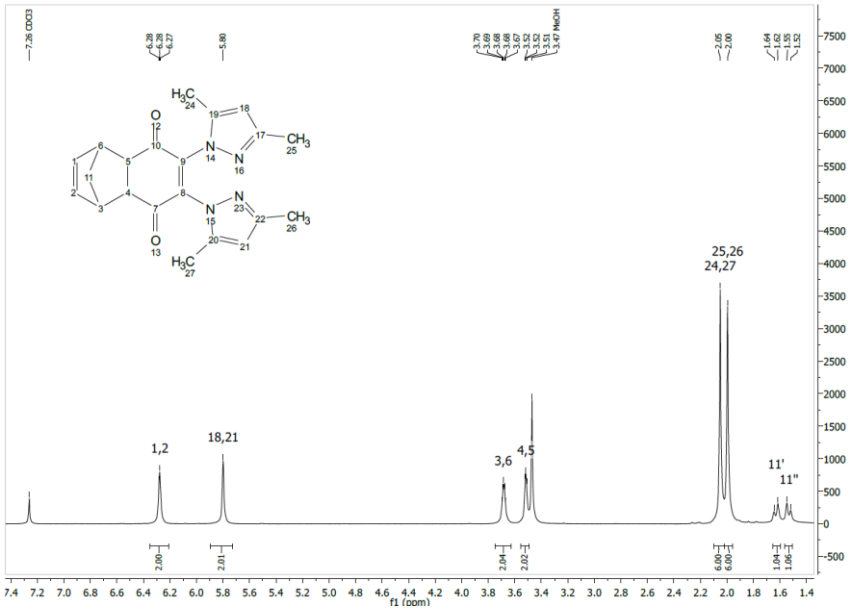

Figure 14 ^{1}H NMR spectrum of **11** *in* $CDCl_3$

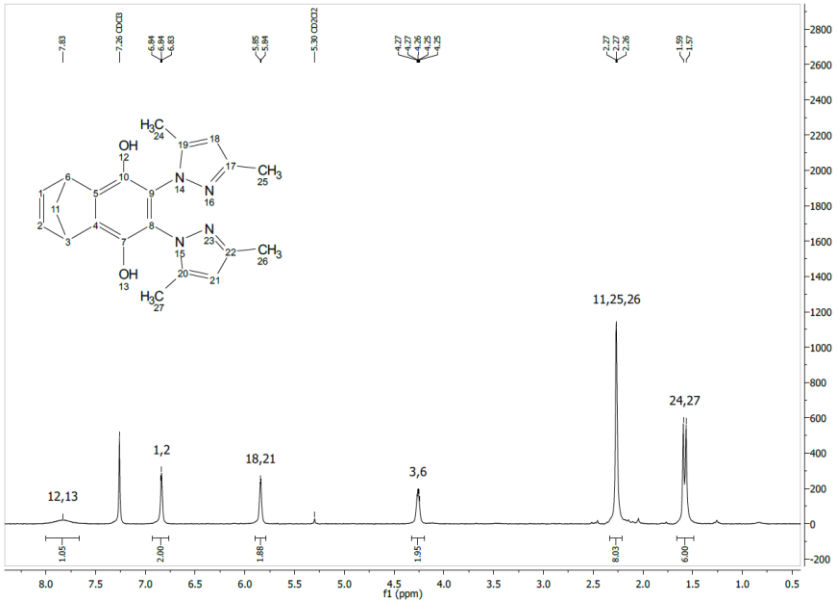

Figure 15 ^{1}H NMR spectrum of **12** in $CDCl_3$

3.3 Polymerisation of Redox-Active Monomers

Ring-opening metathesis polymerisation (ROMP) was performed for all the synthesized monomers as depicted in Table 3. All polymerisations were carried out using standard Schlenk technique and nitrogen as protective gas. As initiators, the third generation Grubbs' catalyst **M31** and the second-generation initiator **M2** provided by Umicore were tested in a ratio of 1:100 (Figure 16)

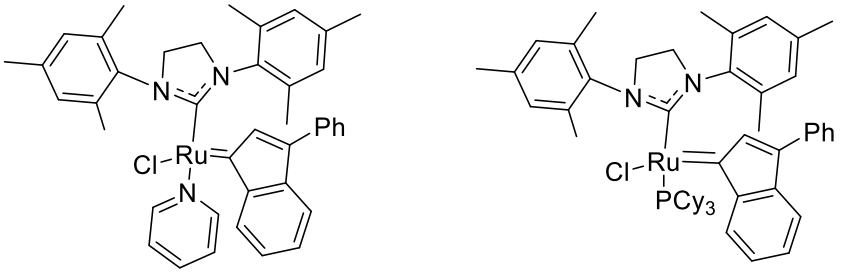

Figure 16 Used initiators for ROMP

Several solvents have been tested, including methylene chloride, tetrahydrofuran and toluene.

The best techniques for each monomer are summarized in Table 3.

Table 3 Attempted polymerisations of monomer **1-8**, M31 initiator (1:100)

Reaction	Successful / Ideal conditions
 **1** **poly1**	**Yes** DCM, room temperature, 18 hours
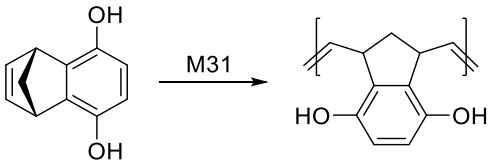 **2** **poly2**	**Yes** THF, room temperature, 6 hours
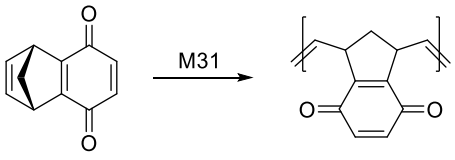 **3** **poly3**	**No conversion observed**

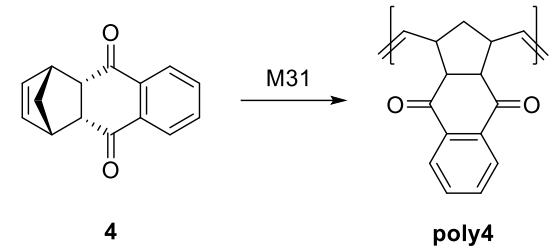

4 **poly4**

Yes
DCM, room temperature, 18 hours

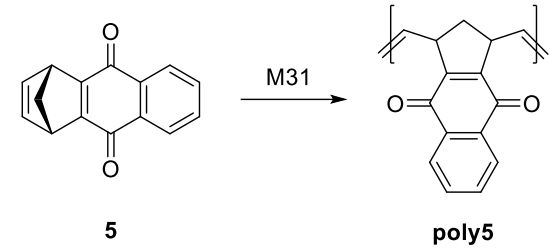

5 **poly5**

No conversion observed

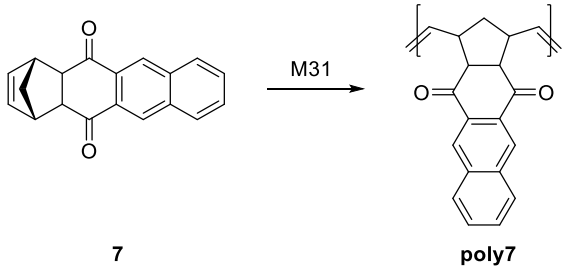

7 **poly7**

Yes
Not fully elaborated, best method:
DCM, room temperature, 96 hours

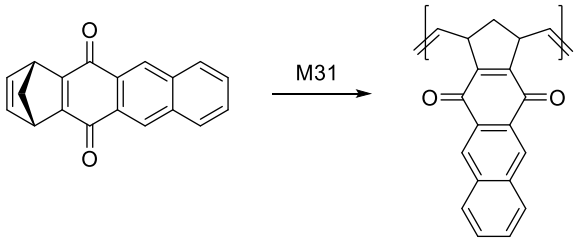

8 **poly8**

No conversion observed

The *endo* isomers of monomer **1** and **4** could successfully be polymerised with the initiator **M31** in methylene chloride and tetrahydrofuran. After completion of the reaction has been detected via ^{1}H NMR spectroscopy, polymers were precipitated from methanol and dried under reduced pressure. **Poly1** is an insoluble, tough material which can hardly be broken whereas **Poly4** was obtained as greyish powder. Experimental details and NMR data are presented in the experimental section.

It is well known, that substituents with oxygen functionalities in *endo* position to the norbornene moiety significantly reduce polymerisation efficiency. This can be explained with chelation of the double bond and oxygen functionality to the metal centre which is only possible for the *endo* isomer.[62] We have shown that full conversion can be achieved when **M31** is used as initiator in a ratio of 1:100 after a stirring time of 24 hours.

Polymerisation of **8** is extremely slow compared to **1** and **4**. As chelation of the metal centre should be equally likely for all *endo* monomers, electronic effects caused by the additional aromatic rings might be the reason for a deceleration of the reaction.

The stiffness of an aromatic ring as in **2** leads to planarity of the monomer disabling coordination of the oxygen atom to the metal centre and subsequent hindrance of polymerisation. Polymerisation was performed in tetrahydrofuran since **2** is not soluble in methylene chloride and full conversion was achieved after 6 hours of stirring.

The norbornadiene containing monomers **3**, **5** and **8** could neither be polymerised with initiator **M31** nor with initiator **M2**. As solvents, methylene chloride, tetrahydrofuran and toluene were tested at room and refluxing temperature. The monomer remained unchanged in all experiments but the ^{1}H NMR spectrum of the attempted polymerisation of **3** revealed traces of monomer **2** indicating that a redox reaction has occurred. Thus, the initiator **M31** might have been oxidized by the monomer rendering it inactive towards polymerisation. After the polymerisation attempts of **5** and **8**, no additional species could be observed in the ^{1}H NMR spectrum.

3.3.1 Post-Synthetic Modifications

Polymers of the oxidized monomers **3**, **5** and **8** would have been most attractive for the fabrication of electrodes because they have a redox-active quinone moiety that is converted into an aromatic system upon reduction.

Therefore, it was tried to synthesize these polymers post-synthetically. **Poly1**, **poly2** and **poly3** were dissolved in 1,4-dioxane and two equivalents of DDQ were added. After 18 hours of stirring at reflux, a poorly soluble black solid formed. In the ^{1}H-NMR spectrum, peaks that could be attributed to polymers could not be detected. Instead, either a paramagnetic material could have formed, or partial oxidation of the polymer could have led to the formation of insoluble quinhydrone like species.

3.3.2 Polymerisation of N-functionalized Naphthalene Derivatives

Next, polymerisation of **11** and **12** was attempted with the same conditions that have been applied for the polymerisation of **1** and **2**. For these reactions, a Schlenk tube was charged with the educt and tetrahydrofuran as solvent. Nitrogen was bubbled through the solution to get rid of oxygen. Grubbs' third generation initiator **M31** in a molar ratio of 1:50 (I:M) was dissolved in a small amount of the solvent and added to the monomer. Upon addition, the light yellow-reddish monomer solution immediately turned dark green. Nevertheless, ^{1}H-NMR spectroscopy didn't show any conversion in both cases, even after 22 hours of stirring in refluxing tetrahydrofuran.

In a second attempt, the second-generation Grubbs' catalyst **M2** in combination with toluene was tested but also this catalyst was not able to initiate polymerisation of the monomers although a higher reaction temperature could be applied.

The failure of these polymerisations can probably be assigned to binding of the Ru centre of the catalyst to the ligand forming a stable complex inactive as catalyst.

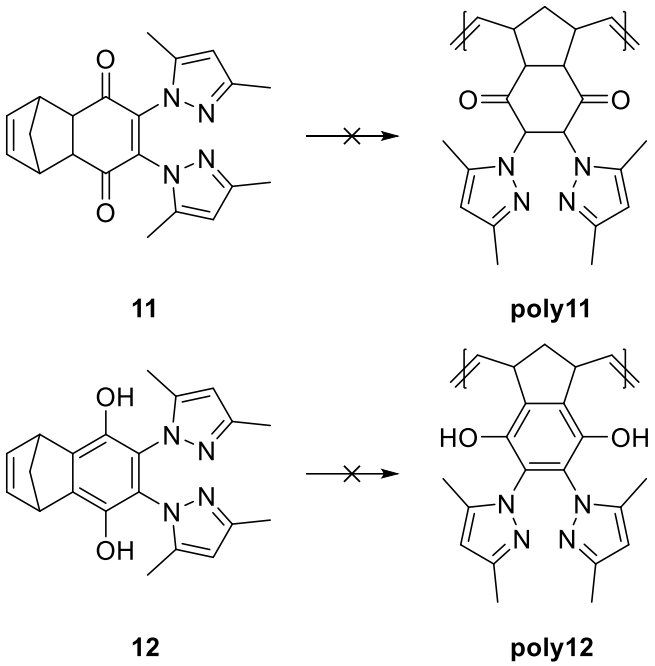

Scheme 19 Attempted polymerisations of **11** and **12** in tetrahydrofuran with **M31** (1:50) as initiator

3.4 Metal Complexes with Redox-Active Ligands

Due to the bonding affinity of the ruthenium atom to the nitrogen atoms of the monomers, we tried to use them as ligands for other metal ions as well. Both ligands containing 3,5-dimethylpyrazole moieties (**9**, **12**) are capable of coordinating to metal ions through their nitrogen atoms. It was decided to use only the reduced hydroquinone forms because upon deprotonation of the hydroxy groups an anionic ligand is provided which is supposed to chelate to metal ions through the N and O atoms.

3.4.1 Metal Complexes with 2,3-bis(3,5-dimethylpyrazole)hydroquinone Ligands

Literature research revealed that there are many metal complexes and coordination polymers known that are based on 2,5-bis(1H-pyrazole)hydroquinone.[58,63–66] Complexes containing a 2,3-bis(3,5-dimethylpyrazole)hydroquinone are much rarer, probably because of increased steric interaction between the pyrazole rings and the metal centre[54,67]. The ones that are known in literature are shown in Figure 17.

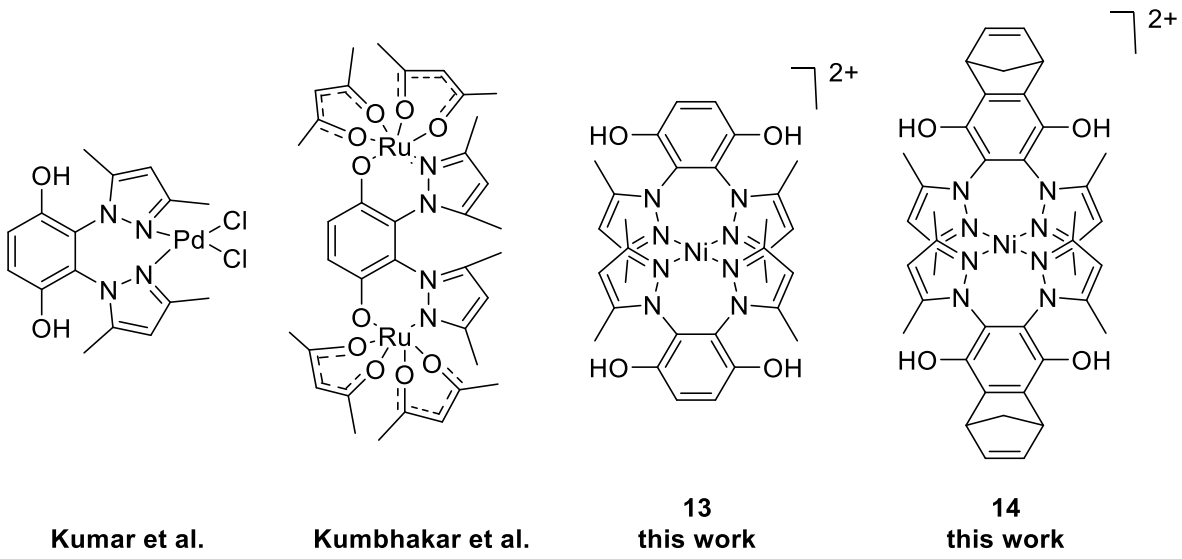

Figure 17 Metal complexes containing the 2,3-bis(3,5-dimethylpyrazole)hydroquinone ligand

The palladium complex by Kumar and co-workers[54] was prepared via the reaction of the ligand with $Pd(MeCN)_2Cl_2$ in refluxing acetonitrile and exclusion of light. The nitrogen atoms of the pyrazole moieties chelate to the palladium atom forming a seven-membered ring. Two chloride ions satisfy the remaining coordination sites.

The ruthenium atoms in the complex that has been prepared by Khumbarkar and co-workers[67] coordinates to the ligand through N and O^- donors forming a six-membered ring each. The remaining coordination sites are satisfied through the coordination of two acetylacetonate groups. The compound was prepared by adding $Ru(acac)_2(CH_3CN)_2$ and triethylamine to the ligand. The latter acts as base and

deprotonates the phenolic group enabling coordination to the metal centre. This example might also show why the ruthenium-based initiators are not active in polymerisation of monomers **11** and **12**.

During this work, ligand **9** was reacted with various metal salts including nickel nitrate, nickel acetate copper nitrate, copper acetate, zinc acetate, zinc nitrate and iron chloride. A turquoise crystalline solid, was only obtained after the reaction of nickel nitrate and the ligand. The other combinations yielded either a brownish precipitate or for the case of nickel acetate a clear red solution.

For the synthesis of compound **13**, both nickel nitrate (1.0 equiv.) and the ligand (1.0 equiv.) were dissolved, respectively suspended in methanol. After combination of the solutions, the resulting clear blue solution was left to stand overnight at 40°C which yielded crystals suitable for single crystal x-ray diffraction analysis (Figure 18).

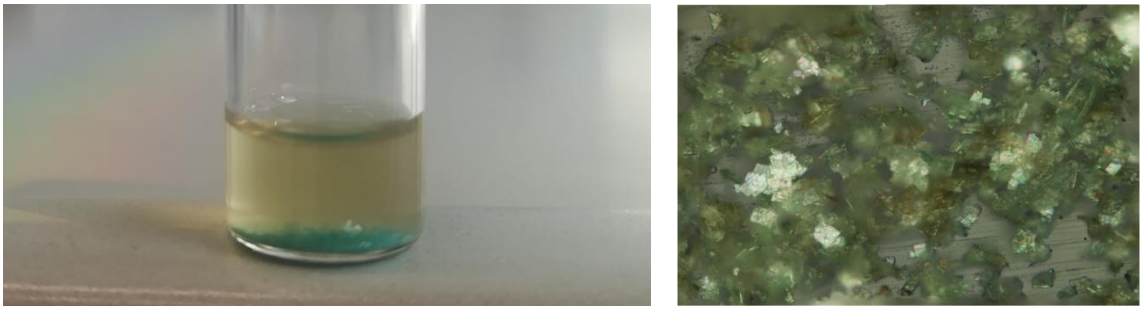

Figure 18 Crystals suitable for SC-XRD analysis of compound **13**

Single crystal X-ray diffraction analysis

The unit cell contains 16 nickel complexes that are made up of three different geometries (i.e. slightly different bond lengths and angles). The unit cell is displayed Figure 19 indicating that the nickel atom is octahedrally coordinated.

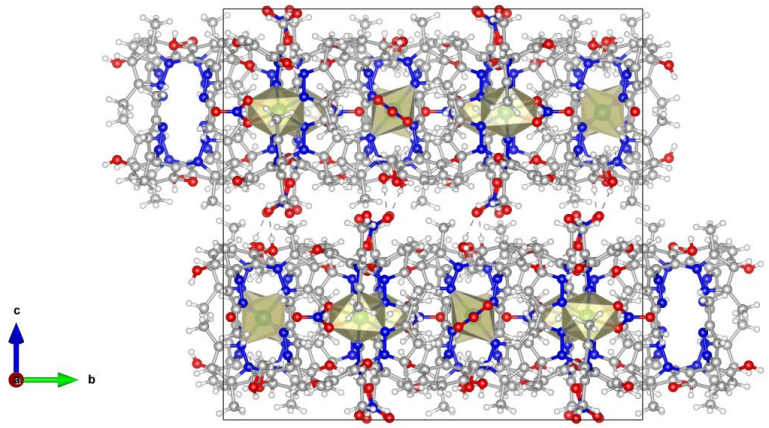

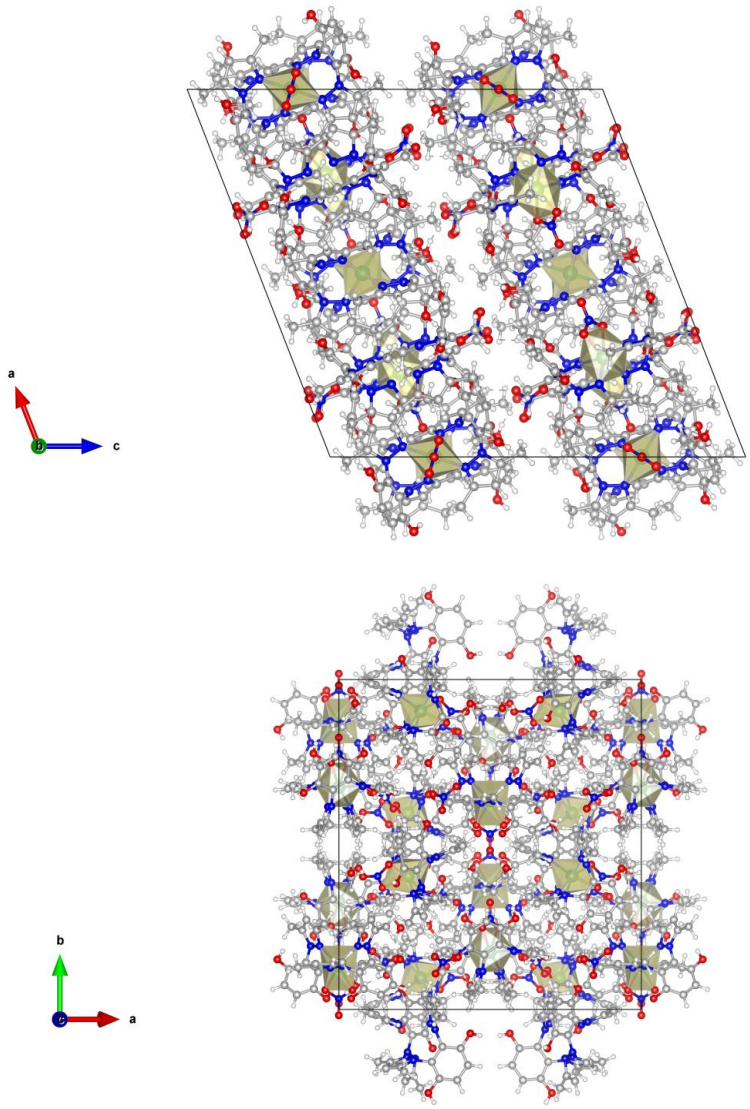

Figure 19 Unit cell of **13**, plane a-c

The compound with a molecular formula of $C_{32}H_{36}N_9NiO_7 \cdot NO_3 \cdot CH_4O$ (**13**, Figure 20) corresponding to a molecular weight of 811.44 g/mol crystallizes in the monoclinic space group C2/c. Crystallographic data are displayed in Table 4. Nickel can be considered as Ni^{II} with an anionic nitrate ligand coordinated to the metal as well as two neutral pyrazole based ligands. Charge neutrality is guaranteed by a second nitrate acting as counter ion. One methanol molecule per metal complex is also part of the crystal structure. The distance between the nitrogen atoms and the metal centre are 2.087 Å (Ni-N16) and 2.110 Å (Ni-N14), respectively (Figure 20). The bond length between the coordinated nitrate and the nickel is 2.1412 Å. Considering the obtained structure, the reaction should preferably be performed with two equivalents of ligand.

Table 4 Crystallographic data of **13**

Compound	**13**
Formula	$C_{32}H_{36}N_9NiO_7 \cdot NO_3 \cdot CH_4O$
Fw (g mol^{-1})	811.44
a (Å)	24.8268(15)
b (Å)	24.8382(15)
c (Å)	26.3874(15)
α (°)	90
β (°)	111.464(3)
γ (°)	90
V ($Å^3$)	15143.4 (16)
Z	16
Crystal size (mm)	0.04 × 0.04 × 0.01
Crystal habit	Plate, blue
Crystal system	Monoclinic
Space group	*C*2/*c*
d_{calc} (mg/m^{-3})	1.424

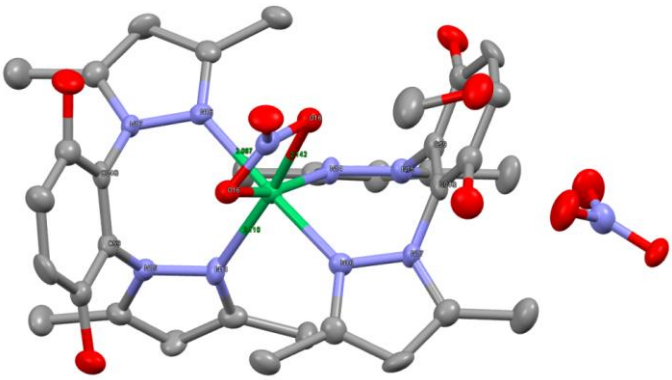

Figure 20 Crystal structure of **13**, hydrogen atoms omitted for clarity

The metal centre is symmetrically coordinated by two ligands with equal bond lengths as indicated by the labelling. The pyrazole rings are rotated relative to each other as can be seen in Figure 21 and Table 5.

Table 5 Torsional angles and angles characterizing the relative position of the pyrazole rings in complex **13**

Atoms	Angle [°]
N15-N14-Ni-N16	139,18
N15-N14-Ni-N14	-126,08
N15-N14-Ni-N16	-34.85
N16-Ni-N16-N17	-96.19
N17-N16-Ni-N14	129.83
N17-N16-Ni-N14	37.61
N16-Ni-N16	171.73
N14-Ni-N14	92.14

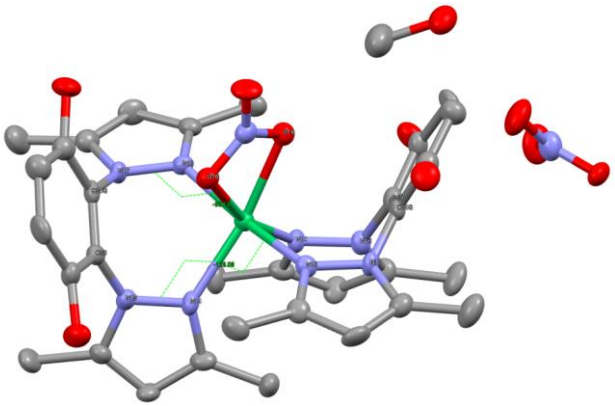

Figure 21 Torsional angles around the nickel centre for compound **13**

IR spectroscopy

A comparison of the IR spectra of the ligand and the metal complex is displayed in Figure 22. The bands at 1497 and 1222 cm^{-1} of the ligand are missing in the spectrum of the complex. New bands appear at 3241, 1420 and 808 cm^{-1}. The question remains whether the quinone moiety of the ligand is still in the reduced form, the hydroquinone, or if oxidation to the corresponding benzoquinone happened during the crystallization process. This assumption is conceivable as the ligand is sensitive to air[58], especially under the presence of a redox-active metal. However, this can be excluded as the IR spectrum does not show any carbonyl bands that can be associated with the oxidized form and the bond lengths of quinone moiety from SC-XRD clearly correspond to an aromatic compound.

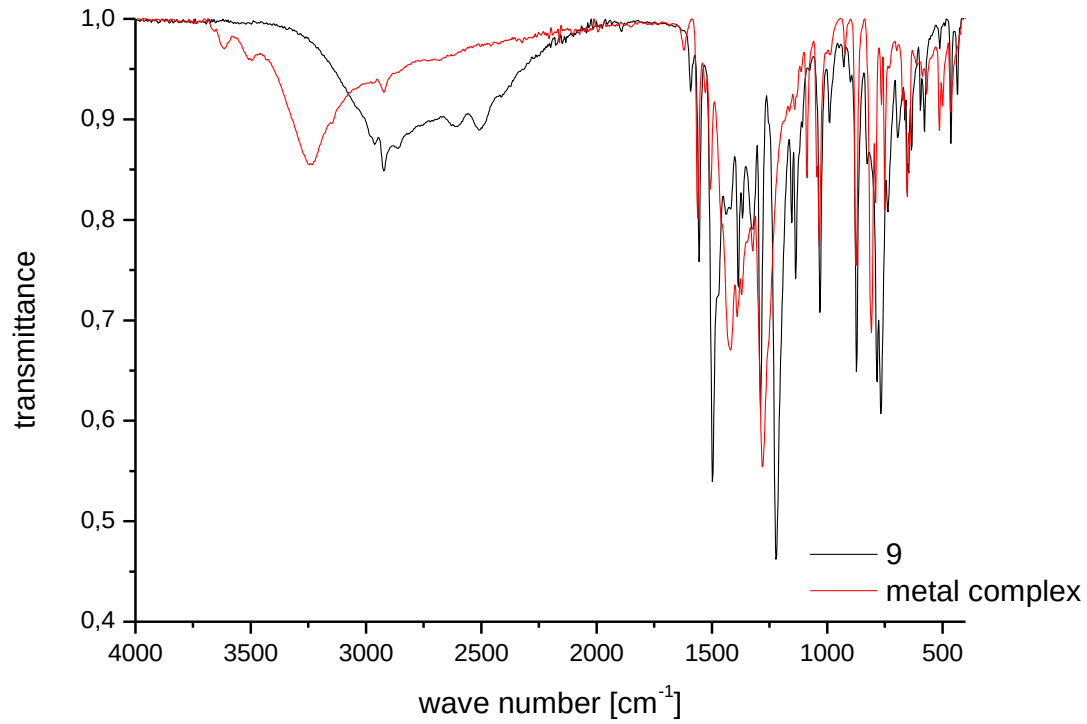

Figure 22 Comparison of ATR-FTIR spectra of the ligand **9** and the corresponding nickel complex

NMR spectroscopy

The complex is soluble in dimethyl sulfoxide as well as large volumina of methanol allowing investigation via ^{1}H NMR spectroscopy. The peaks of ligand **9** are not shifted upon coordination of the nickel atom.

DFT calculations

The crystal structure of the complex was used as input for a computational optimisation to investigate the minimum structure of this compound. Pre-optimisation using a force-field calculation was done using Avogadro before full optimization of the structure on def2-SVPD/PBE D3 level. Single-point energy of this optimised structure was calculated with the combination def2-TZVPPD/B3-LYP D3. The six-fold coordination of the nickel centre is replaced by an energetically favoured square planar coordination. Thus, two Ni-N bonds (Ni-N14, see Figure 20) have to break to allow 4-fold coordination of the nickel atom by two oxygen atoms of the nitrate and two nitrogen atoms of the pyrazole heterocycles. The minimum structure is displayed in Figure 23.

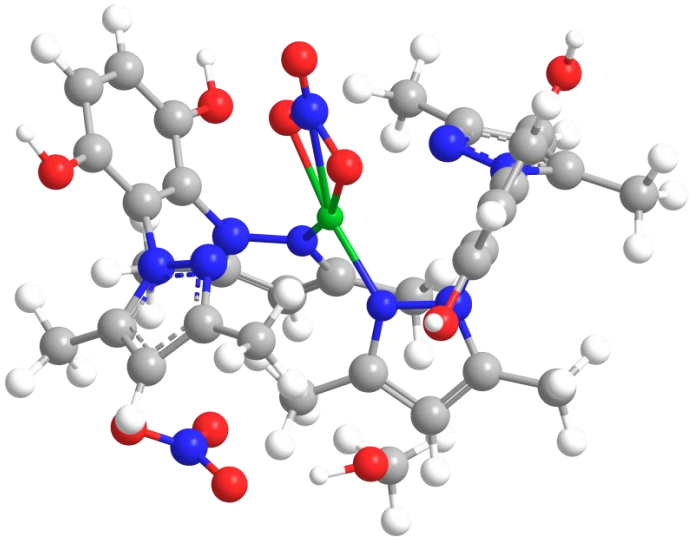

Figure 23 DFT optimized structure of complex **13**

Further considerations

As the oxygen atoms of the quinone moiety do not take part in coordination to the metal centre, a metal complex is formed instead of a coordination polymer. This preferential formation can surely be attributed to the steric clash of the methyl groups forcing non-planar geometry but may also be due to the absence of a base during the reaction. Addition of a base would have deprotonated the phenolic group facilitating coordination to a metal centre through the oxygen atoms.

In a later experiment, this deprotonation was attempted using two equivalents of sodium hydroxide as a base which lead to a colour change of the solution to dark brown and the formation of an insoluble black powder which could not be analysed via ^{1}H-NMR spectroscopy and SC-XRD analysis. Literature research revealed that 2,5(1H-pyrazole)hydroquinone is oxidized spontaneously to the corresponding quinhydrone complex (Figure 24) upon standing in methanol at ambient atmosphere.[58] This pronounced sensitivity of quinones towards oxygen and light as well as the characteristic appearance of the formed solid leads to the assumption that this reaction also happened here.

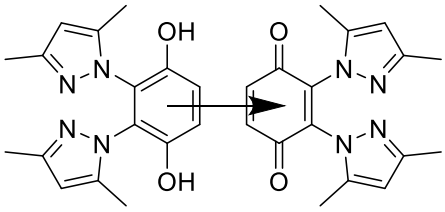

Figure 24 Postulated formation of a quinhydrone complex of ligand 9

Formation of the quinhydrone like adducts can possibly be hindered via in-situ deprotonation of the ligand before the addition of the metal salt which avoids long stirring times under light and ambient atmosphere.

3.4.2 Nickel Complexes with Ligand 12

As crystals suitable for SC-XRD analysis could only be grown from 2,3-bis(3,5-dimethylpyrazole)hydroquinone and nickel nitrate, only this metal salt was used in the reaction with 6,7-bis(3,5-dimethyl-1H-pyrazol-1-yl)-1,4-dihydro-1,4-methanonaphthalene-5,8-diol (**12**).

Ligand **12 (**1.0 equiv.) and nickel nitrate (1.0 equiv.) were dissolved in methanol and combined. After combination, a clear green solution was formed which was heated to 40°C overnight whereupon orange crystals suitable for SC-XRD analysis were obtained (Figure 25)

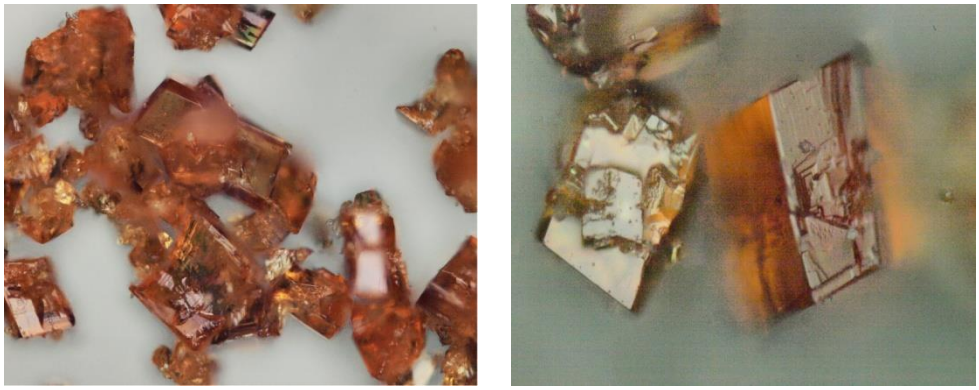

Figure 25 Crystals suitable for SC-XRD of 14

Single crystal X-ray diffraction analysis

The unit cell is displayed in Figure 26 and clearly shows square-planar coordination of the nickel atom without a nitrate ion directly bonded to the metal centre. The unit cell is comprised of two metal complexes with the same geometry.

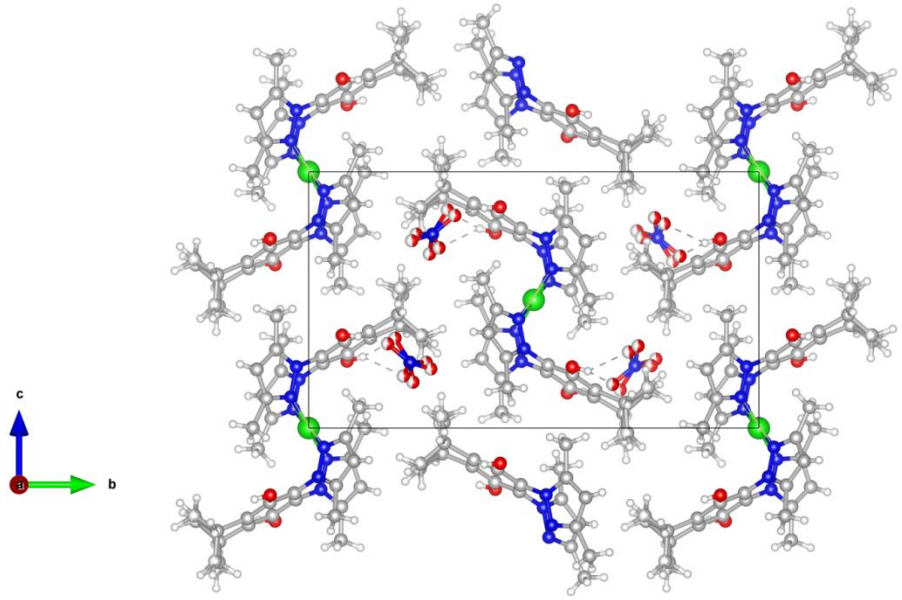

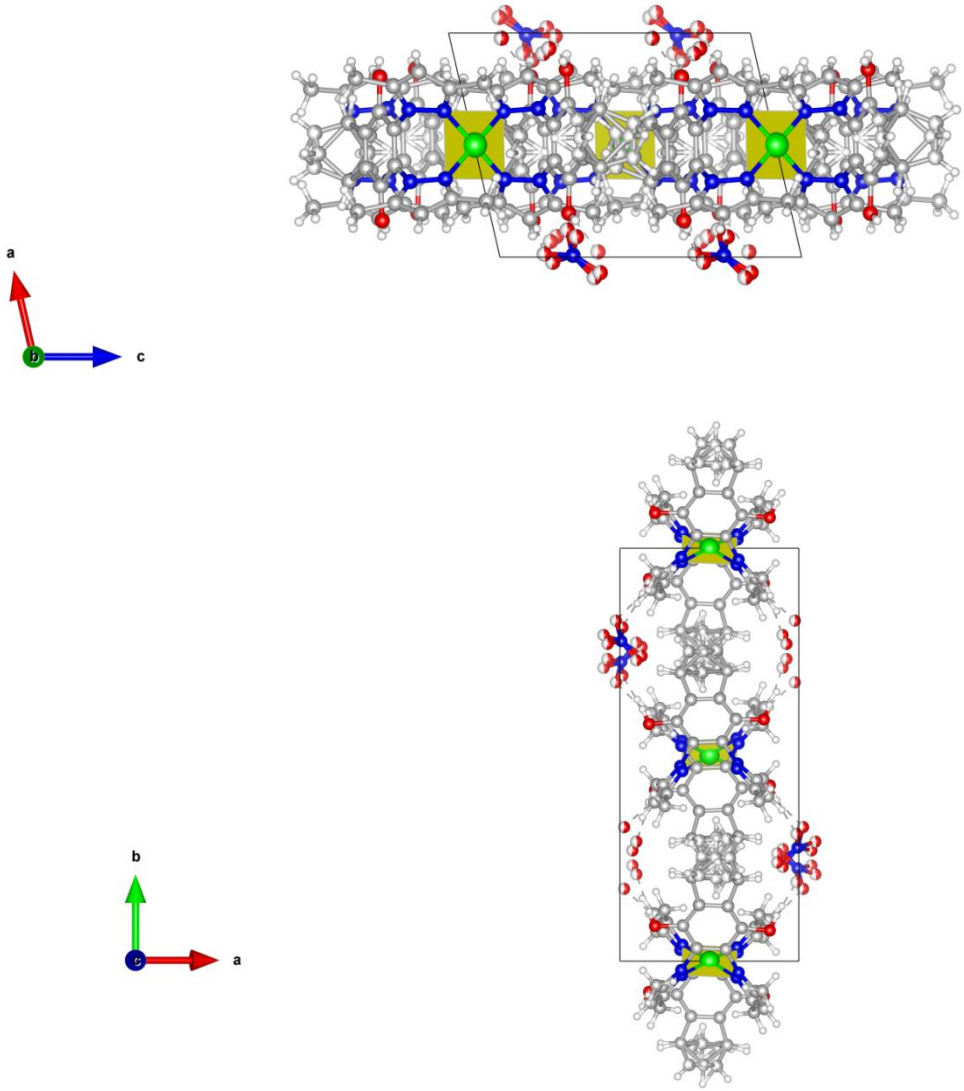

Figure 26 Unit cell of **14**, plane a-c

The molecular structure is displayed in Figure 27 and crystallographic data are presented in Table 6. The unit cell consists of two metal complexes, each of them coordinated by two neutral pyrazole based ligands. Charge of Ni^{2+} is compensated by two nitrate counter ions as can be seen in the unit cell. These nitrate ions and the norbornene moiety of one pyrazole ligand are disordered, each of them having two different orientations. Proper convergence of refinement was possibly not achieved because of poor crystal quality or insufficient cooling during measurement.

In contrast to compound **13**, the distance of the pyrazole rings to the nickel centre is 1.90 Å for both ligands. Square-planar geometry is characterised by an angle of 180° of both N1-Ni-N1 and N3-Ni-N3 and equal bond lengths between the nitrogen atoms and the metal centre. The pyrazole rings are symmetrically arranged and not rotated towards each other like in complex **13** (Figure 21).

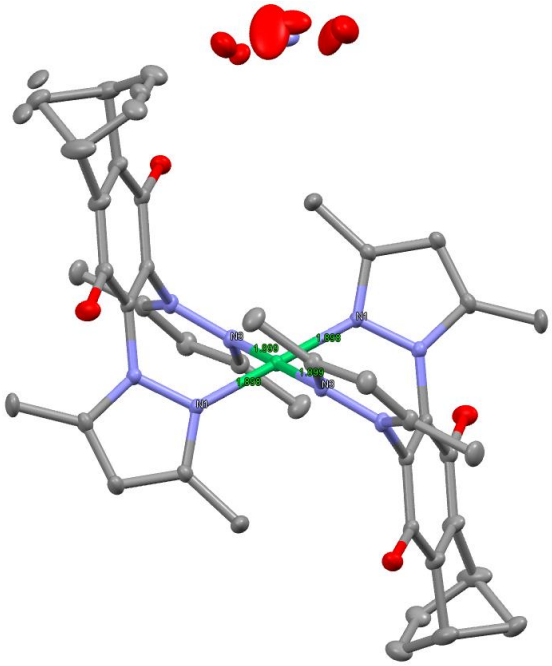

Figure 27 Molecular structure of **14**

Table 6 Crystallographic data of **14**

Compound	**14**
Formula	$C_{42}H_{44}N_8NiO_4 \cdot 2(NO_3)$
Fw (g mol^{-1})	907.58
a (Å)	8.9084 (5) Å
b (Å)	20.0382 (13) Å
c (Å)	11.6827 (7) Å
α (°)	90
β (°)	102.900 (3)
γ (°)	90
V (Å^3)	2032.8 (2)
Z	2
Crystal size (mm)	0.07 × 0.07 × 0.07
Crystal habit	Block, orange
Crystal system	Monoclinic
Space group	$P2_1/c$
d_{calc} (mg/m^{-3})	1.483

IR spectroscopy

In Figure 28 the IR spectra of the metal complex and the corresponding ligand are compared. The broad band at 3460-2683 which can be assigned to the OH group is still present in the spectrum of the complex indicating that coordination does not occur via the oxygen atoms.

The bands of the free ligand are shifted to lower frequencies upon coordination which is shown in

Table 7. Furthermore, a new band appears at 1264 cm^{-1}.

Table 7 Comparison of IR bands of ligand **12** and metal complex **14**

Ligand 12	Metal complex 14
1473 cm^{-1}	1416 cm^{-1}
1308 cm^{-1}	1297 cm^{-1}
1036 cm^{-1}	1026 cm^{-1}
867 cm^{-1}	818 cm^{-1}
690 cm^{-1}	639 cm^{-1}
773 cm^{-1}	743 cm^{-1}

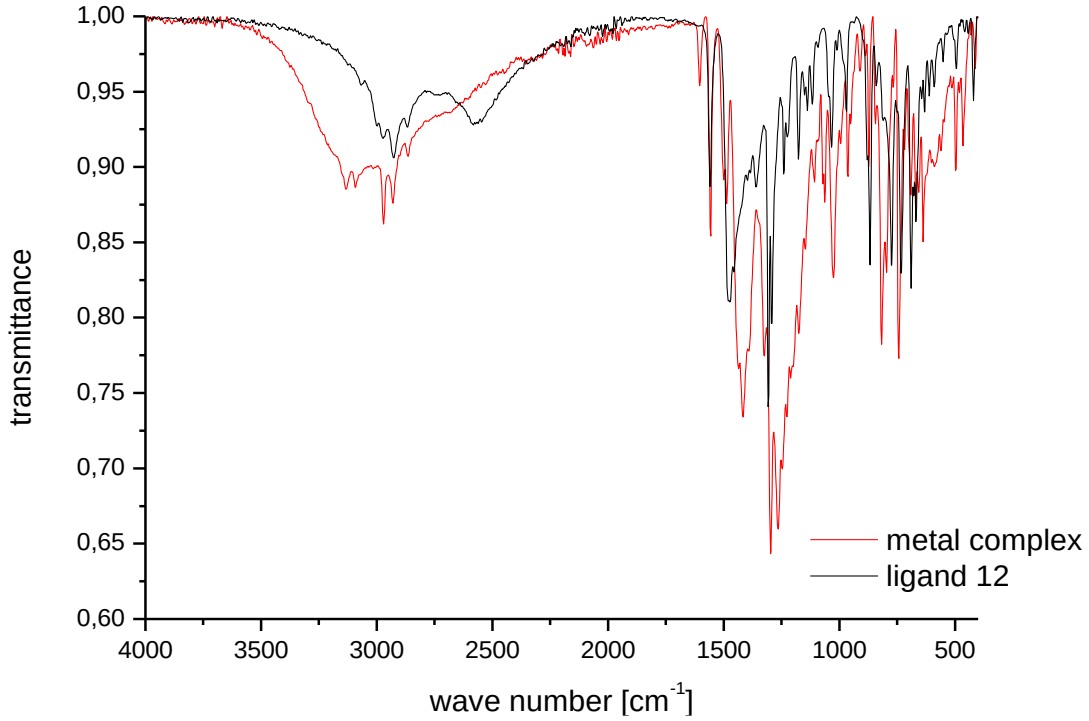

Figure 28 Comparison of ATR-FTIR spectra of metal complex **14** and ligand **12**

DFT calculations

DFT optimization of the crystal structure did not lead to any significant changes of the geometry as in complex **13**. Square planar coordination of the nickel centre seems to be the thermodynamically favoured coordination mode.

3.5 Coordination Polymers

As the combination of metal salts with ligands **5** and **8** only yielded discrete metal complexes, (±)*endo*,*exo*-5-norbornene-2,3-dicarboxylic acid (Figure 29) was chosen as linker to explore the formation of coordination polymers. Advantages of this linker are its commercial availability, the existence of two carboxylic groups capable of coordination to a metal ion and the presence of a norbornene moiety which can potentially be functionalized or cross-linked via ring-opening metathesis polymerisation. Besides, it is sterically less bulky since the quinone and pyrazole moieties are missing enhancing the formation of polymers instead of complexes.

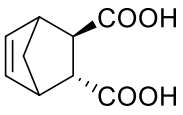

Figure 29 (±)*endo*,*exo*-5-norbornene-2,3-dicarboxylic acid (NDC)

The isomeric form, of this ligand, cis-5-norbornene-endo-2,3-dicarboxylic acid, is well known to act as ligand in various metal complexes containing manganese[68,69], cobalt[69] and nickel[69]. It can also be used as bidentate ligand to connect adjacent metal ions to develop dimers of cadmium[70,71], manganese[72] and copper[73]. Hydrogen bonds can extend a dinuclear structure into a 1D or 3D polymeric network as reported for copper[74,75], manganese[75] and nickel[74].

Networks which have not been formed via weak interactions like π-π or hydrogen bonding have been reported for cadmium where the linker forms 1D chains with metal ions which are then connected via 4,4′-bipy ligands to form a 3D network.[74] Polymers can also be formed for manganese, zinc or lead when 1,3-bis(pyrazol-1'-yl)propane (bpp)[76,77], phenanthroline (phen)[78, 79,80] or 1-methylimidazole (1-MeIm)[81] ligands are added.

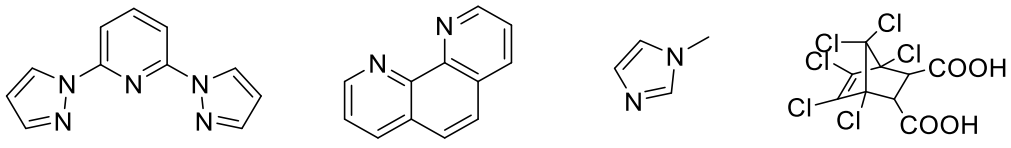

Figure 30 Commonly used ligands to promote formation of a multidimensional coordination polymer

Polymeric materials containing only the linker and metal ions are reported for cadmium where chlorendic acid (HET)[82] was used as linker. The structure features a 1D chain which is further connected by hydrogen bonds and Cl-Cl halogen bonds to form a 3D network. The molecular structure consists of two Cd ions unsymmetrically coordinated by two HET ligands, three coordinated water molecules and two uncoordinated DMF molecules.

In this work it was tried to extend the research on coordination polymers based only on (±)*endo,exo*-5-norbornene-2,3-dicarboxylic acid (NDC) and metal ions. All reactions were performed in water or methanol to avoid expensive and toxic solvents like DMF, DEF or NMP conventionally used in the fabrication of metal-organic frameworks.[83] In contrast to solvothermal methods, where high temperatures for MOF formation are necessary, we performed reactions either at room temperature or at maximum 80°C making the whole process environmentally friendly and economically more attractive.

3.5.1 The Linker – Acid vs. Salt

Basic salts like carbonates, acetates, hydroxides or oxides can be directly combined with NDC in water. These salts are formed upon neutralization of a strong base with a weak acid. When they get hydrolysed, the pH of the corresponding solution is basic.[84] Consequently, the linker gets deprotonated and is able to coordinate to the metal ion.

The poor solubility of NDC in water and the necessity of a base like NaOH, Na_2CO_3 or Et_3N upon combination of NDC with a neutral or acidic salt (sulphates or nitrates) make the direct combination of NDC with metal salts unattractive. Alternatively, the disodium salt of NDC can be used. This "linker-salt approach" was introduced by Sánchez-Sánchez et al. who used alkaline-based salts of organic linkers instead of the protonated form enabling "green" synthesis in water at room temperature.[85,86]

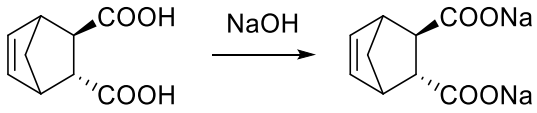

Scheme 20 Deprotonation of NDC with NaOH to yield NDC-Na

The disodium salt of (±)*endo,exo*-5-norbornene-2,3-dicarboxylic acid (NDC-Na) was synthesized via a simple deprotonation reaction in water as displayed in Scheme 20. NDC was suspended in water, 2.02 equivalents of sodium hydroxide were added, and the mixture was stirred overnight at 80°C. After drying at 80°C, the product was obtained quantitatively and used without further purification. It was analysed via ^{1}H- NMR spectroscopy in D_2O. In the IR spectrum of NDC-Na, the broad band at 3200-2500 cm-1 indicative for the COOH group of the acid disappears and the carbonyl vibration is shifted (Figure 31).

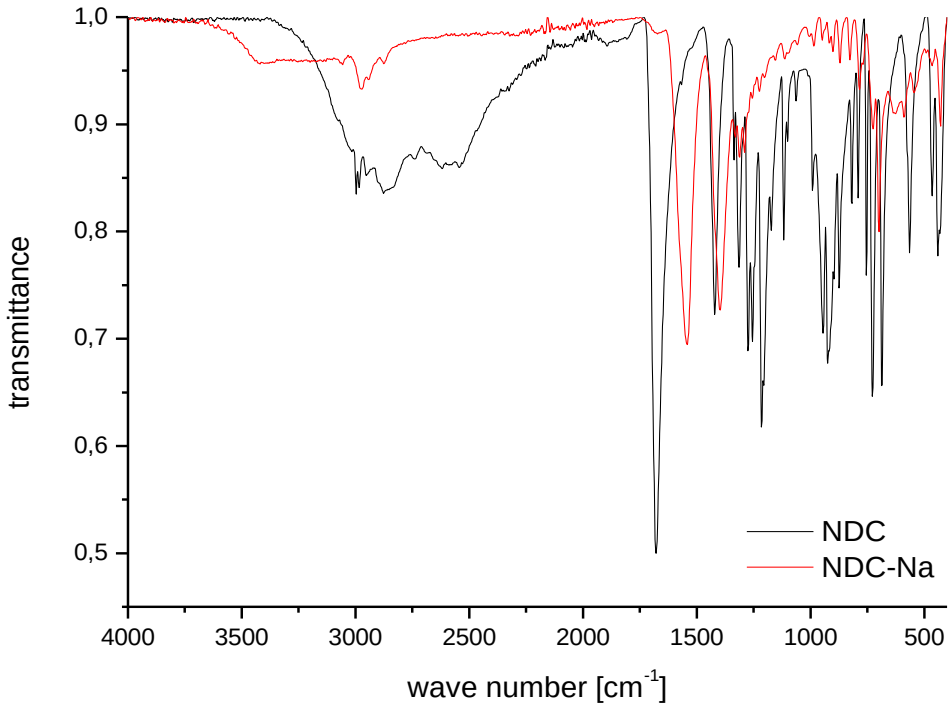

Figure 31 Comparison of ATR-FTIR spectra of NDC and NDC-Na

All syntheses of coordination polymers were attempted both with NDC as well as NDC-Na as linker

3.5.2 Zinc Containing Coordination Polymer (15)

Zinc containing coordination polymers are formed upon combination of NDC and either zinc acetate or zinc oxide in a molar ratio of 3:4 (linker to metal). WAXS analysis revealed that the same product formed upon combination of NDC-Na and zinc nitrate in the same molar ratio (Figure 32)

The coordination polymer formed in each case precipitated from the solution as a fine, white powder and was left to stand at 80°C. The product is insoluble in water, methanol, methylene chloride, isopropanol, methylene chloride and toluene. Interestingly, the product floats on water.

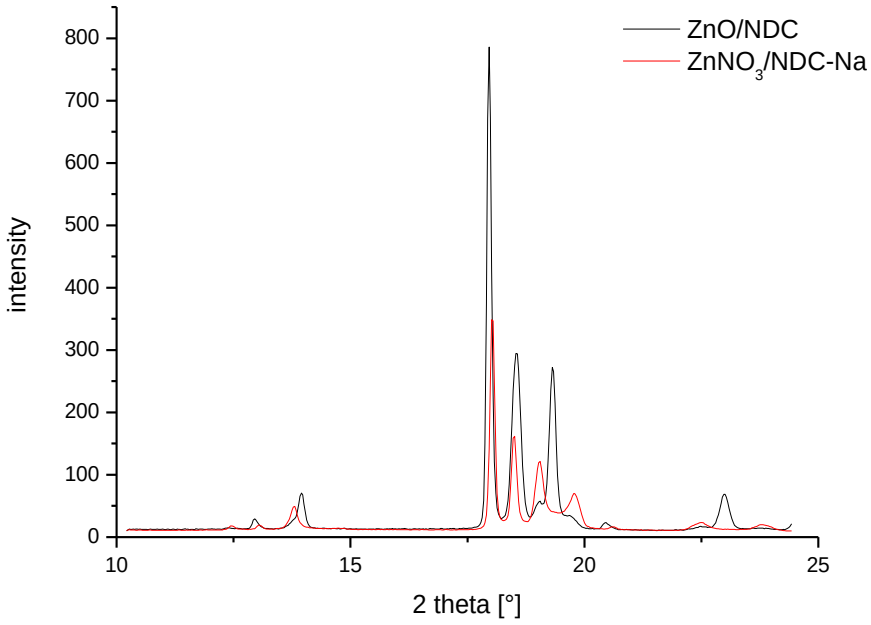

Figure 32 WAXS analysis of ZnO-NDC (black) and $ZnNO_3$-NDC-Na (red)

SC-XRD measurements could not be performed because of the small size of the crystals. Different methods have been tried to grow bigger crystals which were all unsuccessful. Duration of storage at 80°C (two days or two weeks) does not influence the size or properties of the crystals. Addition of 1 mL of a Tris-HCl buffer[VI] solution reduced the pH from 10-12 to 7-8 but this change did not have any effects on the crystal size. Increasing the linker to metal ratio to 2:1 also lead to the formation of the coordination polymer whereby the excess ligand remained in solution. However, coordination polymers did not form upon further increasing this ratio to 10:1, and only the linker could be detected in the IR spectrum. It was also tried to change the amount of solvent, in this case water, during the reaction. Both, more and less solvent did not influence the size of the crystals. Lastly, the reaction was performed in an Anton Paar Monowave 50 for 14 hours at 160°C without changing the properties of the product.

In the IR spectrum characteristic bands appear at 2975, 1610, 1522, 1430, 783, 718 cm^{-1}.

BET surface analysis revealed a surface of 25.5 m^2/g.

Thermal stability was investigated via **TGA/DSC analysis** revealed one mass loss step of 64% at 400°C.

[VI] Tris buffer: 100 mM tris(hydroxymethyl)aminomethane in water has a pkA of 8.07, implying that the buffer has a pH range between 7.0 and 9.0. Tris hydrochloride; MSDS No. PHG0002; Sigma-Aldrich Handels GmbH: Vienna, Austria, Aug 19, 2019.

3.5.3 Manganese Containing Coordination Polymer (16)

Thin plates of coordination polymer **16** can be prepared via combination of NDC and manganese carbonate in a molar ratio of 1:1, 1:1.33, 1:2, or 1:5. The amount of metal salt determines the shape of the plates – a large excess of metal salt leads to the formation of a flat and stable plate, the ratios 1:1.33 and 1:2 lead to the formation of a curved one and combination of the linker and the metal salt in a ratio of 1:1 produces small pieces.

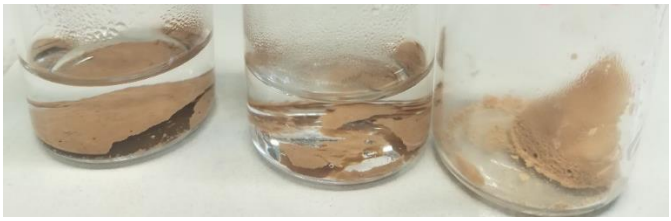

Figure 33 Formation of plates upon combination of NDC and manganese carbonate in different ratios (linker:metal) – left: 1:5, middle: 1:1, right: 1:1.33

The plates form spontaneously after combination of a solution of NDC with solid manganese carbonate and heating up to 80°C overnight without stirring.

It was found that the pH is crucial for the formation of the plates. A solution of 100 mg of NDC in 4 ml of water has a pH of 3 which is necessary to break manganese carbonate and enable coordination of the carboxylate moieties of the linker to the metal ion. Thus, formation of the plates was not possible upon addition of manganese carbonate to buffered solutions or solutions of NDC-Na (pH=8).

If the metal salt is changed to manganese sulphate and combined with NDC-Na, small white crystals form upon storage in an oven at 80°C for 2 days. However, WAXS analysis revealed that the crystal structure of all manganese containing polymers is the same (Figure 34).

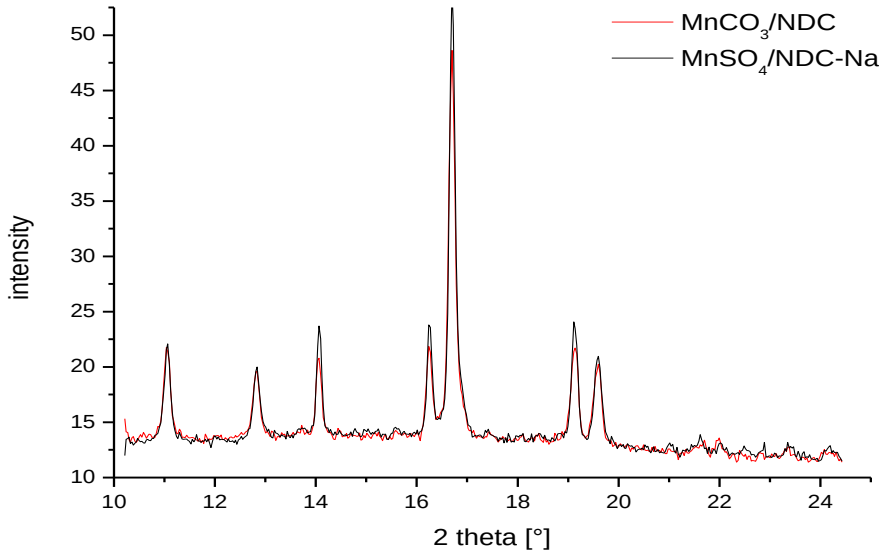

Figure 34 WAXS spectrum of $MnCO_3$/NDC (red) and $MnSO_4$/NDC-Na (black)

The product was characterised via **IR spectroscopy**, where characteristic bands appear at 1624, 1563 and 1400 cm^{-1}.

BET surface analysis revealed that the compound has a surface of 14.3 m^2/g. However, the low porosity is indicative of a non-porous compound and the surface can be considered as the outer surface of the crystal grains. The adsorption isotherms are presented in the appendix.

The products exhibited, according to **TGA/DSC analysis**, an exceptional high thermal stability as decomposition started at 460°C without any weight loss before that temperature.

3.5.4 Copper Containing Coordination Polymer (17)

Coordination polymers with copper as metal ion can be formed through the combination of copper acetate and NDC or copper nitrate and NDC-Na. As solvents, water or methanol can be used. Changing the metal salt to CuO or Cu_2O lead to the formation of black precipitates which were not further analysed. Using $CuCO_3$*$Cu(OH)_2$ as metal source did not lead to any conversion.

The linker was dissolved in water or methanol and the metal salt (1.0 equiv.) in the same solvent. The metal salt solution was slowly dropped into the linker solution. A plate-like amorphous precipitate is formed directly after combination (Figure 36 and Figure 37, left) which is then converted to turquoise crystals (Figure 36 and Figure 37, right). This conversion takes place both for copper nitrate/NDC-Na and copper acetate/NDC-Na but it is significantly faster when copper nitrate is used as metal source (Figure 35).

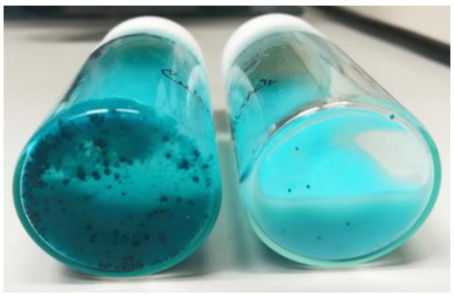

Figure 35 Formation of turquoise needles from a light blue suspension, left: copper nitrate/NDC-Na, right: copper acetate/NDC-Na, after 16 hours.

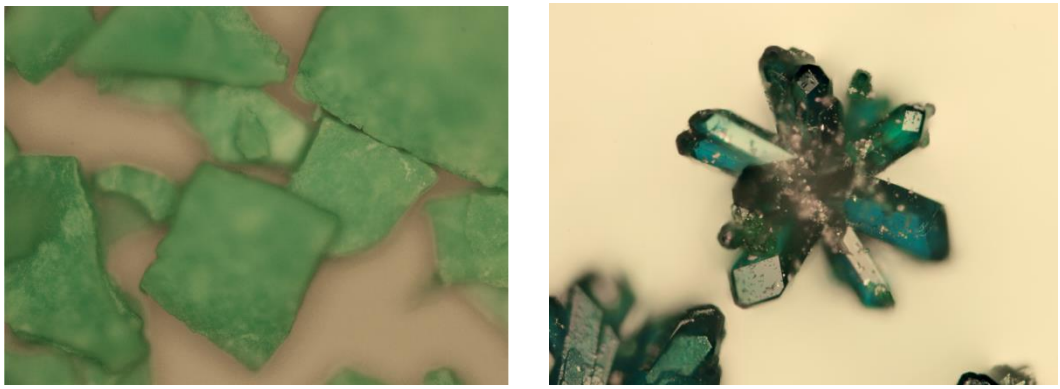

Figure 36 Plate like precipitate formed immediately after combination of copper nitrate and NDC-Na (left) and turquoise needles formed overnight (right), 10x magnification

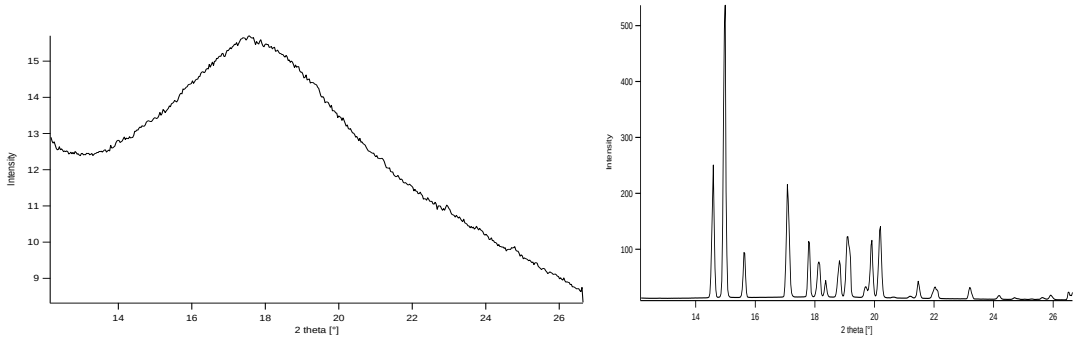

Figure 37 WAXS spectra of light blue plates (left) and turquoise needles (right) formed upon combination of copper nitrate/NDC-Na in water at rt

SC-XRD measurements were done for the turquoise needles. Because of the poor quality of the crystals, proper refinement was not possible and crystallographic data could not be generated. The crystal structure of the secondary building unit (SBU) is displayed in Figure 38. A molecular weight of approximately 842 g/mol can be assigned.

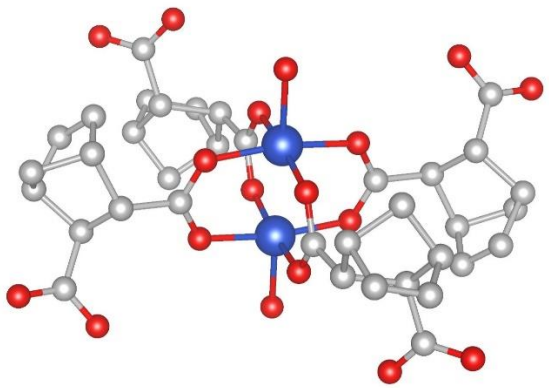

Figure 38 SBU of coordination polymer **17**

The 3D coordination polymer exhibits typical copper paddle wheel SBUs interconnected by the ligand. The copper atoms are octahedrally coordinated to two ligands. Cu-O distances are 1.964 and 1.972 Å. One water molecule is loosely coordinated to each Cu atom with a bond length of 2.182 Å. The Cu-Cu distances are 2.595 Å. This SBU is also present in HKUST-1 which has a Cu-O bond length of 1.96 Å and a Cu-Cu distance of 2.521 Å.[87,88]

The unit cell of the coordination polymer is displayed in Figure 39 and shows channels along the c-axis which are clogged with water and methanol (Figure 40).

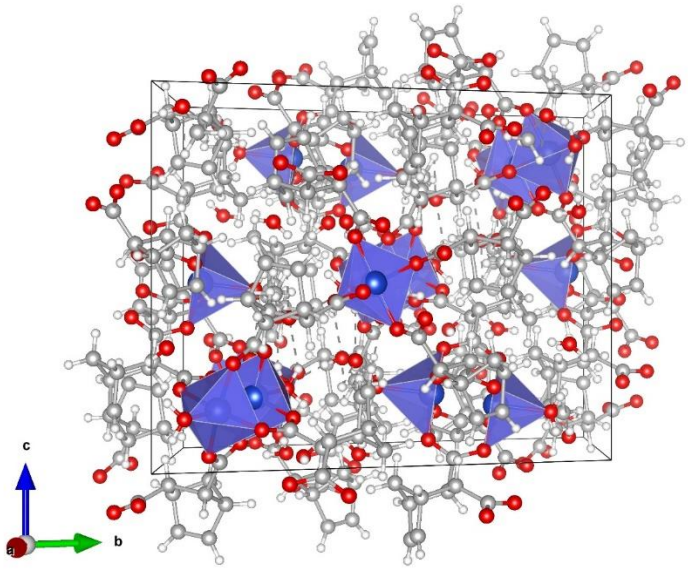

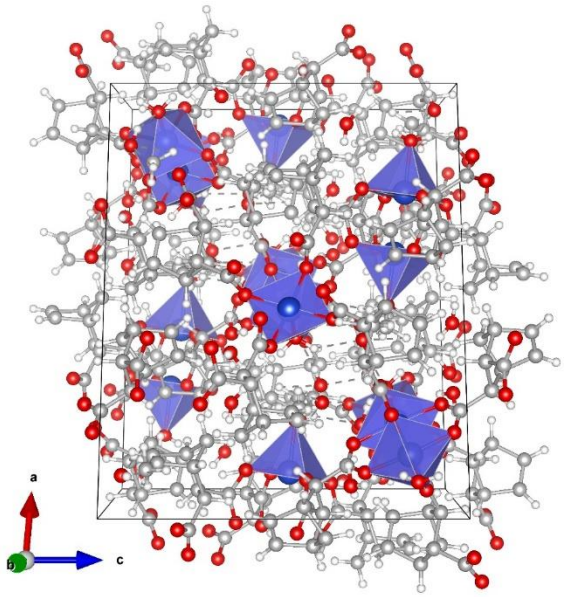

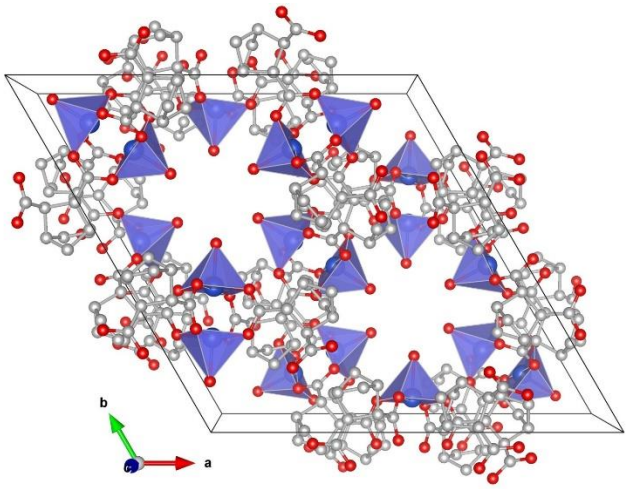

Figure 39 Unit cell of **17**, plane a-c

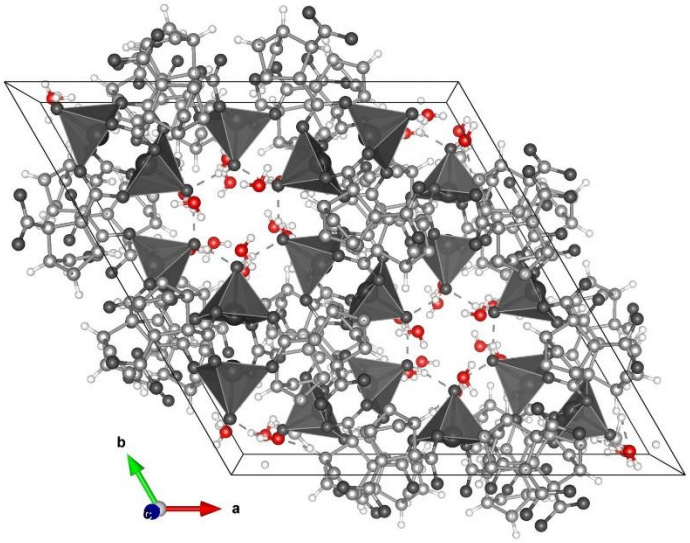

Figure 40 Unit cell of **17** seen along the c-axis (solvent molecules shown in colour to illustrate the pore clocking)

The crystals were washed with methanol and water to get rid of excess ligand potentially clogging the pores. The compound itself is insoluble in methylene chloride, methanol, toluene, nitromethane, tetrahydrofuran, cyclohexane, ethyl acetate and partly soluble in dimethyl sulfoxide and dimethyl formamide. The reflexes of **17** broaden upon drying under reduced pressure which is indicative for a loss of crystallinity (see Appendix).

BET surface analysis (see Appendix) revealed a porosity of 18.2 m^2/g which is vanishingly low compared to HKUST-1 having a porosity of 1055 m^2/g.[87] This low porosity can be attributed to the clogged pores (Figure 40) and the non-planarity of the linker which significantly reduces the pore size and symmetry of the compound generating voids only along the c axis whereas HKUST-1 is completely symmetric and porous along all lattice planes.[88]

The IR spectrum of the compound is characterised by few bands indicative for symmetric coordination of the ligands. Strong bands appear at 1585 and 1395 cm^{-1}.

TGA/DSC analysis of wet samples revealed three major mass losses (15% inflection point 100°C, 22% inflection point 250°C, 25% inflection point 330°C). The remaining 38% of mass correspond to a molecular weight of 320 g/mol which can be attributed to four CuO units.

Furthermore, it was found that **17** is only formed if the reaction is performed at room temperature. The structure collapses upon heating even in wet state forming a brown precipitate and a supernatant green liquid (Figure 41). The precipitate was characterised via IR spectroscopy which revealed that the bands which can be associated with the product decrease in intensity while new bands at 1761, 1353 and 834 cm^{-1} appear. This decomposition happens at 80°C within six hours and at 40°C within a few days. This pronounced thermal instability is ascribed to weak and labile Cu(II)-carboxylate bonds which are known to cause structural decomposition. In HKUST-1, the copper paddlewheel SBU even collapses upon contact with water.[89]

Figure 41 Copper nitrate/NDC-Na after 6 hours of storage at 80°C (left) and room temperature (right)

3.5.5 Cobalt and Iron Containing Coordination Polymers

It was also tried to assemble coordination polymers from cobalt (cobalt nitrate, cobalt carbonate) or iron salts (iron sulfate, iron chloride) and the NDC linker. These attempts were not successful in all cases since only dark powders were obtained which could not be analysed with SC-XRD measurements. As WAXS analysis of these powders revealed amorphous phases for all products, further investigation was not attempted.

4 Conclusion

In this work, the syntheses and characterisation of seven different redox-active monomers with different sizes of the conjugated system have been presented. The aromatic rings do not influence the Diels-Alder addition of cyclopentadiene to the quinones since it works equally well for the naphthalene, the anthracene and the tetracene derivatives. Aromatisation was only successful for tetrahydro-1,4-methanonaphthalene-5,8-dione (**1**). In the other cases vast product mixtures of oxidized products and epoxides have formed. However, oxidation of the Diels-Alder addition products **1**, **4** and **7** was successful in all cases yielding norbornadiene derivatives which have a pronounced sensitivity to light.

Furthermore, the functionalisation of tetrahydro-1,4-methanonaphthalene-5,8-dione (**1**) and 1,4-dihydro-1,4-methanonaphthalene-5,8-dione (**3**) with pyrazoles or imidazoles was investigated. This Aza-Michael addition was not successful when **1** was applied as acceptor and could only be realized for **3** when 3,5-dimethylpyrazole was used as donor which can be correlated with its high nucleophilicity. Nevertheless, yield and reaction time were not satisfactory making the elaboration of an alternative synthetic route necessary. In a 4-step sequence, 6,7-bis(3,5-dimethyl-1H-pyrazol-1-yl)-1,4-dihydro-1,4-methanonaphthalene-5,8-diol (**12**) could finally be synthesized.

Next, ring-opening metathesis polymerisation (ROMP) of the obtained monomers was attempted. While it was successful for the direct Diels-Alder addition products **1**, **4** and **7** and the aromatic product **2**, the norbornadiene containing monomers (**3**, **5** and **8**) could not be polymerised. This may be due to the higher redox potential of these monomers leading to an oxidation of the initiator and a concomitant reduction of the monomers. The pyrazole functionalized monomers (**11**, **12**) could not be polymerized via ROMP, probably because of the chelation of the ruthenium centre of the catalyst rendering it inactive.

However, these monomers can be used as ligands for nickel forming stable complexes in methanol. The structures of **13** and **14** could be elucidated via SC-XRD revealing the metal centre to be coordinated by two ligands. It will further be investigated if the norbornene moiety can be cross-linked to yield a three-dimensional polymeric structure. The formation of coordination polymers was investigated with (±)*endo*,*exo*-5-norbornene-2,3-dicarboxylic acid as linker and zinc, manganese and copper as metal centres. The structure of the copper containing coordination polymer could be elucidated via SC-XRD revealing a 3D-polymeric network that is composed of the typical paddlewheel SBU.

Summarizing, different precursor materials (monomers, polymers and metal complexes) containing quinones as redox centres have been prepared. Their electrochemical characterisation has not yet taken place but their straightforward synthesis from easily available starting materials has been demonstrated.

5 Experimental Section

5.1 General Information

5.1.1 Chemicals

All chemicals have been purchased from Sigma-Aldrich, Fluka and TCI and were, unless specified otherwise, used as received. Solvents used for reactions and work-up were of analytical grade and used as received. If purification of compounds was done via column chromatography, silica gel 60 was used as stationary phase.

5.1.2 Instruments

NMR spectroscopy

^{1}H and ^{13}C nuclear magnetic resonance spectra were recorded on an Avance 3 by Bruker Ultrashield 300 coupled to an autosampler. Spectra were obtained either in deuterated chloroform ($CDCl_3$), dimethyl sulfoxide (DMSO-d_6) or deuterated water (D_2O) at 300.36 MHz for ^{1}H and 75.53 MHz for ^{13}C. Chemical shifts for the ^{1}H spectra are reported in parts per million (ppm) relative to the singlet of $CDCl_3$ at 7.26 ppm, DMSO-d_6 at 2.50 ppm and D_2O at 4.79. The chemical shifts for the ^{13}C-spectra are reported relative to the signal of $CDCl_3$ at 77.16 ppm and 39.52 of DMSO-d_6. For D_2O a TMS standard was added. The shape of the peaks is specified as follows: s (singlet), bs (broad singlet), d (doublet), t (triplet), m (mulitplet). Data analysis was performed with TopSpin.

IR spectroscopy

Infrared spectra were measured on an Alpha FT-IR spectrometer by Bruker with a Platinum ATR single reflection diamond ATR module.

SC-XRD

Single crystal x-ray diffraction analysis was conducted by Ana Torvisco, Ph.D, Institute of Inorganic Chemistry, on an APEX diffractometer by Bruker with Mo-K_α radiation (λ= 0.71073 Å) and a CCD area detector.

XRD

Small- and wide-angle X-ray scattering (SAXS/WAXS) measurements were performed at the Austrian SAXS beamline of the electron storage ring Elettra (Trieste, Italy) using 8 keV branch corresponding to a wavelength of 1.54 Å; 1 s exposure time was used to collect the diffraction images. Data were analysed using the Igor Pro software Package (WaveMetrics Inc.).

TGA

Thermogravimetral analysis was performed on a Netzsch STA 449 C. As purge and protective gas helium with a flow rate of 50 ml/min was used. The temperature range of the experiment ranged from 20 to 550 K with a heating rate of 10 K/min.

BET

Brunauer-Emmett-Teller surface measurements were conducted at AIT using a Quantachrome ASiQwinTM instrument. As absorbate nitrogen was used at a bath temperature of 11.35 K using a cell diameter of 9 mm. Data were analysed by multipoint BET and BJH. Sample weight was about 100 mg.

TLC

Silica gel 60 F254 sheets were used for thin-layer chromatography. Visualization was done via UV light exposure or dipping into an aqueous solution of $KMNO_4$ (1%).

GPC

Weight average of molecular mass (Mw) and polydispersity indices (PDI) were determined via gel permeation chromatography in tetrahydrofuran. A Shimadzu LabSolutions GPC machine was used.

5.1.3 Computational Details

All calculations were performed using density functional theory (DFT) methods as implemented in TURBOMOLE V6.7 using gas phase optimizations either with the quality basis set def2-SVPD in combination with the generalized gradient approximation functional PBE+D3 or the triple-zeta basis set def2-TZVPDD with the hybrid functional B3-LYP. Grimme's empirical correction D3 for dispersive interactions was applied in all calculations.

For the former functional/basis set combination, vibrational energies, temperature effects and zero-point energies were calculated with RI-DFT using rigid-rotor approximation (RRHO). The scaling factor of 1.0203 was used to account for anharmonic effects. Solvent effects were considered for methanol with a dielectric constant of 32.6 and a radius of 2.53 and were calculated employing the conductor like screening model COSMO. For graphical visualization *Avogadro* and *Molden* were used. Input structures and preoptimization was done with *Avogadro*.

5.2 Monomer Synthesis

5.2.1 Diels-Alder Addition

1,4,4a,8a-Tetrahydro-1,4-methanonaphthalene-5,8-dione (1)

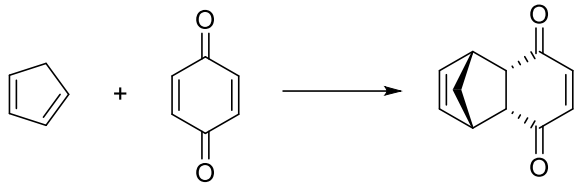

1

The synthesis of **1** has been performed by an adapted procedure of L.K. Chen et al.[27]

Freshly distilled cyclopentadiene (2.98 g, 0.98 equiv., 45.1 mmol) in 10 ml of cooled methanol was slowly dropped to a suspension of freshly sublimed 1,4-benzoquinone (1.0 equiv., 4.90 g, 45.3 mmol) in 100 ml of methanol cooled to 0°C with an ice/water bath. The mixture was stirred for 17 hours and allowed to warm up to room temperature. The clear yellow solution was concentrated under reduced pressure and 200 ml of water were added to remove the unreacted 1,4-benzoquinone via steam distillation with a rotary evaporator. The product was obtained as dark-yellow crystals in 82.8 % yield (6.53 g, 37.5 mmol).

^{1}H-NMR (δ, 20°C, $CDCl_3$): 6.56 (s, 2H, CH), 6.06 (s, 2H, CH), 3.54 (s, 2H, CH), 3.21 (s, 2H, CH), 1.52-1.41 (m, 2H, CH_2)

^{13}C-NMR (δ, 20°C, $CDCl_3$): 199.5, 142.2, 135.4, 48.9, 48.9, 48.5

1,4,4a,9a-tetrahydro-1,4-methanoanthracene-9,10-dione (4)

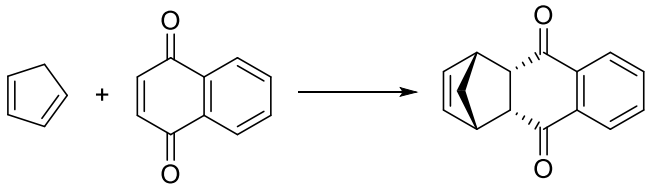

4

Synthesis was performed according to published patents.[30,90]

A round-bottom flask was charged with 2.65 g (1.0 equiv., 16.76 mmol) of 1,4-naphtoquinone and 100 ml of ethanol. The solution was cooled to 0°C and 2 ml of cyclopentadiene (1.44 equiv., 24.21 mmol) were added under stirring. Upon completion of the reaction, the solvent was removed under reduced

pressure and the crude product was washed with cold ethanol (2x15 ml) to give 2.7143 g of a light beige solid (7.29 mmol, 72.4 % yield).

^{1}H-NMR (δ, 20°C, $CDCl_3$): 8.00-7.98 (m, 2H, aryl-CH), 7.68-7.65 (m, 2H, aryl-CH), 5.95 (s, 2H, CH=CH), 3.63(s, 2H), 3.43 (s, 2H), 1.51 (m, 2H, CH_2)

^{13}C-NMR (δ, 20°C, $CDCl_3$): 197.8 (C=O), 135.6, 135.9, 34.2, 126.9, 49.6, 49.3

5.2.2 Aromatisation and Epoxidation

1,4-Dihydro-1,4-methanonaphthalene-5,8-diol (2)

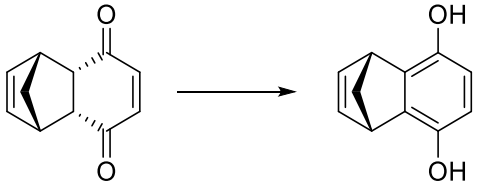

1 **2**

Synthesis was performed according to a procedure published by J. Benkhoff et al.[32]

A three-neck round-bottom flask equipped with a reflux condenser was charged with **1** (4.44 g, 25.5 mmol) 90 ml of methanol and 23.5 g of basic aluminium oxide under nitrogen atmosphere. Under vigorous stirring, the reaction mixture was heated to 65°C and stirred overnight. Then, the mixture was cooled, and aluminium oxide was filtered off and washed several times with methanol. The solvent was evaporated yielding the crude product as brown, sticky oil (4.3107 g, 97.0 % crude yield). Approximately 20 ml of chloroform were added, and the flask was put in an ultrasound bath whereupon the pure product crystallised as white powder (2.70 g, 15.5 mmol, 60.8% yield).

Alternatively, the aromatisation with sodium acetate based on the published procedures has been optimized.[33,91]

1 (118.3 mg, 1.00 equiv., 0.679 mmol) and sodium acetate (168.0 mg, 3.01 equiv., 2.05 mmol) were dissolved in 5 ml of methanol and stirred for 12 hours at 65°C. The reaction mixture was then extracted with tetrahydrofuran (3 x 10 ml) to give the crude product in 78.0% yield (92.27 mg, 0.530 mmol)

^{1}H-NMR (δ, 20°C, $CDCl_3$): 6.80 (s, 2H, CH), 6.35 (s, 2H, CH), 4.30 (s, 2H, OH), 4.08 (s, 2H, CH), 2.24-2.21 (m, 2H, CH_2)

^{1}H-NMR (δ, 20°C, DMSO-d_6): 8.39 (s, 2H, OH), 6.73 (s, 2H, CH), 6.18 (s, 2H, CH), 4.03 (s, 2H, CH), 2.04-1.94 (m, 2H, CH_2)

^{13}C-NMR (δ, 20°C, DMSO-d_6): 144.2, 142.5, 136.5, 113.6, 68.6, 46.2

1,4-dihydro-4a,9a-epoxy-1,4-methanoanthracene-9,10-dione (6a, 6b)

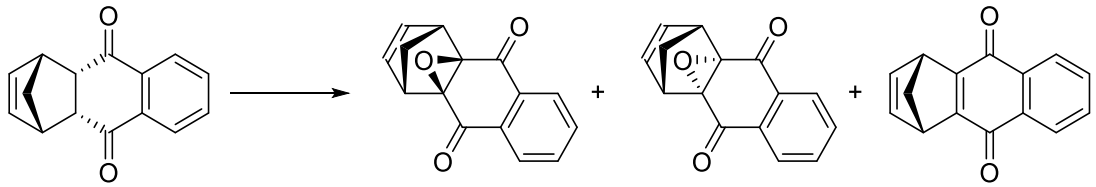

4 **6a** **6b** **5**

A 10 ml Schlenk tube was charged with **7** (113.4 mg, 1.0 equiv., 0.506 mmol) dissolved in a solvent mixture of 4 ml of dimethyl acetamide and 4 ml of water. Then, 100 µl of a sodium hydroxide solution in water were added to adjust the pH to 10. The solution turned dark red and was stirred for three hours at 80°C. After cooling, the solution was acidified with hydrochloric acid to a pH of 2-3 whereupon a brown precipitate formed which was dried and analysed. The yield was very poor because the product had to be consumed for NMR measurements.

^{1}H-NMR (δ, 20°C, $CDCl_3$): **6a**: 8.09-7.93 (m, 2H, aryl-H), 7.72-7.70 (m, 2H, aryl-H), 6.60 (s, 2H, CH), 3.60 (s, 2H, CH), 1.64-1.68 (m, 2H, CH_2); **6b**: 7.90-7.40 (m, 2H, aryl-H), 7.43 (m, 2H, aryl-H), 6.17 (s, 2H, CH), 3.76 (s, 2H, CH), 1.64-1.81 (m, 2H, CH_2)

^{13}C-NMR (δ, 20°C, $CDCl_3$): **6a**: not all quaternary carbons visible, 142.1 (CH), 134.3 (CH), 127.3 (CH), 42.6 (CH_2), 42.1 (q-C), **6b** could not be detected

5.2.3 Oxidation

1,4-dihydro-1,4-methanonaphthalene-5,8-dione (3)

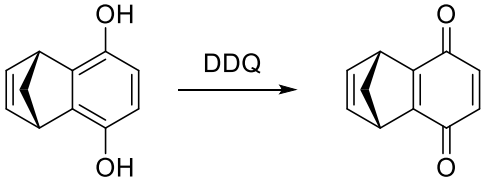

2 **3**

2,3-Dichloro-5,6-dicyano-1,4-benzoquinone (DDQ) (0.5803 g, 1.00 equiv., 2.56 mmol) suspended in 3 ml of 1,4-dioxane were added to a round bottom flask charged with **2** (0.4495 g, 1.00 equiv., 2.58 mmol) dissolved in 5 ml of the same solvent. The reaction mixture was stirred for 4 hours whereupon the clear orange solution turned turbid. The precipitate was filtered off and the filtrate was evaporated in vacuum giving the product as a yellow solid in 95.6 % yield (0.4296 g, 2.50 mmol).

Alternatively, the oxidation of **2** works with ceric ammonium nitrate (CAN) as oxidant as well. For this procedure, a round-bottom flask was charged with ceric ammonium nitrate (0.8363 g, 2.0 equiv.,

1.53 mmol) and dissolved in 1 ml of water. The solution was cooled to 0°C. **2** (0.1333 g, 1.0 equiv., 0.765 mmol) was dissolved in 15 ml of acetonitrile and slowly dropped into the CAN solution. The reaction mixture was stirred for 1 hour at 0°C and another hour at room temperature. After completion of the reaction has been detected via TLC, 10 ml of water were added, and the reaction mixture was extracted with 4x10 ml of diethyl ether. The combined organic phases were washed with saturated sodium chloride solution and dried over sodium sulphate. The filtrate was concentrated under reduced pressure to yield product 3 (0.0718 mg, 0.417 mmol, 54.5 % yield)

^{1}H-NMR (δ, 20°C, $CDCl_3$): 6.85 (s, 2H, CH), 6.56 (s, 2H), 4.10 (s, 2H, CH), 2.30-2.26 (m, 2H, CH_2)

^{13}C-NMR (δ, 20°C, $CDCl_3$): 184.2 (C=O), 160.9, 142.7, 135.9, 74.0, 48.5

1,4-dihydro-1,4-methanonaphthalene-5,8-dione (3)

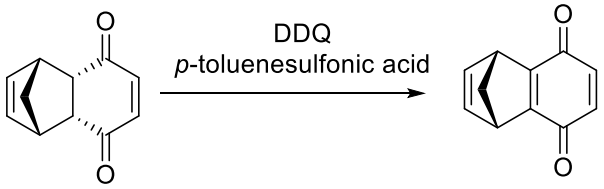

1 **3**

Product **3** can also be obtained directly via oxidation of **1** with DDQ. It was prepared according to the procedure of Zhao et al.[43] A Schlenk tube was charged with **1** (198.5 mg, 1.0 equiv., 1.14 mmol) dissolved in 4.5 ml of 1,4-dioxane. 1.3 equiv. of DDQ (348.8 mg, 1.54 mmol) and 0.1 equiv. of *p*-toluenesulfonic acid (26,6 mg, 0.140 mmol) were added and the reaction mixture was kept at 110°C for 20 hours. Completion of the reaction was detected via thin layer chromatography. Then, the reaction mixture was diluted with 5 ml of water and extracted with ethyl acetate (3x10 ml). The combined organic layers were washed with brine, dried over Na_2SO_4, filtered and concentrated under reduced pressure whereupon a dark-yellow solid formed. The crude product was purified via column chromatography using cyclohexane and ethyl acetate (3:1) as the mobile phase. The light-yellow product could be obtained in 69.5 % yield (136.4 mg, 0.7921 mmol). As the product is not stable under ambient conditions, it was stored under nitrogen atmosphere.

1,4-dihydro-1,4-methanoanthracene-9,10-dione (5)

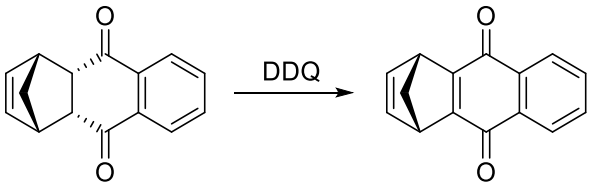

4 **5**

Synthesis is based on a procedure published by Zhao Y. et al.[43]

1.0 equiv. of **8** (484.5 mg, 2.16 mmol) were dissolved in 12 ml of 1,4-dioxane. 1.2 equiv. DDQ (613.1 mg) and 0.11 equiv. of p-toluenesulfonic acid (44.4 mg, 0.233 mmol) were added to the reaction mixture which was then stirred for 10 hours. After completion of the reaction, it was diluted with 20 ml of water and extracted with ethyl acetate (3x 15 ml). The combined organic layers were washed with brine and dried over sodium sulphate. After filtration of the solid, the filtrate was concentrated under reduced pressure. The crude product was purified via column chromatography using cyclohexane and ethyl acetate (5:1) as the mobile phase. The product was obtained as a light-yellow solid in 71.0 % yield (0.3407 g, 1.53 mmol). The product is not stable at ambient conditions and therefore stored under nitrogen atmosphere and light exclusion.

^{1}H-NMR (δ, 20°C, $CDCl_3$): 8.06-8.03 (m, 2H, aryl-CH), 7.68-7.66 (m, 2H, aryl-CH), 6.89 (s, 2H, CH=CH), 4.24 (s, 2H, CH), 2.36-2.33 (m, 2H, CH_2)

^{13}C-NMR (δ, 20°C, $CDCl_3$): 181.7 (C=O), 163.1 (q-C), 142.6 (CH), 133.3 (CH), 132.8 (q-C), 126.2 (CH), 73.4 (CH_2), 48.7 (q-C)

1,4-dihydro-1,4-methanotetracene-5,12-dione (8)

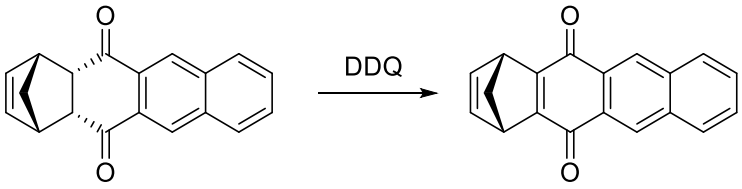

7 **8**

Synthesis was performed according to the procedure published by Y. Zhao et al.[43]

1.0 equiv. of **7 (**127.4 mg, 0.464 mmol) was dissolved in 2 ml of 1,4-dioxane in a 10 ml Schlenk tube. Then, 1.1 equiv. of DDQ (115.1 mg, 0.507 mmol) and 0.1 equiv. of p-toluenesulfonic acid (8.88 mg, 0.0467 mmol) were added and the reaction mixture was stirred at 110°C overnight. Upon completion of the reaction, the reaction mixture was diluted with 5 ml of water and extracted with ethyl acetate

(3x10 ml). The combined organic layers were washed with brine, dried over sodium sulphate, filtered and concentrated under reduced pressure. The crude product was purified via column chromatography using toluene as the mobile phase. Fractions of 80 ml were collected. The product was isolated as an orange-red solid in 43.1% yield (54.3 mg, 0.200 mmol). The product is not stable at ambient atmosphere and therefore stored under nitrogen atmosphere and exclusion of light.

^{1}H-NMR (δ, 20°C, $CDCl_3$): 8.59 (s, 2H, CH), 8.05-8.02 (m, 2H), 7.67-7.64 (m, 2H), 6.94 (s, 2H), 4.31 (s, 2H), 2.39-2.38 (m, 2H)

5.3 Polymer Synthesis

5.3.1 Poly(1,4,4a,8a-Tetrahydro-1,4-methanonaphthalene-5,8-dione) (poly1)

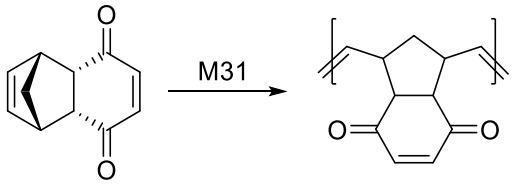

1 **poly1**

A Schlenk tube was charged with **1** (210.3 mg, 1.0 equiv., 1.21 mmol) and 20 ml of methylene chloride. Nitrogen was bubbled through the solution for 20 minutes to get rid of oxygen. Then, M31 (0.01 equiv., 8.60 mg, 0.0115 mmol) was added and the solution was stirred for 24 hours at room temperature. Upon completion of the reaction, 50 µl of ethyl vinyl ether was added to stop the polymerisation. The polymer solution was slowly dropped into methanol whereupon a dark grey solid precipitated which was separated via centrifugation. The polymer was washed with methanol and dried in vacuum to yield a black and insoluble product.

^{1}H-NMR (δ, 20°C, DMSO-d_6): 6.67, 5.44, 2.89, 1.86

IR [cm^{-1}]: 3486, 2946, 1667, 1267, 1098, 747

GPC: poor solubility in THF and $CHCl_3$ makes measurement impossible

5.3.2 Poly(1,4-Dihydro-1,4-methanonaphthalene-5,8-diol) (poly2)

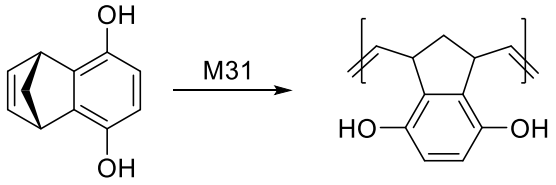

2 **poly2**

A Schlenk tube was charged with 202 mg of **1** (1.0 equiv., 1.16 mmol) and 20 ml of tetrahydrofuran. Nitrogen was bubbled through the solution for 20 minutes to get rid of oxygen. Then, M31 (0.01 equiv., 8.60 mg, 0.0115 mmol) was added and the solution was stirred for 6 hours at room temperature. Upon completion of the reaction, 50 µl of ethyl vinyl ether was added to stop the polymerisation. The polymer solution was slowly dropped into methanol whereupon a grey solid precipitated which was separated via centrifugation. The polymer was washed with methanol and dried in vacuum to obtain 78.8 mg of pure product.

^{1}H-NMR (δ, 20°C, DMSO-d_6): 8.39-8.32, 8.02-7.95, 6.44, 5.41, 4.32, 1.61-1.57

^{13}C-NMR (δ, 20°C, DMSO-d_6): 147.1-145.9, 132.1, 114.8, 67.1, 48.6, 25.1

IR [cm^{-1}]: 3470, 1650, 1485, 1200, 1142, 806

GPC: poor solubility in THF and $CHCl_3$ makes measurement impossible

5.3.3 Poly(1,4,4a,9a-tetrahydro-1,4-methanoanthracene-9,10-dione) (poly4)

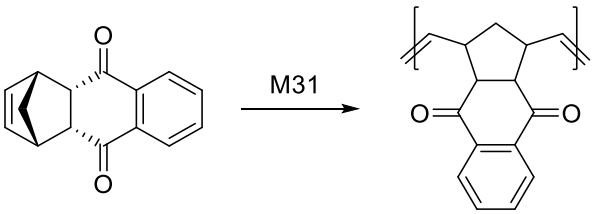

4 **poly4**

A Schlenk tube was charged with 104.9 mg of **9** (1.0 equiv., 0.4678 mmol). 4 ml of tetrahydrofuran were added, and nitrogen was bubbled through the solution for 20 minutes to get rid of oxygen. Then, M31 (0.01 equiv., 3.57 mg, 0.004775 mmol) was added and the reaction mixture was stirred for 24 hours. Upon completion, 200 µl of ethyl vinyl ether was added to stop the polymerisation. Tetrahydrofuran was removed under reduced pressure and the remaining black solid was dissolved in a small amount of chloroform. The solution was slowly dropped into methanol whereupon a light-grey volu-

minous precipitate formed which was separated via centrifugation. The solid polymer was washed with methanol (2x5ml) and dried in vacuum to obtain 50.8 mg of pure product.

^{1}H-NMR (δ, 20°C, $CDCl_3$): 7.91, 7.69, 5.41-5.37, 3.26, 2.81, 1.91-1.25

^{13}C-NMR (δ, 20°C, $CDCl_3$): 197.09, 136.67, 134.00, 131.04, 126.37, 55.92, 55.42, 46.19

IR [cm^{-1}]: 2946, 1681, 1591, 1298, 1250, 973, 743, 722

GPC: Average molecular weight: 28600 g/mol, PDI: 1.8

5.3.4 Poly(,4,4a,12a-tetrahydro-1,4-methanotetracene-5,12-dione) (poly7)

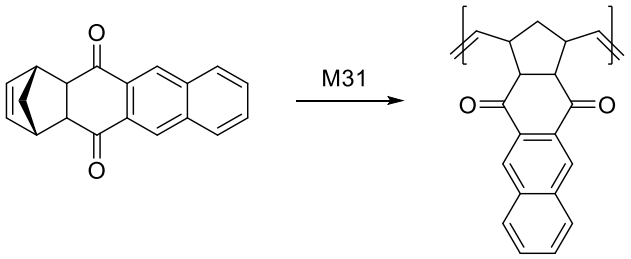

7 **poly7**

A 10 ml Schlenk tube was charged with **7** (0.040 mg, 0.1458 mmol, 1.0 equiv.) dissolved in 5 ml of methylene chloride. Nitrogen was bubbled through the solution for 20 minutes to get rid of oxygen. Then, M31 (1.09 mg, 0.01 equiv., 0.00146 mmol) was added and the reaction mixture was stirred for 96 hours at room temperature before 100 µl of ethyl vinyl ether was added to the reaction mixture. Since precipitation from methanol failed, the solvent was removed under reduced pressure.

^{1}H-NMR (δ, 20°C, $CDCl_3$): 8.44-8.42, 7.96, 7.59, 2.79-2.71; monomer still present in sample

5.4 Quinone Functionalisation

5.4.1 2,3-bis(3,5-dimethyl-1H-pyrazol-1-yl)benzene-1,4-diol (9)

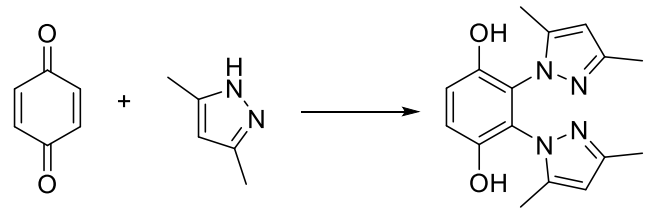

9

The published procedure for the synthesis of **9** by P. Ballesteros et al.[49] was adapted.

A three-neck round-bottom flask equipped with a reflux condenser was charged with 65 ml of 1,4 dioxane and nitrogen was bubbled through for 20 minutes. Then, 1,4-benzoquinone (4.7 g, 43.5 mmol) and 3,5-dimethylpyrazole (4.1846 g, 43.5 mmol, 1.0 equiv.) were added and the reaction mixture was refluxed for 18 hours. The obtained crude brown product was washed with approximately 200 ml of diethyl ether to remove the hydroquinone side product. The pure product was obtained as a white solid in 81.8 % yield (5.0786 g, 17.02 mmol).

^{1}H-NMR (δ, 20°C, DMSO-d6): 9.32 (2H, s, OH), 6.95 (2H, s, CH), 5.68 (2H, s, CH), 2.01-1.94 (6H, d, CH_3)

IR [cm^{-1}]: 2923, 1557, 1497, 1289, 1222, 1032, 873, 765

2,3-bis(3,5-dimethyl-1H-pyrazol-1-yl)cyclohexa-2,5-diene-1,4-dione (10)

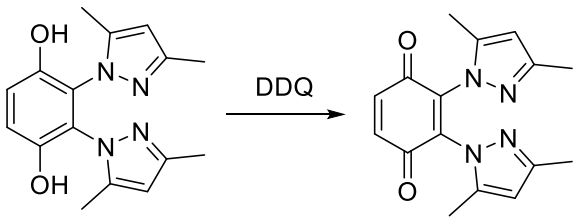

9 **10**

Synthesis was done according to the procedure published by P. Ballesteros et al.[49]

A round-bottom flask was charged with **4** (3.8038 g, 12.75 mmol) suspended in 1,4-dioxane. DDQ (2.9086 g, 12.81 mmol, 1.00 equiv.) was dissolved in 20 ml of the same solvent and was added dropwise under stirring during a period of 10 minutes at room temperature. Then, the mixture was continuously stirred for 2 hours whereupon a precipitate formed which was then filtered off. The filtrate was taken to dryness yielding 3.722 g of pure product (12.56 mmol, 98.5 % yield).

^{1}H-NMR (δ, 20°C, $CDCl_3$): 6.95 (2H, s, CH), 5.82 (2H, s, CH), 2.07 (s, 3H, CH_3), 1.94 (s, 3H, CH_3)

^{13}C-NMR (δ, 20°C, $CDCl_3$): 182.13, 151.43, 143.13, 137.35, 135.84, 107.35, 13.41, 11.16

IR [cm^{-1}]: 2928, 1677, 1567, 1391, 1296

6,7-bis(3,5-dimethyl-1H-pyrazol-1-yl)-1,4,4a,8a-tetrahydro-1,4-methanonaphthalene-5,8-dione (11)

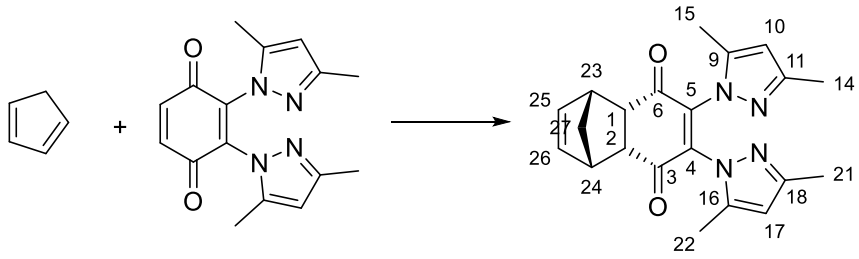

Freshly distilled cyclopentadiene (1.0 equiv., 847 µl, 10.25 mmol) was added to a solution of **5** (1.0 equiv., 3.0369 g, 10.25 mmol) in methanol maintained at 0°C. The reaction mixture gradually turned turbid and was stirred for 3.5 hours. Methanol was removed under reduced pressure and the crude yellow product was used without further purification. It was obtained in 97.8% yield (3.6303 g, 10.02 mmol).

^{1}H-NMR (δ, 20°C, $CDCl_3$): 6.28 (s, 2H, *H*C=C*H*), 5.80 (s, 2H, pyrazole), 3.68 (s, 2H), 3.52 (s, 2H), 2.05-2.00 (d, 12H, CH_3), 1.64-1.52 (m, 2H, CH_2)

^{13}C-NMR (δ, 20°C, $CDCl_3$): 193.9 (C3, C6), 151.2 (C9, C16), 143.36 (C11, C18), 136.0 (C25, C26), 107.2 (C10, C17), 49.52, 49.17, 49.10 (CH_2, C1, C2, C23, C24), 13.6 (C15, C22), 11.7 (C14, C21)

6,7-bis(3,5-dimethyl-1H-pyrazol-1-yl)-1,4-dihydro-1,4-methanonaphthalene-5,8-diol (12)

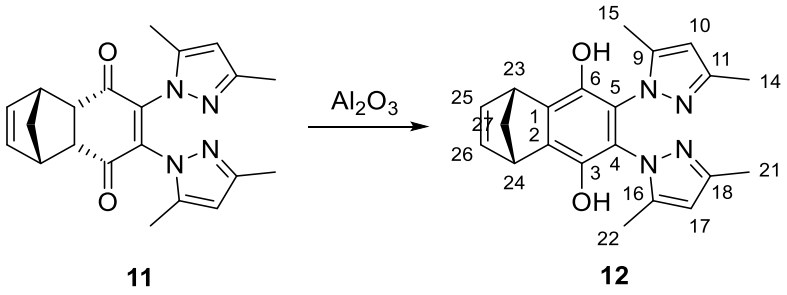

A round-bottom flask was charged with **6** (2.6413 g, 7.29 mmol) and 155 ml of ethyl acetate. 15.50 g of aluminium oxide were added in one batch and the reaction mixture was stirred vigorously overnight. Upon completion of the reaction, the solid was filtered off and aluminium oxide was washed several times with ethyl acetate and methanol. Then, the filtrate was concentrated under reduced pressure whereupon of the product was obtained as a white solid (0.7509 g, 2.07 mmol, 28.43% yield).

^{1}H-NMR (δ, 20°C, $CDCl_3$): 7.84-7.60 (bs, 2H, OH), 6.83 (s, 2H, *H*C=C*H*), 5.84 (d, 2H, CH pyrazole), 4.25 (s, 2H, norbornene CH), 2.26 (8H, CH_3, CH_2), 1.59-1.56 (s, 6H, CH_3)

^{13}C-NMR (δ, 20°C, $CDCl_3$): 151.5 (C9, C16), 143.31 (C11, C18), 142.46 (C25 or C26), 142.37 (C25 or C26), 139.84, 139.64, 139.36, 139.22 (C1, C2, C3, C6), 118.31 (C4, C5), 106.73 (C10, C17), 69.32 (C27), 47.35, 47.12 (C23, C24), 13.53 (C15, C22), 10.65 (C14, C21)

IR [cm^{-1}]: 2926, 2587, 1559, 1473, 1308, 1036, 867, 773, 735, 690

5.5 Metal Complex Synthesis

5.5.1 Nickel-bis{2,3-bis(3,5-dimethyl-1H-pyrazol-1-yl)benzene-1,4-diol} (13)

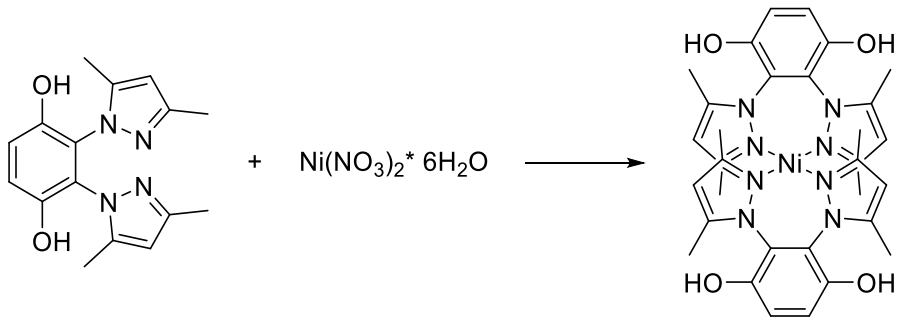

9 **13**

4 (1.0 equiv., 0.0502 g, 0.168 mmol) was suspended in 2 ml of methanol. Then, nickel nitrate (2.0 equiv., 0.09748 g, 0.335 mmol) dissolved in 2 ml of the same solvent was added in one batch whereupon a blue precipitate formed immediately. The reaction mixture was left to stand at 40°C for two days. The precipitate was separated from the supernatant clear liquid and washed with methanol. Upon drying under reduced pressure, a light green solid was obtained. Crystals suitable for SC-XRD analysis were obtained directly from the reaction mixture.

^{1}H-NMR (δ, 20°C, DMSO-d_6): 9.30 (s, 2H, OH), 6.95 (s, 2H, CH), 5.68 (s, 2H, CH), 2.01-1.94 (d, 6H, CH_3)

IR [cm^{-1}]: 3244, 1561, 1420, 1281, 1034, 875, 808

5.5.2 Nickel-bis{6,7-bis(3,5-dimethyl-1H-pyrazol-1-yl)-1,4-dihydro-1,4-methanonaphthalene-5,8-diol} (14)

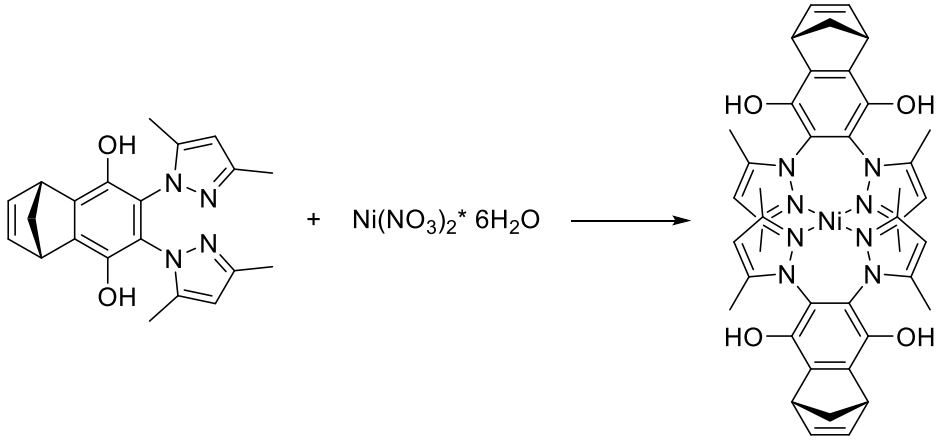

12 **14**

7 (1.0 equiv., 0.05 g, 0.138 mmol) was dissolved in 2 ml of methanol and heated to 40°C. Then, a solution of 1.0 equiv. of nickel nitrate (0,0398 g, 0.137 mmol) in 1 ml of methanol was added whereupon a clear green solution formed. The solution was left to stand at 40°C overnight. Subsequently, the formation of orange crystals large enough for SC-XRD measurement could be obtained.

IR [cm^{-1}]: 3460-2683 (broad), 1557, 1416, 1297, 1264, 1026, 818, 743

5.6 Coordination Polymer Synthesis

5.6.1 Synthesis of NDC-Na

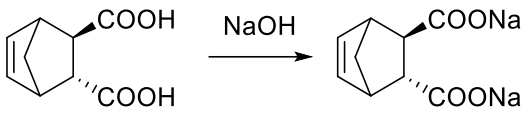

NDC **NDC-Na**

A 4 ml vial was charged with (±)*endo*,*exo*-5-norbornene-2,3-dicarboxylic acid (NDC) (30 mg, 1.0 equiv., 0.165 mmol) suspended in 2.5 ml of water. Then, sodium hydroxide 5.55 M was added (13.83 mg, 2.0 equiv., 0.346 mmol) and the resulting reaction mixture was stirred overnight at 80°C. After completion of the reaction, the solvent was evaporated and the product (NDC-Na) was obtained as a white solid.

^{1}H-NMR (δ, 20°C, D_2O): 6.32 (dd, 1H, =CH), 6.06 (dd, 1H, =CH), 3.15 (1H, CH, bridge head), 3.11-3.10 (t, 1H, exo-CH), 3.01 (s, 1H, CH bridge head), 2.39 (s, 1H, endo-CH), 1,56-1.53 (dd, 1H, CH_2), 1.39-1.36 (dd, 1H, CH_2)

^{13}C-NMR (δ, 20°C, D_2O): 140.90 (C=*H*), 137.68 (C=*H*), 53.79 (exo-CH), 53.36 (endo-CH), 51.18 (CH norbornene), 50.25 (CH norbornene), 49.15 (CH_2); q-C not visible

IR [cm^{-1}]: 2972, 1542, 1398, 700

5.6.2 Zinc Containing Coordination Polymer (15)

A glass vial was equipped with (±)*endo*,*exo*-5-norbornene-2,3-dicarboxylic acid (NDC) (0.1025 g, 1.0 equiv., 0.563 mmol) suspended in 2.5 ml of H_2O. The mixture was heated with a heat gun until the solid has fully dissolved. $Zn(OAc)_2$ (0.1399 g, 1.35 equiv., 0.762 mmol) was dissolved in 2.5 ml of H_2O and added to the linker solution. The resulting solution was heated to 80°C for two days whereupon a fine, white precipitate formed. The product was washed with water and methanol several times and analysed via IR spectroscopy.

The same product was formed upon combination of NDC and zinc oxide and upon combination of the NDC-Na with $Zn(NO_3)_2$*3 H_2O

IR [cm^{-1}]: 2975, 1610, 1522, 1430, 783, 718

TGA: decomposition at 400.0°C

BET surface: 25.5 m^2/g

5.6.3 Manganese Containing Coordination Polymer (16)

A glass vial was equipped with NDC (0.1280 g, 1.0 equiv, 0.7026 mmol) suspended in approx. 2.5 ml of H_2O. Then, $MnCO_3$ (0.0892 g, 1.10 equiv., 0.776 mmol) was added to the linker solution. A light beige plate formed overnight upon heating the reaction mixture to 80°C without stirring. The plate was separated via decantation and washed several times with water.

IR [cm^{-1}]: 1624, 1563, 1400, 1300, 704

TGA: decomposition at 459.3°C

BET surface: 14.3 m^2/g

5.6.4 Copper Containing Coordination Polymer (17)

$Cu(NO_3)_2*3H_2O$ (100 mg, 0.414 mmol, 1.0 equiv.) was dissolved in 2.5 ml of water and slowly dropped into a solution of NDC-Na in water (93.61 mg, 0.414 mmol) whereupon a turbid, light-blue suspension formed which was left to stand at room temperature. Overnight, turquoise crystals grew which were separated via centrifugation and subsequently washed with methanol and water.

The same product forms upon combination of $Cu(OAc)_2*H_2O$ with NDC-Na in a molar ratio of 1:1.

IR [cm^{-1}]: 1585, 1395, 712

TGA: three weight loss steps (15%, inflection point 100°C; 22%, inflection point 250°C; 25%, inflection point 330°C).

BET surface: 18.2 m^2/g

6 List of Abbreviations

Analytical methods

BET	Brunauer-Emmett-Teller model
ATR	Attenuated total reflection
IR	Infrared
MHz	Megahertz
NMR	Nuclear magnetic resonance
D	Doublet
M	Multiplet
T	Triplet
S	singlet
Ppm	Parts per million
SC-XRD	Single crystal X-ray diffraction
XRD	X-ray powder diffraction
WAXS	Wide angle X-ray scattering
SAXS	Small angle X-ray scattering
TGA	Thermogravimetric analysis
DSC	Differential scanning calorimetry
GPC	Gel permeation chromatography
TLC	Thin layer chromatography

Chemicals

PTVE	poly(2,2,6,6-tetramethylpiperidinyloxy-4-yl vinylether)
PVdF	Polyvinylidene difluoride
TBA	Tetrabutylammonium
DDQ	2,3-dichloro-5,6-dicyano-1,4-benzoquinone
CAN	Ceric ammonium nitrate
DDQ-HQ	2,3-Dichloro-5,6-dicyano-1,4-hydroquinone
PzH	pyrazole
Ru	ruthenium
NDC	5-norbornene-endo,exo-2,3-dicarboxylic acid
NDC-Na	Disodium 5-norbornene-endo,exo-2,3-carboxylate
Na_2CO_3	Sodium carbonate
Et_3N	Triethylamine
NaOH	Sodium hydroxide
DMF	Dimethyl formamide
DEF	Diethyl formamide
NMP	N-methyl-2-pyrrolidon
DMSO-d_6	Deuterated dimethyl sulfoxide
$CDCl_3$	Deuterated chloroform
D_2O	Deuterated water
TMS	Trimethylsilylpropionic acid, sodium salt
M31	[(SIMes)Ru(py)(Ind)Cl_2], [1,3-Bis(2,4,6-trimethylphenyl)-2-imidazolidinylidene]dichloro(3-phenyl-1H-inden-1-ylidene)(pyridyl)ruthenium(II)

Others

ROMP	Ring-opening metathesis polymerisation
CP	Coordination polymer
MOF	Metal-organic framework
UV	Ultraviolet
DFT	Density functional theory
SBU	Secondary building unit

7 List of Figures

8 List of Schemes

9 List of Tables

10 References

(1) Muench, S.; Wild, A.; Friebe, C.; Häupler, B.; Janoschka, T.; Schubert, U. S. Polymer-Based Organic Batteries. *Chemical Reviews*. American Chemical Society August 24, 2016, pp 9438–9484. https://doi.org/10.1021/acs.chemrev.6b00070.

(2) Muench, S.; Winsberg, J.; Friebe, C.; Wild, A.; Brendel, J. C.; Lex-Balducci, A.; Schubert, U. S. PNTQS: Easily Accessible High-Capacity Redox-Active Polymer for Organic Battery Electrodes. *ACS Appl. Energy Mater.* **2018**, *1* (8), 3554–3559. https://doi.org/10.1021/acsaem.8b00734.

(3) Suga, T.; Konishi, H.; Nishide, H. Photocrosslinked Nitroxide Polymer Cathode-Active Materials for Application in an Organic-Based Paper Battery. *Chem. Commun.* **2007**, No. 17, 1730. https://doi.org/10.1039/b618710b.

(4) Kawai, T.; Oyaizu, K.; Nishide, H. High-Density and Robust Charge Storage with Poly(Anthraquinone-Substituted Norbornene) for Organic Electrode-Active Materials in Polymer-Air Secondary Batteries. *Macromolecules* **2015**, *48* (8), 2429–2434. https://doi.org/10.1021/ma502396r.

(5) Speer, M. E.; Kolek, M.; Jassoy, J. J.; Heine, J.; Winter, M.; Bieker, P. M.; Esser, B. Thianthrene-Functionalized Polynorbornenes as High-Voltage Materials for Organic Cathode-Based Dual-Ion Batteries. *Chem. Commun.* **2015**, *51* (83), 15261–15264. https://doi.org/10.1039/c5cc04932f.

(6) Xiang, J.; Chang, C.; Li, M.; Wu, S.; Yuan, L.; Sun, J. A Novel Coordination Polymer as Positive Electrode Material for Lithium Ion Battery. *Cryst. Growth Des.* **2008**, *8* (1), 280–282. https://doi.org/10.1021/cg070386q.

(7) Haas, O.; Mu, K.; Haas, O. Electrochemically Active Polymers for Rechargeable Batteries Electrochemically Active Polymers for Rechargeable Batteries. **2015**, No. MARCH 1997. https://doi.org/10.1021/cr941181o.

(8) Janoschka, T.; Hager, M. D.; Schubert, U. S. Powering up the Future: Radical Polymers for Battery Applications. *Adv. Mater.* **2012**, *24* (48), 6397–6409. https://doi.org/10.1002/adma.201203119.

(9) Liang, Y.; Tao, Z.; Chen, J. Organic Electrode Materials for Rechargeable Lithium Batteries. *Advanced Energy Materials*. July 2012, pp 742–769. https://doi.org/10.1002/aenm.201100795.

(10) Häupler, B.; Wild, A.; Schubert, U. S. Carbonyls: Powerful Organic Materials for Secondary Batteries. *Adv. Energy Mater.* **2015**, *5* (11). https://doi.org/10.1002/aenm.201402034.

(11) Han, C.; Li, H.; Shi, R.; Zhang, T.; Tong, J.; Li, J.; Li, B. Organic Quinones towards Advanced Electrochemical Energy Storage: Recent Advances and Challenges. *J. Mater. Chem. A* **2019**. https://doi.org/10.1039/c9ta05252f.

(12) Yokoji, T.; Kameyama, Y.; Maruyama, N.; Matsubara, H. High-Capacity Organic Cathode Active Materials of 2,2′-Bis-p-Benzoquinone Derivatives for Rechargeable Batteries. *J. Mater. Chem. A* **2016**, *4* (15), 5457–5466. https://doi.org/10.1039/c5ta10713j.

(13) Dong, T.; Zhang, J.; Xu, G.; Chai, J.; Du, H.; Wang, L.; Wen, H.; Zang, X.; Du, A.; Jia, Q.; et al. A Multifunctional Polymer Electrolyte Enables Ultra-Long Cycle-Life in a High-Voltage Lithium Metal Battery. *Energy and Environmental Science*. Royal Society of Chemistry May 1, 2018, pp 1197–1203. https://doi.org/10.1039/c7ee03365f.

(14) Wang, Y.; Zhu, S.; Zou, L.-H. Recent Advances in Direct Functionalization of Quinones. *European J. Org. Chem.* **2019**, *0* (0). https://doi.org/10.1002/ejoc.201900028.

(15) Saitou, K.; Nagasaki, K. I.; Yamakawa, H.; Hu, H. Y.; Fujie, K.; Katayama, A. Linear Relation between the Amount of Respiratory Quinones and the Microbial Biomass in Soil. *Soil Sci. Plant Nutr.* **1999**, *45* (3), 775–778. https://doi.org/10.1080/00380768.1999.10415843.

(16) Juliasih, N. L. G. R.; Yuan, L. C.; Sago, Y.; Atsuta, Y.; Daimon, H. Supercritical Fluid Extraction of Quinones from Compost for Microbial Community Analysis. *J. Chem.* **2015**, *2015*. https://doi.org/10.1155/2015/717616.

(17) Guin, P. S.; Das, S.; Mandal, P. C. Electrochemical Reduction of Quinones in Different Media: A Review. *Int. J. Electrochem.* **2011**, *2011* (January), 1–22. https://doi.org/10.4061/2011/816202.

(18) Wu, Y.; Zeng, R.; Nan, J.; Shu, D.; Qiu, Y.; Chou, S. L. Quinone Electrode Materials for Rechargeable Lithium/Sodium Ion Batteries. *Adv. Energy Mater.* **2017**, *7* (24). https://doi.org/10.1002/aenm.201700278.

(19) Kim, J.; Kim, J. H.; Ariga, K. Redox-Active Polymers for Energy Storage Nanoarchitectonics. *Joule* **2017**, *1* (4), 739–768. https://doi.org/10.1016/J.JOULE.2017.08.018.

(20) Albagli, D.; Bazan, G.; Schrock, R. R.; Wrighton, M. S. Electrochemistry of Well-Defined Redox Active Block Polymers Prepared by Ring-Opening Metathesis Polymerisation. *Mol. Cryst. Liq. Cryst. Sci. Technol. Sect. A. Mol. Cryst. Liq. Cryst.* **1992**, *216* (1), 123–128. https://doi.org/10.1080/10587259208028760.

(21) Zheng, Q.; Niu, Z.; Ye, J.; Zhang, S.; Zhang, L.; Li, L.; Zhao, Y.; Zhang, X. High Voltage, Transition Metal Complex Enables Efficient Electrochemical Energy Storage in a Li-Ion Battery Full Cell. *Adv. Funct. Mater.* **2017**, *27* (4). https://doi.org/10.1002/adfm.201604299.

(22) Pan, F.; Wang, Q. Redox Species of Redox Flow Batteries: A Review. *Molecules*. MDPI AG November 18, 2015, pp 20499–20517. https://doi.org/10.3390/molecules201119711.

(23) Batten, S. R.; Champness, N. R.; Chen, X.-M.; Garcia-Martinez, J.; Kitagawa, S.; Öhrström, L.; O'Keeffe, M.; Paik Suh, M.; Reedijk, J. Terminology of Metal–organic Frameworks and Coordination Polymers (IUPAC Recommendations 2013). *Pure Appl. Chem.* **2013**, *85* (8), 1715–1724. https://doi.org/10.1351/PAC-REC-12-11-20.

(24) Batten, S. R.; Champness, N. R.; Chen, X.-M.; Garcia-Martinez, J.; Kitagawa, S.; Öhrström, L.; O'Keeffe, M.; Suh, M. P.; Reedijk, J. Coordination Polymers, Metal–organic Frameworks and the Need for Terminology Guidelines. *CrystEngComm* **2012**, *14* (9), 3001. https://doi.org/10.1039/c2ce06488j.

(25) Zhu, J. P.; Wang, X. H.; Zuo, X. X. The Application of Metal-Organic Frameworks in Electrode Materials for Lithium–ion and Lithium–sulfur Batteries. *R. Soc. Open Sci.* **2019**, *6* (7), 190634. https://doi.org/10.1098/rsos.190634.

(26) Tormena, C. F.; Lacerda, V.; De Oliveg, K. T. Revisiting the Stability of Endo/Exo Diels-Alder Adducts between Cyclopentadiene and 1,4-Benzoquinone. *J. Braz. Chem. Soc.* **2010**, *21* (1), 112–118. https://doi.org/10.1590/S0103-50532010000100017.

(27) Chen, L.-K.; Wu, C.-S.; Chen, M.-C.; Hsu, K.-L.; Li, H.-C.; Hsieh, C.-H.; Hsiao, M.-H.; Chang, C.-L.;

Chu, P. P.-J. Cross-Linked Norbornene Sulfonated Poly(Ether Ketone)s for Proton Exchange Membrane. *J. Memb. Sci.* **2010**, *361* (1–2), 143–153. https://doi.org/10.1016/J.MEMSCI.2010.05.060.

(28) Clark, C. A.; Lee, D. S.; Pickering, S. J.; Poliakoff, M.; George, M. W. UV PhotoVap: Demonstrating How a Simple and Versatile Reactor Based on a Conventional Rotary Evaporator Can Be Used for UV Photochemistry. *Org. Process Res. Dev.* **2018**, *22* (5), 595–599. https://doi.org/10.1021/acs.oprd.8b00037.

(29) Cookson, R. C.; Crundwell, E.; Hill, R. R.; Hudec, J. 586. Photochemical Cyclisation of Diels–alder Adducts. *J. Chem. Soc.* **1964**, *0* (0), 3062–3075. https://doi.org/10.1039/jr9640003062.

(30) Zhang, J.; Zhang, L.; Shkrob, I. A. Two-Electron Redox Catholyte for Redox Flow Batteries., February 14, 2019.

(31) Eyring, H. The Activated Complex in Chemical Reactions. *J. Chem. Phys.* **1935**, *3*, 107. https://doi.org/10.1063/1.1749604.

(32) Benkhoff, J.; Boese, R.; Klärner, F.-G. Synthesis of Sterically Rigid Macrocycles by The Use of Pressure-Induced Repetitive Diels–Alder Reactions. *Liebigs Ann.* **1997**, *1997* (3), 501–516. https://doi.org/10.1002/jlac.199719970310.

(33) Marchand, A. P.; Alihodzic, S.; Shukla, R. A Simple Procedure for Preparing Annulated P-Benzoquinones. Improved Synthesis of 1,4-Dihydro-1,4-Methanonaphthalene-5,8-Dione. *Synth. Commun.* **1998**, *28* (3), 541–546. https://doi.org/10.1080/00397919808005109.

(34) Mitra, A. K.; Gawandi, V. B.; George, K.; Mohan, H.; Mukherjee, T. Investigations on the Antioxidant Activity of 5,8-Dihydroxy-1,4-Dihydro-1, 4-Methanonaphthalene (DDMN). *Res. Chem. Intermed.* **2009**, *35* (1), 13–20. https://doi.org/10.1007/s11164-008-0007-3.

(35) Numata, S.; Sakurai, T.; Naito, T.; Yamada, A.; Nagasawa, Y. 10-Substituted 1,4-Dihydro-1,4-Methanoanthracen-9-Yl (Meth)Acrylates Having High Refractivity and Manufacture Thereof., May 9, 2013.

(36) Ching, A. L.; Liew, C. V.; Chan, L. W.; Heng, P. W. S. Modifying Matrix Micro-Environmental PH to Achieve Sustained Drug Release from Highly Laminating Alginate Matrices. *Eur. J. Pharm. Sci.* **2008**, *33* (4–5), 361–370. https://doi.org/10.1016/J.EJPS.2008.01.007.

(37) Giles, R. G. F.; Green, I. R.; Mitchell, P. R. K.; Raston, C. L.; White, A. H. Epoxidation of 1,4-Dihydro-1,4-Methanoanthraquinones. Photochemistry and Crystal Structure Determination of the Products. *J. Chem. Soc. Perkin Trans. 1* **1979**, 719. https://doi.org/10.1039/p19790000719.

(38) Marchand, A. P.; Dong, E. Z.; Bott, S. G. Synthesis and Acid- and Base-Promoted Ring Opening of Polycarbocyclic Oxiranes. *Tetrahedron* **1998**, *54* (18), 4459–4470. https://doi.org/10.1016/S0040-4020(98)00162-8.

(39) Paquette, L. A.; Bellamy, F.; Bohm, M. C.; Gleiter, R. Electronic Control of Stereoselectivity. 6. Directionality of Singlet Oxygen Addition to 1,4-Dimethoxynaphthalenes Laterally Fused to Bridged Bicyclic Systems. *J. Org. Chem.* **1980**, *45* (24), 4913–4921. https://doi.org/10.1021/jo01312a019.

(40) Valderrama, J. A.; Espinoza, O.; González, M. F.; Tapia, R. A.; Rodríguez, J. A.; Theoduloz, C.; Schmeda-Hirschmann, G. Studies on Quinones. Part 40: Synthesis and Cytotoxicity Evaluation of Anthraquinone Epoxides and Isomerization Products. *Tetrahedron* **2006**, *62* (11), 2631–2638.

https://doi.org/10.1016/j.tet.2005.12.038.

(41) Huynh, M. T.; Anson, C. W.; Cavell, A. C.; Stahl, S. S.; Hammes-Schiffer, S. Quinone 1 E- and 2 e-/2 H+ Reduction Potentials: Identification and Analysis of Deviations from Systematic Scaling Relationships. *J. Am. Chem. Soc.* **2016**, *138* (49), 15903–15910. https://doi.org/10.1021/jacs.6b05797.

(42) Wendlandt, A. E.; Stahl, S. S. Quinone-Catalyzed Selective Oxidation of Organic Molecules. *Angew. Chemie - Int. Ed.* **2015**, *54* (49), 14638–14658. https://doi.org/10.1002/anie.201505017.

(43) Zhao, Y.; He, Y.; Swager, T. M. Porous Organic Polymers via Ring Opening Metathesis Polymerisation. *ACS Macro Lett.* **2018**, *7* (3), 300–304. https://doi.org/10.1021/acsmacrolett.8b00041.

(44) Derikvand, F.; Bigi, F.; Maggi, R.; Piscopo, C. G.; Sartori, G. Oxidation of Hydroquinones to Benzoquinones with Hydrogen Peroxide Using Catalytic Amount of Silver Oxide under Batch and Continuous-Flow Conditions. *J. Catal.* **2010**, *271* (1), 99–103. https://doi.org/10.1016/J.JCAT.2010.02.015.

(45) Suzuki, T.; Yamashita, Y.; Mukai, T.; Miyashi, T. Photocyclization of Norbornadienes Fused with Quinone Units. *Tetrahedron Lett.* **1988**, *29* (12), 1405–1408. https://doi.org/10.1016/S0040-4039(00)80309-3.

(46) Maruyama, Kazuhiro; Terada, Kazutoshi; Yamamoto, Y. Exploitation of Solar Energy Storage Systems Table I. Photochemical Isomerization of La to 2a in the Presence of Copper(I)-Nitrogen Ligand Catalysts0. *J. Org. Chem* **1981**, *46*, 5294–5300.

(47) Bren', V. A.; Dubonosov, A. D.; Minkin, V. I.; Chernoivanov, V. A. Norbornadiene–quadricyclane — an Effective Molecular System for the Storage of Solar Energy. *Russ. Chem. Rev.* **1991**, *60* (5), 451–469. https://doi.org/10.1070/rc1991v060n05abeh001088.

(48) Gauβ, W.; Heitzer, H.; Petersen, S. Umsetzungen von Chinonen Mit Stickstoffhaltigen Heteroaromaten. *Justus Liebigs Ann. Chem.* **1973**, *764* (1), 131–144. https://doi.org/10.1002/jlac.19727640116.

(49) Ballesteros, Paloma; Claramunt, Rosa M.; Escolástico, Consuelo; Santa Maria, M. D. *Reaction of Pyrazole Addition to Quinones*; 1992; Vol. 57.

(50) Catalán, J.; Fabero, F.; Soledad Guijarro, M.; Claramunt, R. M.; Dolores Santa María, M.; de la Concepción, M.; Hernández Cano, F.; Elguero, J.; Sastre, R. Photoinduced Intramolecular Proton Transfer as the Mechanism of Ultraviolet Stabilizers: A Reappraisal. *J. Am. Chem. Soc.* **1990**, *112* (2), 747–759. https://doi.org/10.1021/ja00158a039.

(51) Escolástico, C.; Dolores Santa María, M.; María Claramunt, R.; Luisa jimeno, M.; Alkorta, I.; Foces-Foces, C.; Hernández Cano, F.; Elguero, J. Imidazole and Benzimidazole Addition to Quinones. Formation of Meso and d,l Isomers and Crystal Structure of the d,l Isomer of 2,3-Bis(Benzimidazol-1'-Yl)-1,4-Dihydroxybenzene. *Tetrahedron* **1994**, *50* (43), 12489–12510. https://doi.org/10.1016/S0040-4020(01)89555-7.

(52) KOUNO, K.; OGAWA, C.; SHIMOMURA, Y.; YANO, H.; UEDA, Y. O. Interaction of Imidazole Derivatives with Electron Acceptors. II. Reaction Products of Imidazole with p-Benzoquinone. *Chem. Pharm. Bull. (Tokyo).* **1981**, *29* (2), 301–307. https://doi.org/10.1248/cpb.29.301.

(53) Larrañaga, M. D.; Lewis, R. J.; Lewis, R. A. (Robert A.; Hawley, G. G. (Gessner G. *Hawley's Condensed*

Chemical Dictionary.

(54) Kumar, A.; Purkait, K.; Dey, S. K.; Sarkar, A.; Mukherjee, A. A Hydroquinone Based Palladium Catalyst for Room Temperature Nitro Reduction in Water. *RSC Adv.* **2014**, *4* (66), 35233–35237. https://doi.org/10.1039/C4RA06547F.

(55) Grandberg, I. I.; Kost, A. N. No Title. *Zh. Obs. Khim.* **1959**, *29* (4), 1099.

(56) Thiele, J.; Meisenheimer, J. Ueber Die Addition von Blausäure an Chinon. *Berichte der Dtsch. Chem. Gesellschaft* **1900**, *33* (1), 675–676. https://doi.org/10.1002/cber.190003301115.

(57) Wallenfels, K.; Bachmann, G.; Hofmann, D.; Kern, R. Cyansubstituierte Chinone—II : 2,3-, 2,5- 2,6-Dicyanchinone Und Tetracyanbenzochinon. *Tetrahedron* **1965**, *21* (9), 2239–2256. https://doi.org/10.1016/S0040-4020(01)93879-7.

(58) Wagner, M.; Biani, F. F. de; Margraf, G.; Lerner, H.-W.; Schiemann, O.; Kretz, T.; Bats, J. W.; Boltea, M.; Dürner, G.; Zanello, P. Redox Behaviour of Pyrazolyl-Substituted 1,4-Dihydroxyarenes: Formation of the Corresponding Semiquinones, Quinhydrones and Quinones. *Zeitschrift für Naturforsch. B* **2015**. https://doi.org/10.1515/znb-2006-0304.

(59) Bordwell, F. G.; Cripe, T. A.; Hughes, D. L. Nucleophilicity, Basicity, and the Brønsted Equation; 1987; pp 137–153. https://doi.org/10.1021/ba-1987-0215.ch009.

(60) Bailey, P. J.; Lorono-Gonzales, D.; McCormack, C.; Millican, F.; Parsons, S.; Pfeifer, R.; Pinho, P. P.; Rudolphi, F.; Sanchez Perucha, A. Reaction of Azole Heterocycles with Tris(Dimethylamino)Borane, a New Method for the Construction of Tripodal Borate-Centred Ligands. *Chem. – A Eur. J.* **2006**, *12* (20), 5293–5300. https://doi.org/10.1002/chem.200501323.

(61) Petrosyan, V. A.; Burasov, A. V. Arenium Cation as the Key Intermediate of the Electrosynthesis of N-(2,5-Dimethoxyphenyl)Azoles. A New Approach to the Synthesis of N-(Dimethoxyphenyl)Azoles. *Russ. Chem. Bull.* **2007**, *56* (11), 2175–2183. https://doi.org/10.1007/s11172-007-0342-3.

(62) Hennis, A. D.; Polley, J. D.; Long, G. S.; Sen, A.; Yandulov, D.; Lipian, J.; Benedikt, G. M.; Rhodes, L. F.; Huffman, J. Novel, Efficient, Palladium-Based System for the Polymerisation of Norbornene Derivatives: Scope and Mechanism. *Organometallics* **2001**, *20* (13), 2802–2812. https://doi.org/10.1021/om010232m.

(63) Li Ding, †; Fabrizia Fabrizi de Biani, ‡; Michael Bolte, §; Piero Zanello, ‡; and Matthias Wagner*, †. Reactivity of Ferrocenylboranes: Rearrangements versus Electron Transfer Reactions. **2000**. https://doi.org/10.1021/OM000727W.

(64) Dinnebier, R.; Lerner, H.-W.; Ding, L.; Shankland, K.; David, W. I. F.; Stephens, P. W.; Wagner, M. One-Dimensional Spin Chains from CuII Ions and 2,5-Bis(Pyrazol-1-Yl)-1,4-Dihydroxybenzene. *Zeitschrift für Anorg. und Allg. Chemie* **2002**, *628* (1), 310–314. https://doi.org/10.1002/1521-3749(200201)628:1<310::AID-ZAAC310>3.0.CO;2-3.

(65) Kamatchi, T. S.; Kalaivani, P.; Fronczek, F. R.; Natarajan, K.; Prabhakaran, R. Impact of Chelation on Anticancer Activities of Organometallic Ruthenium(Ii) Complexes Containing 2,5-Di(1H-Pyrazol-1-Yl)-1,4-Benzoquinone: Synthesis, Structure, DNA/Protein Binding, Antioxidant Activity and Cytotoxicity. *RSC Adv.* **2016**, *6* (52), 46531–46547. https://doi.org/10.1039/C6RA05867A.

(66) Margraf, G.; Kretz, T.; Fabrizi de Biani, F.; Laschi, F.; Losi, S.; Zanello, P.; W. Bats, J.; Wolf, B.; Remović-Langer, K.; Lang, M.; et al. Mono-, Di-, and Oligonuclear Complexes of CuII Ions and p-Hydroquinone Ligands: Syntheses, Electrochemical Properties, and Magnetic Behavior. *Inorg. Chem.* **2006**, *45* (3), 1277–1288. https://doi.org/10.1021/ic051016z.

(67) Kumbhakar, D.; Sarkar, B.; Maji, S.; Mobin, S. M.; Fiedler, J.; Urbanos, F. A.; Jiménez-Aparicio, R.; Kaim, W.; Lahiri, G. K. Intramolecular Valence and Spin Interaction in *Meso* and *Rac* Diastereomers of a *p* -Quinonoid-Bridged Diruthenium Complex. *J. Am. Chem. Soc.* **2008**, *130* (51), 17575–17583. https://doi.org/10.1021/ja807043s.

(68) Devereux, M.; Curran, M.; McCann, M.; Casey, M. T.; McKee, V.; McKee, V. Synthesis and Catalase Activity of Manganese(II) Complexes of Cis-5-Norbornene-Endo-2,3-Dicarboxylic Acid (NdaH2): X-Ray Crystal Structure of [Mn(H1η1-Nda)(Phen)2]·EtOH·H2O (Phen = 1,10-Phenantholine). *Polyhedron* **1995**, *14* (15–16), 2247–2253. https://doi.org/10.1016/0277-5387(94)00492-W.

(69) Hartung, H.; Baumeister, U.; Kaplonek, R.; Fechtel, G. Synthese, Kristallstrukturen Und Spektroskopische Untersuchungen von 3d-Übergangsmetall-Komplexen Mit Bicyclo[2.2.1]Hept-5-En-2-Endo,3-Cis-Dicarbonsäure Und N,N-Donorliganden. *Zeitschrift für Anorg. und Allg. Chemie* **1993**, *619* (7), 1196–1202. https://doi.org/10.1002/zaac.19936190708.

(70) Xin, L.-Y.; et al., H.-B.; Guo, H. Crystal Structure of Aqua-Bis-(1,10-Phenanthroline)- (5-Norbornene-2,3-Dicarboxylic Acid)-Cadmium(II)-Hydrate, [Cd(C9H8O4)(C12H8N2)(H2O)]·(H2O), C42H40Cd2N4O12. *Zeitschrift für Krist. - New Cryst. Struct.* **2012**, *227* (3), 351–352. https://doi.org/10.1524/ncrs.2012.0167.

(71) Hai-Xia, W.; Hai-Yan, Z.; Ling-Yun, X. Crystal Structure of Diaquabis(Bicyclo[2.2.1]Hept-5-Ene-2,3-Dicarboxylate-K4O, O′:O′′,O′′′)Bis-(2,2′-Bipyridine-K2N, N′)Dicadmium(II) Hydrate. *Zeitschrift für Krist. - New Cryst. Struct.* **2016**, *231* (1), 101–103. https://doi.org/10.1515/ncrs-2015-0051.

(72) Baumeister, U.; Hartung, H.; IUCr. Bis(μ-Bicyclo[2.2.1]Hept-5-Ene-2- *Exo* ,3- *Exo* -Dicarboxylato-κ ^{2} *O* , *O* ':κ ^{2} *O* ' ', *O* ' ' ')Bis[Aqua(2,2'-Bipyridine- *N* , *N* ')Manganese(II)] Monohydrate. *Acta Crystallogr. Sect. C Cryst. Struct. Commun.* **1997**, *53* (9), 1246–1248. https://doi.org/10.1107/S0108270197004757.

(73) Yang, Y.-Q.; Li, W.; Chen, Z.-M.; Fu, L.-X. Crystal Structure and Properties of a New Copper(II) Complex Cu2(Phen)2[C7H8(COO)2]2 (H2O)4:5. *Zeitschrift für Naturforsch. B* **2012**, *67* (9), 872–876. https://doi.org/10.5560/znb.2012-0097.

(74) Yang, J.; Liu, X.; Wang, X.; Dai, F.; Zhou, Y.; Dong, B.; Zhang, L.; Liu, Y.; Sun, D. Syntheses, Crystal Structures, and Properties of Four Metal–Organic Complexes Based on 1,4,5,6,7,7-Hexachlorobicyclo[2.2.1]Hept-5-Ene-2,3-Dicarboxylic Acid. *Cryst. Growth Des.* **2015**, *15* (9), 4198–4205. https://doi.org/10.1021/acs.cgd.5b00164.

(75) Gao, E.; Ding, Y.; Sun, N.; Zhang, S.; Qiu, X.; Zhan, Y.; Zhu, M. Synthesis, Characterization, DNA Interaction, Apoptosis and Molecular Docking of Cu(II) and Mn(II) Complexes with *Endo* -Norbornene-*Cis* -5,6-Dicarboxylic Acid. *Appl. Organomet. Chem.* **2017**, *31* (3), e3575. https://doi.org/10.1002/aoc.3575.

(76) Gui-Lian, L.; Jia, S.; Yu-Ying, H. Hydrothermal Synthesis and Crystal Structure of Poly[Aqua-(M2-1,3-

Bis(4-Pyridyl)Propane-K2N:N′)-(M2-1,4,5,6,7,7-Hexachlorobicyclo[2.2.1]Hept-5-Ene-2,3-Dicarboxylato-K2O:O′)Manganese(II) Hydrate, C22H20Cl6N2O6Mn. *Zeitschrift für Krist. - New Cryst. Struct.* **2018**, *233* (1), 95–97. https://doi.org/10.1515/ncrs-2017-0187.

(77) Xin, L.; Liu, G.; Ma, L.; Li, G.; Wang, L. Guest Water-Controlled Reversible Crystalline-to-Amorphous Transition and Concomitant Fluorescence Shift in a Polar Open Coordination Polymer. *Inorganica Chim. Acta* **2016**, *443*, 64–68. https://doi.org/10.1016/J.ICA.2015.12.022.

(78) Hu, M.-L.; Zhu, N.-W.; IUCr. *Catena* -Poly[[[Aqua(1,10-Phenanthroline)Manganese(II)]-μ- *Endo* -Norbornene- *Cis* -5,6-Dicarboxylato] Monohydrate]. *Acta Crystallogr. Sect. E Struct. Reports Online* **2005**, *61* (6), m1105–m1107. https://doi.org/10.1107/S1600536805014017.

(79) Gao, E.; Sun, N.; Zhang, S.; Ding, Y.; Qiu, X.; Zhan, Y.; Zhu, M. Synthesis, Structures, Molecular Docking, Cytotoxicity and Bioimaging Studies of Two Novel Zn(II) Complexes. *Eur. J. Med. Chem.* **2016**, *121*, 1–11. https://doi.org/10.1016/J.EJMECH.2016.05.013.

(80) Hu, M. L.; Lü, Y. P.; Zhang, H. M.; Tu, B.; Jin, Z. M. Synthesis and Crystal Structure of Two Novel PbII Compounds of [Pb(Endc)2(Phen)]n and [Pb(Endc)(Phen) · 3H2O]2. *Inorg. Chem. Commun.* **2006**, *9* (9), 962–965. https://doi.org/10.1016/J.INOCHE.2006.06.009.

(81) Zevaco, T. A.; Görls, H.; Dinjus, E. Synthesis and Structural Characterisation of the Zinc Carboxylate Catena-[Monoaqua(Bicyclo [2,2,1]Hept-5-Ene-Cis-2,3-Dicarboxylato) Bis(1-Methylimidazole) Zinc(II)]. *Inorg. Chem. Commun.* **1998**, *1* (5), 170–173. https://doi.org/10.1016/S1387-7003(98)00046-X.

(82) Cui, P.-P.; Cui, L.-F.; Zhang, L.-L.; Sun, D.-F. Halogen Bonding in the Assembly of a 1D Cadmium(II) Polymer Based on Chlorendic Acid (HET). *Zeitschrift für Anorg. und Allg. Chemie* **2013**, *639* (7), 1269–1273. https://doi.org/10.1002/zaac.201300141.

(83) Zhang, B.; Zhang, J.; Liu, C.; Sang, X.; Peng, L.; Ma, X.; Wu, T.; Han, B.; Yang, G. Solvent Determines the Formation and Properties of Metal–organic Frameworks. *RSC Adv.* **2015**, *5* (47), 37691–37696. https://doi.org/10.1039/C5RA02440D.

(84) Cady, H. P.; Elsey, H. M. A General Definition of Acids, Bases, and Salts. *J. Chem. Educ.* **1928**, *5* (11), 1425. https://doi.org/10.1021/ed005p1425.

(85) Sánchez-Sánchez, M.; Getachew, N.; Díaz, K.; Díaz-García, M.; Chebude, Y.; Díaz, I. Synthesis of Metal–organic Frameworks in Water at Room Temperature: Salts as Linker Sources. *Green Chem.* **2015**, *17* (3), 1500–1509. https://doi.org/10.1039/C4GC01861C.

(86) Cheng, L.; Yang, J.; Saulat, H.; Li, L.; Lu, J.; Zhang, Y. Fabrication and Orientation of Ni-LAB Membranes by Linker Salt Approach. *Microporous Mesoporous Mater.* **2019**, *287*, 135–143. https://doi.org/10.1016/J.MICROMESO.2019.05.044.

(87) Li, J.; Cheng, S.; Zhao, Q.; Long, P.; Dong, J. Synthesis and Hydrogen-Storage Behavior of Metal–organic Framework MOF-5. *Int. J. Hydrogen Energy* **2009**, *34* (3), 1377–1382. https://doi.org/10.1016/J.IJHYDENE.2008.11.048.

(88) Yakovenko, A. A.; Reibenspies, J. H.; Bhuvanesh, N.; Zhou, H.-C.; IUCr. Generation and Applications of Structure Envelopes for Porous Metal–organic Frameworks. *J. Appl. Crystallogr.* **2013**, *46* (2), 346–353. https://doi.org/10.1107/S0021889812050935.

(89) Bosch, M.; Zhang, M.; Zhou, H.-C. Increasing the Stability of Metal-Organic Frameworks. *Adv. Chem.* **2014**, *2014*, 1–8. https://doi.org/10.1155/2014/182327.

(90) Himori, S.; Iuchi, K.; Numata, S. Cyclic Diketone Structure-Containing Chain Transfer Agents for Use in Manufacture of Polymers Bearing the Cyclic Diketone Structure with Freedom from the Malodor., May 12, 2014.

(91) Mitra, A. K.; Gawandi, V. B.; George, K.; Mohan, H.; Mukherjee, T. Investigations on the Antioxidant Activity of 5,8-Dihydroxy-1,4-Dihydro-1,4-Methanonaphthalene (DDMN). *Res. Chem. Intermed.* **2009**, *35* (1), 13–20. https://doi.org/10.1007/s11164-008-0007-3.

11 Appendix

11.1 Monomer synthesis

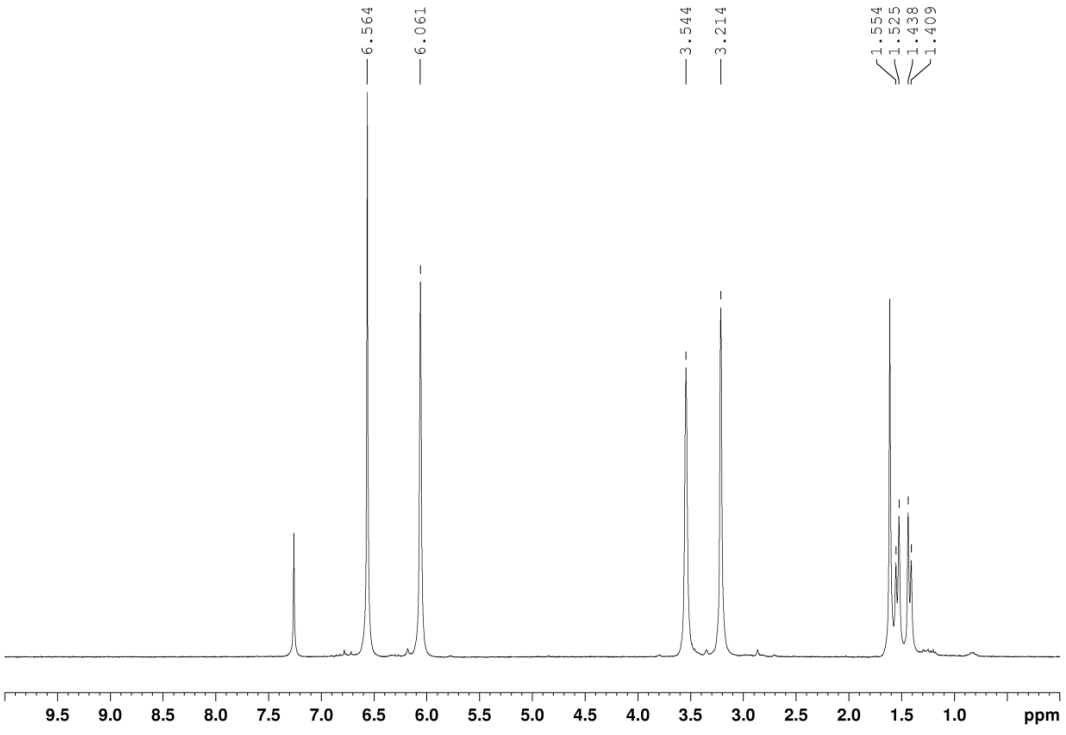

Figure 42 ^{1}H NMR spectrum of **1** in $CDCl_3$

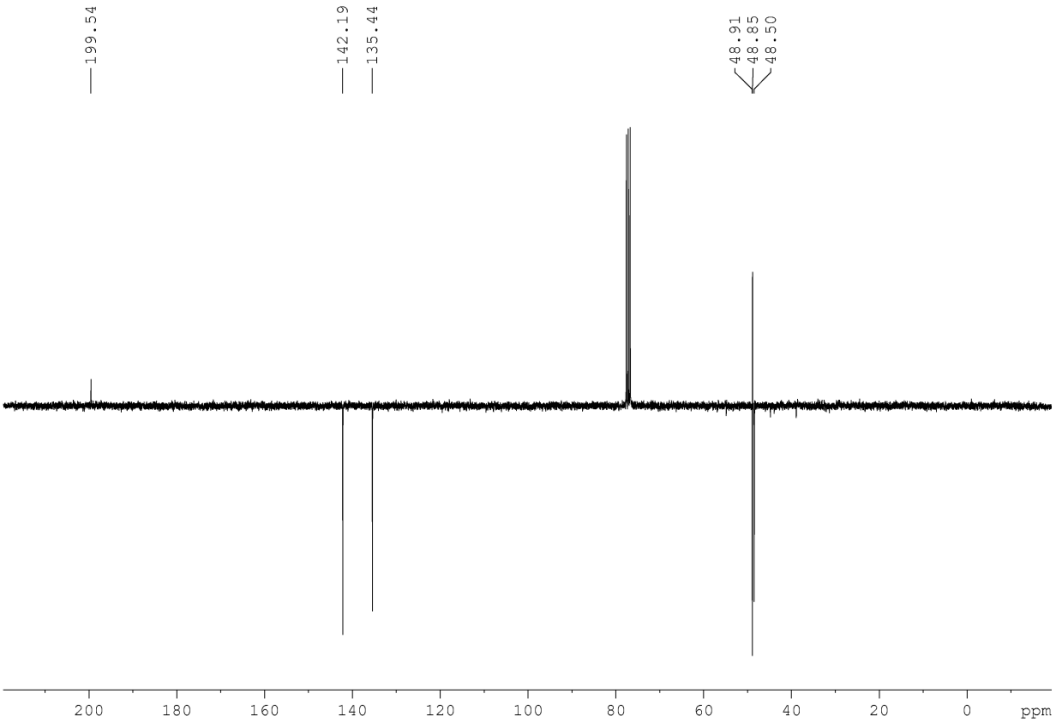

Figure 43 ^{13}C APT spectrum of **1** in $CDCl_3$

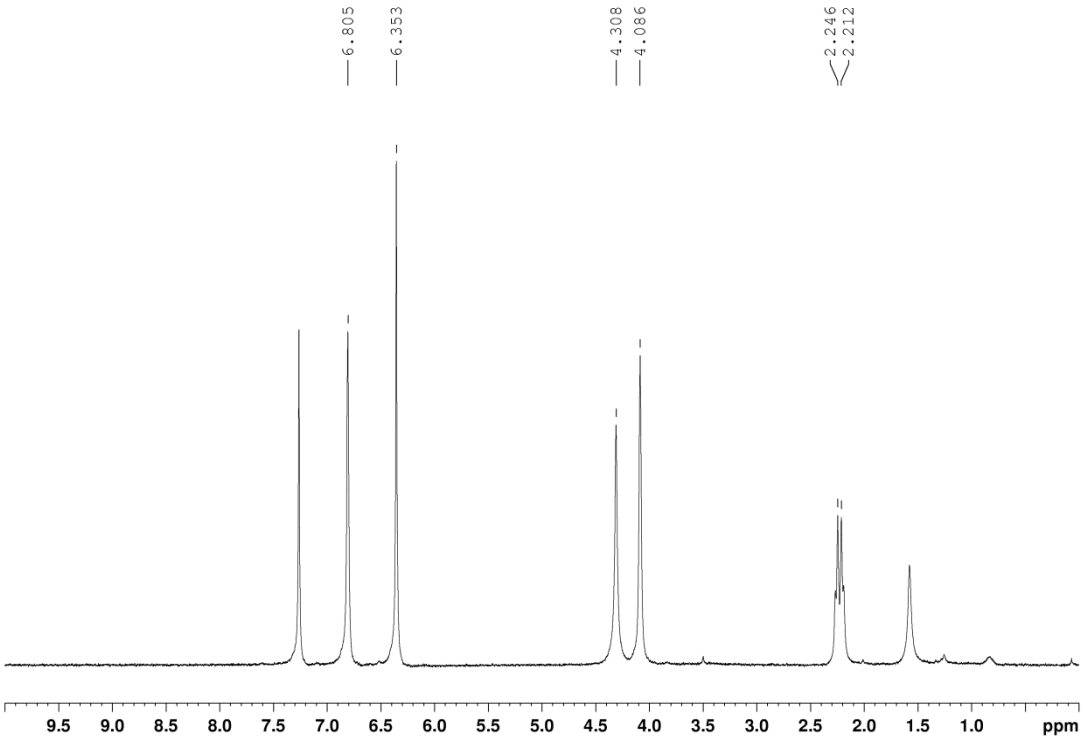

Figure 44 ^{1}H NMR spectrum of **2** in $CDCl_3$

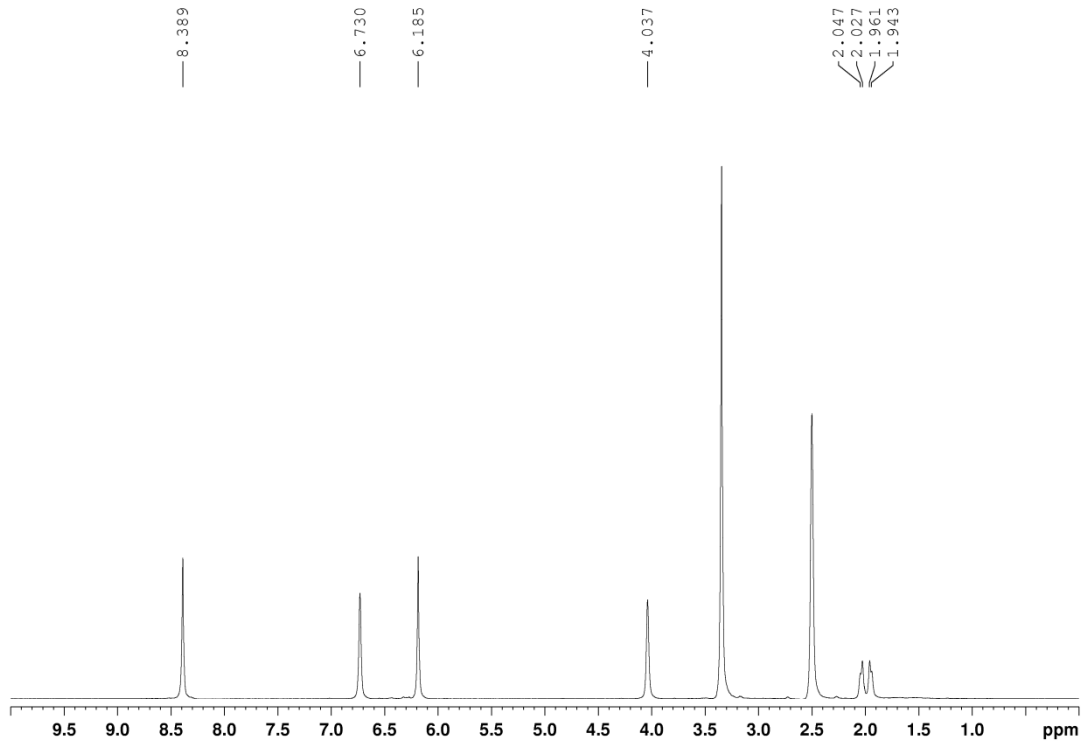

Figure 45 ^{1}H NMR spectrum of **2** in DMSO-d6

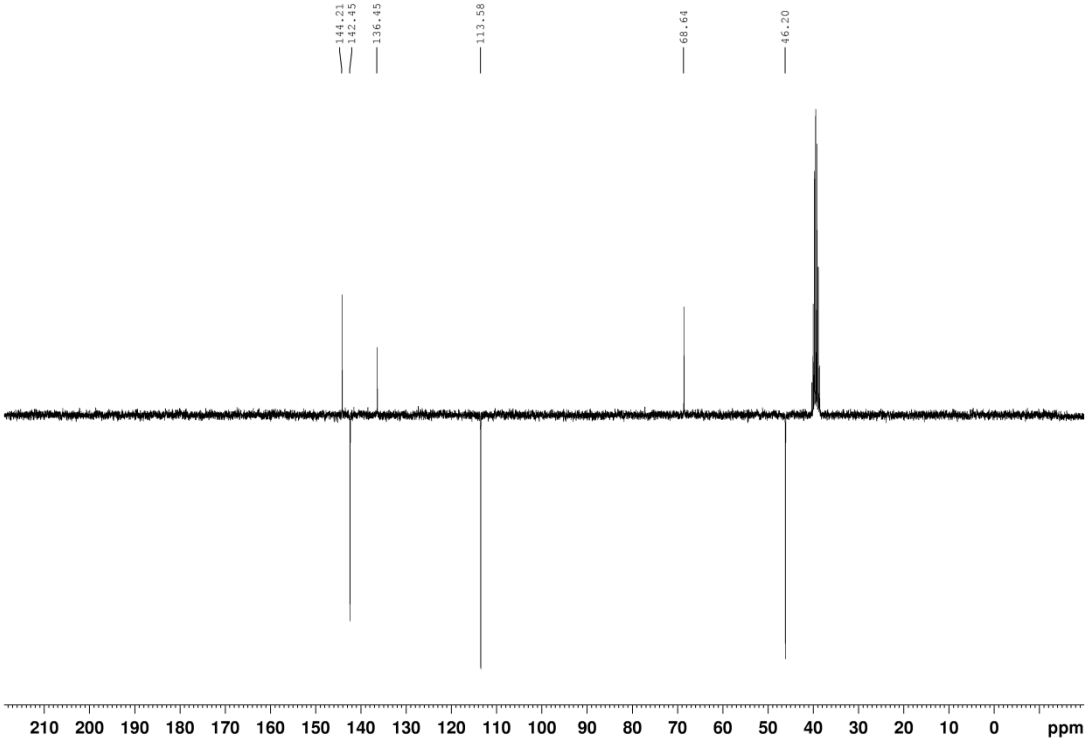

Figure 46 ^{13}C APT spectrum of **2** in DMSO-d6

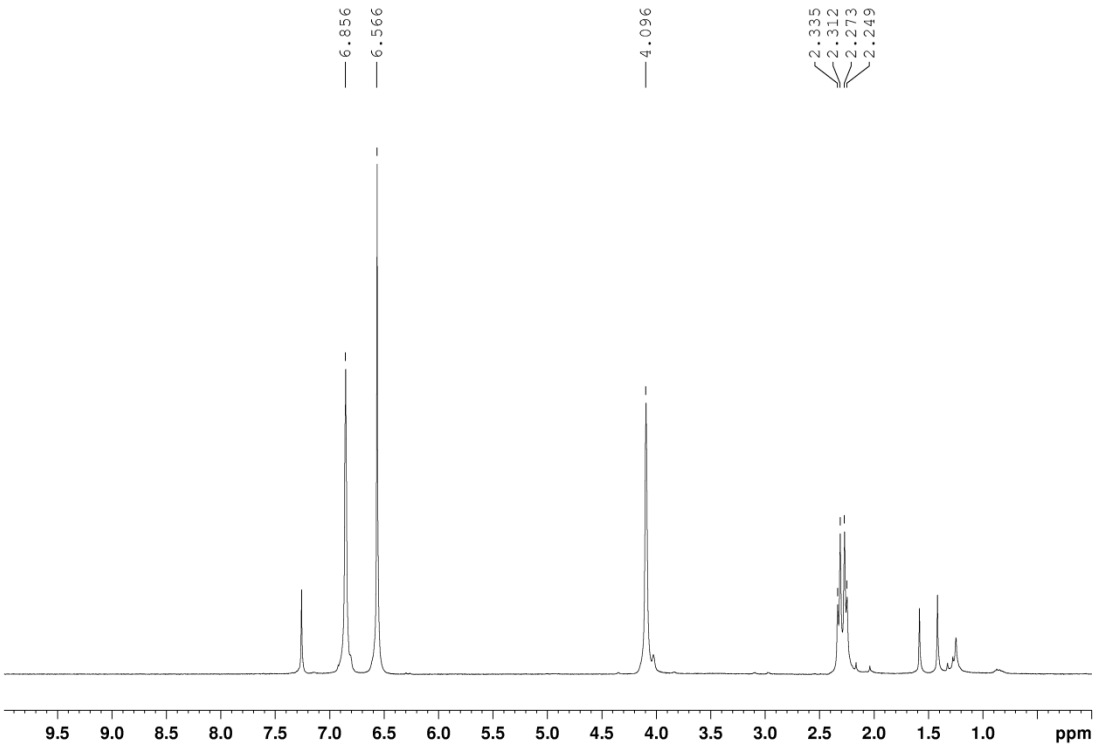

Figure 47 ^{1}H NMR spectrum of **3** in $CDCl_3$

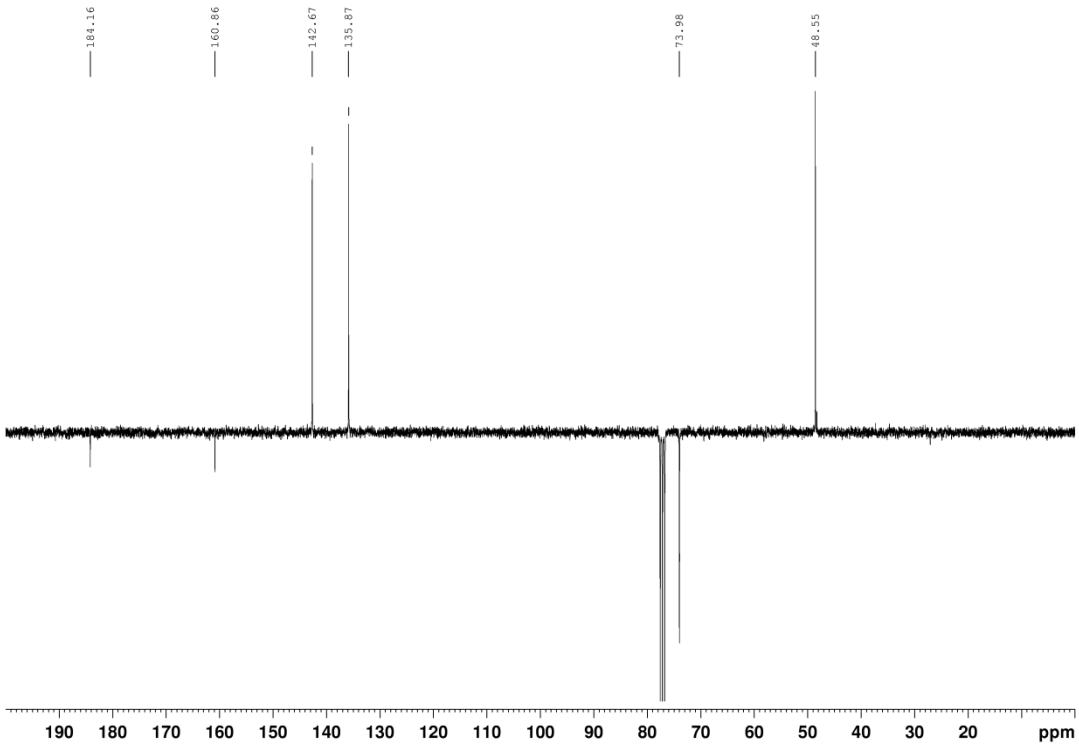

Figure 48 ^{13}C APT spectrum of **3** in $CDCl_3$

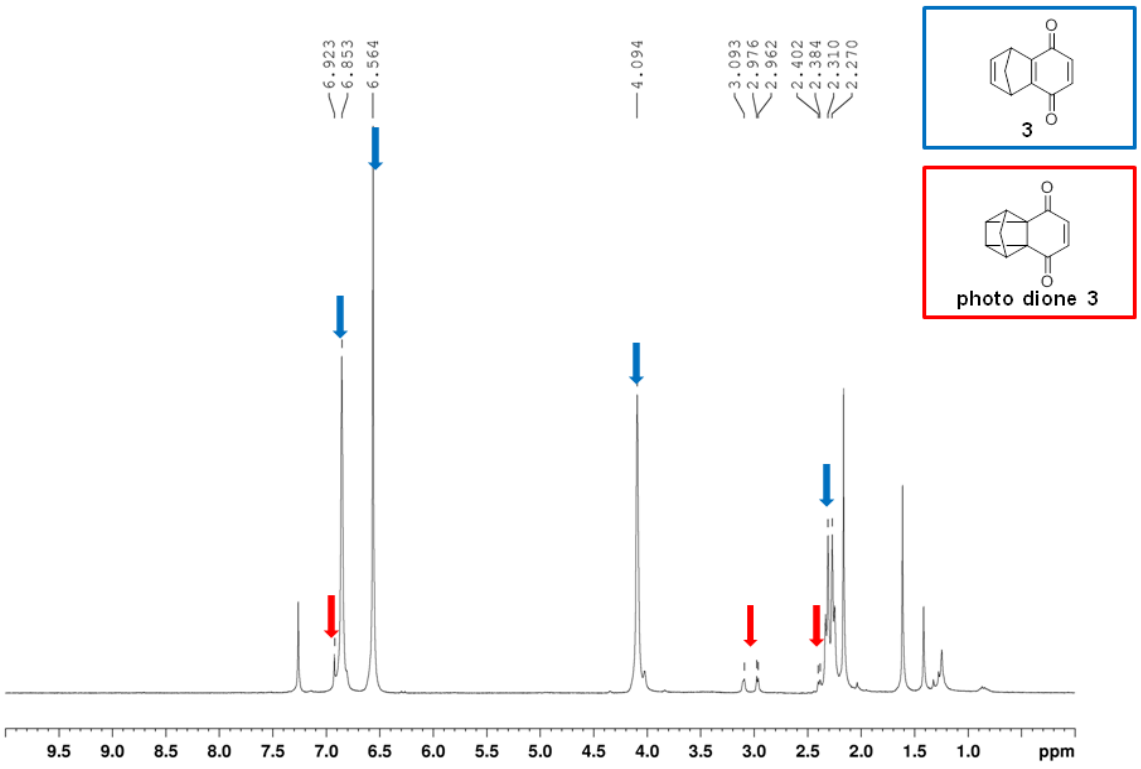

Figure 49 Formation of **photo dione 3** after storage of **3** in chloroform at visible light for 3 hours

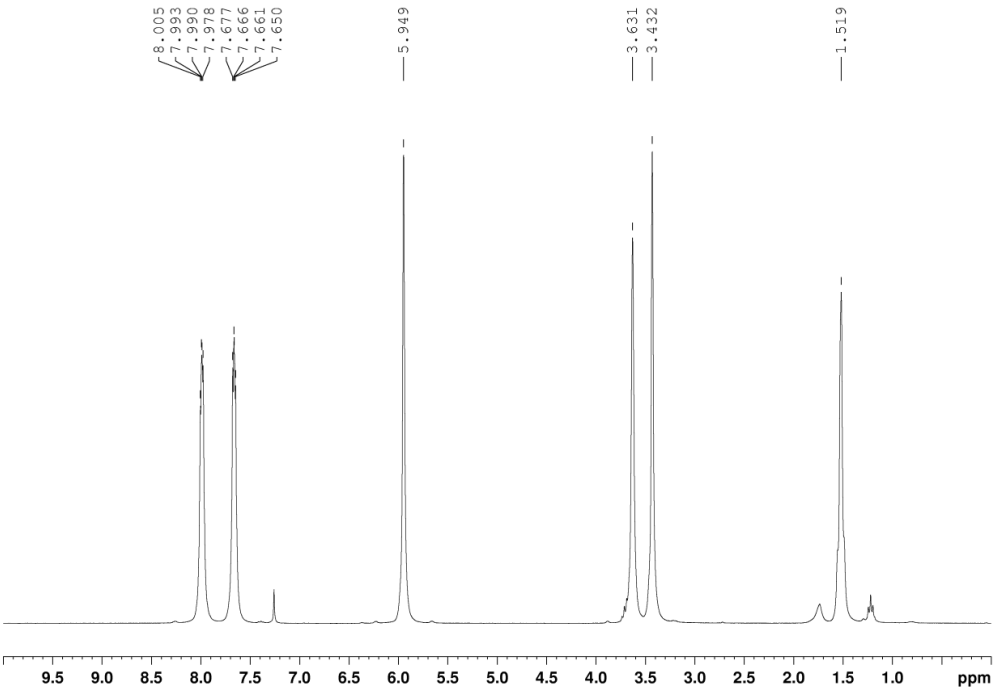

Figure 50 ^{1}H NMR spectrum of **4** in $CDCl_3$

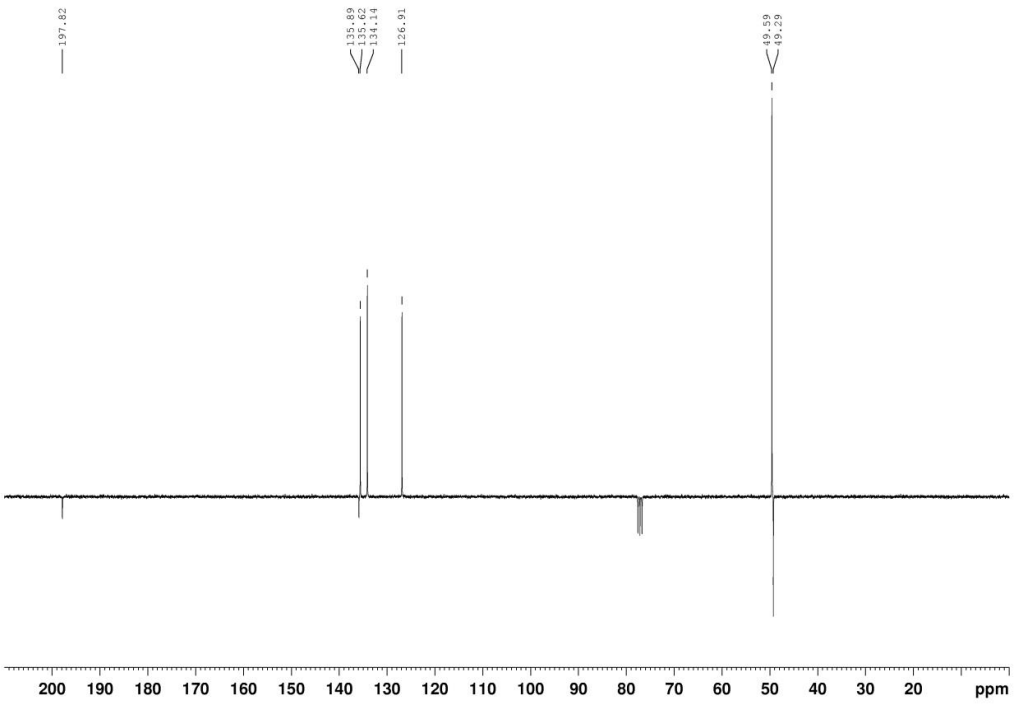

Figure 51 ^{13}C APT spectrum of **4** in $CDCl_3$

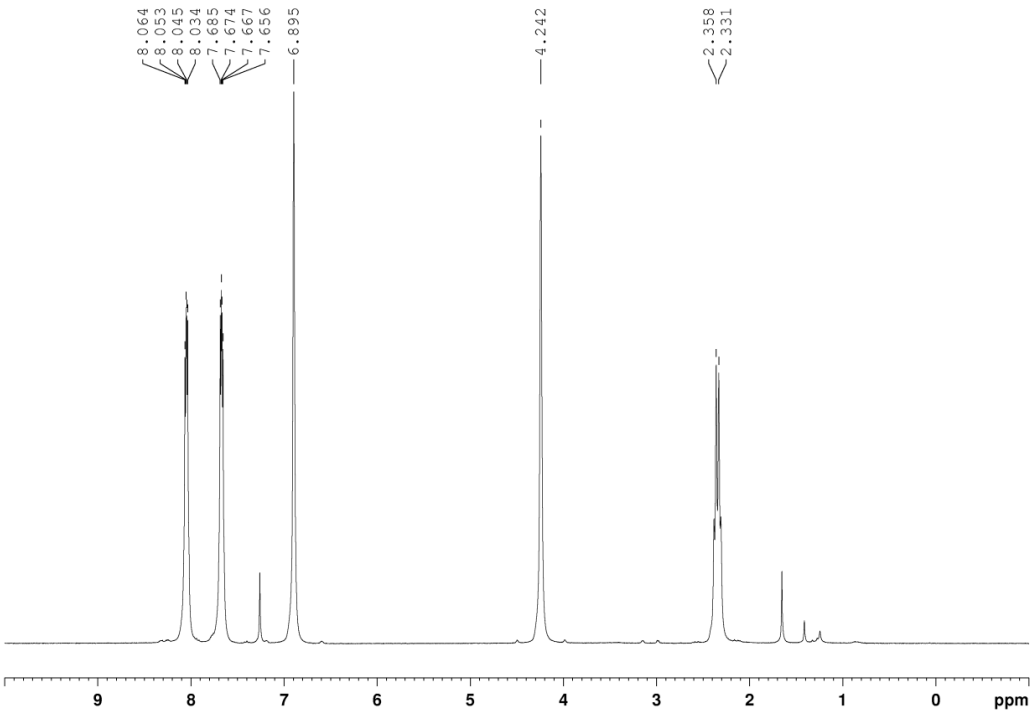

Figure 52 ^{1}H spectrum of **5** in $CDCl_3$

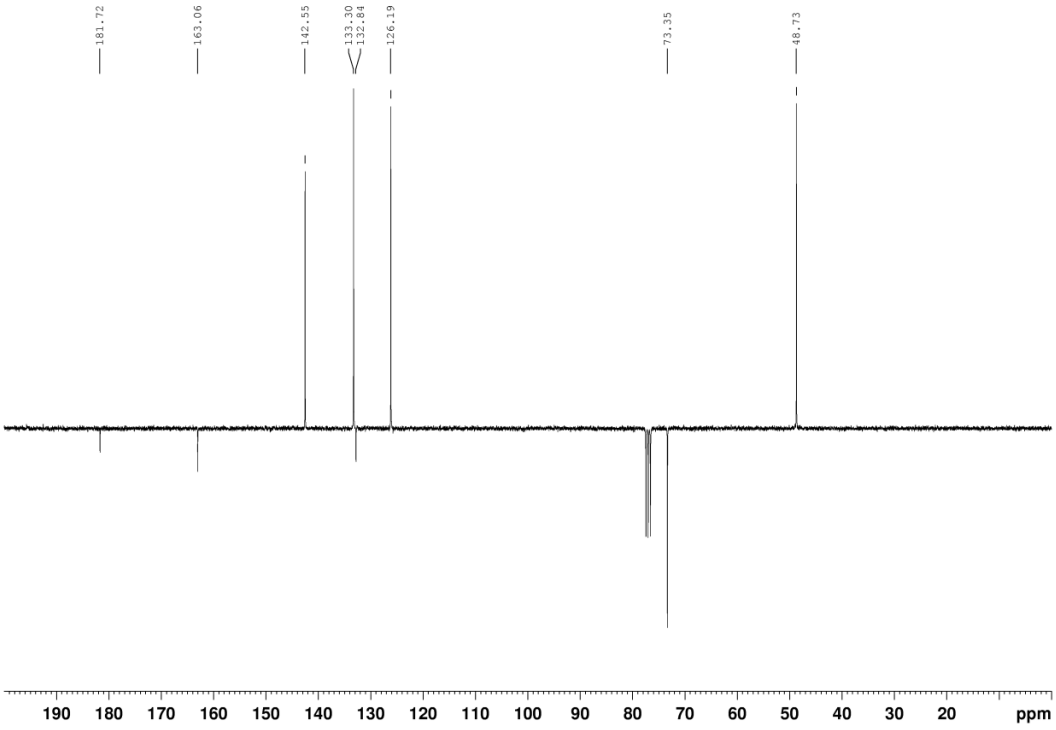

Figure 53 ^{13}C APT spectrum of **5** in $CDCl_3$

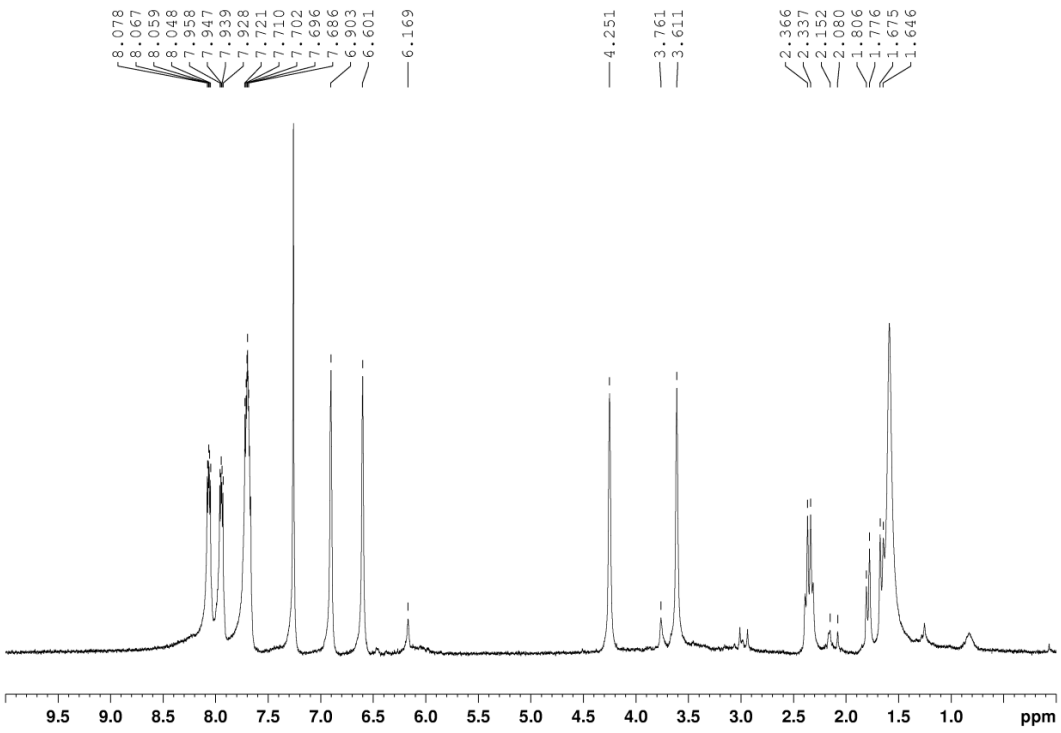

Figure 54 ^{1}H NMR spectrum of **5**, **6a** and **6b** in $CDCl_3$

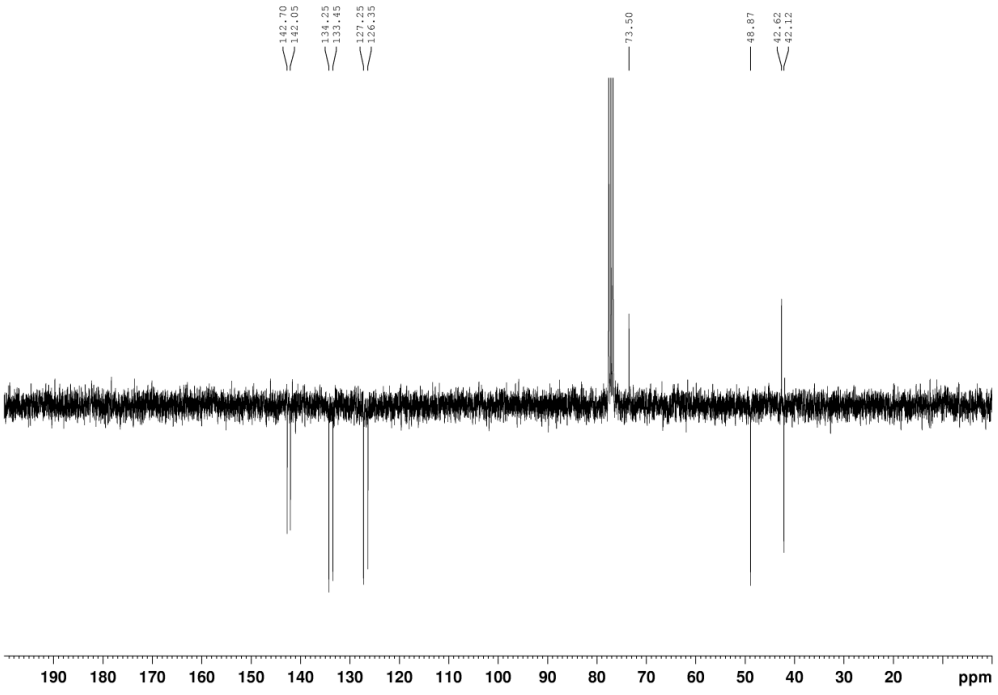

Figure 55 ^{13}C APT spectrum of **5**, **6a** and **6b** in $CDCl_3$

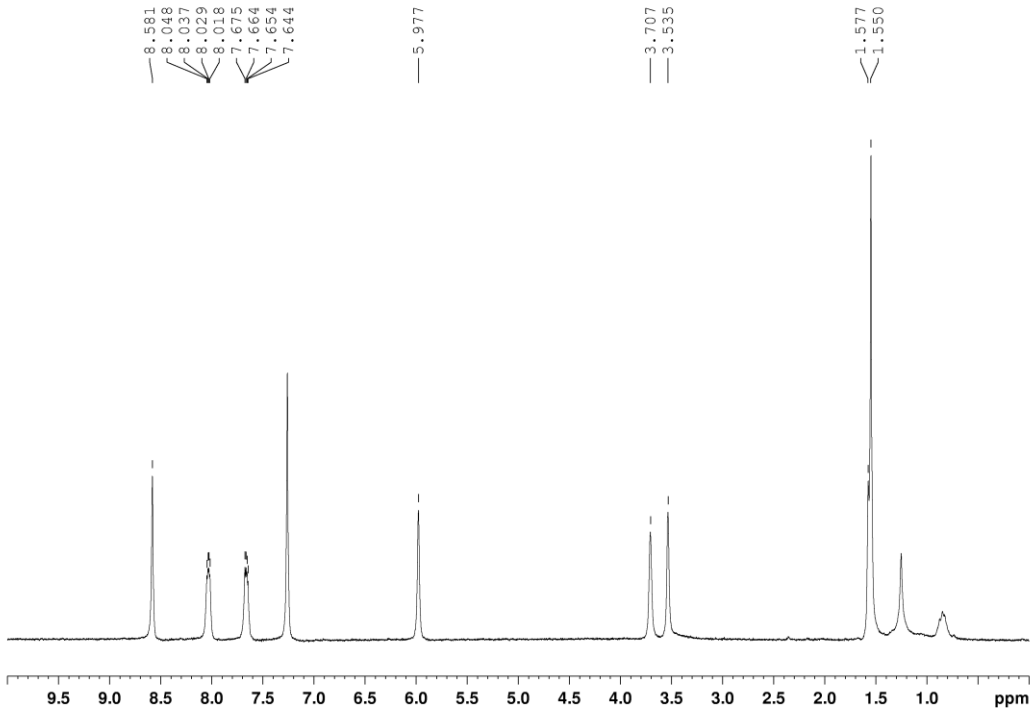

Figure 56 ^{1}H NMR spectrum of **7** in $CDCl_3$

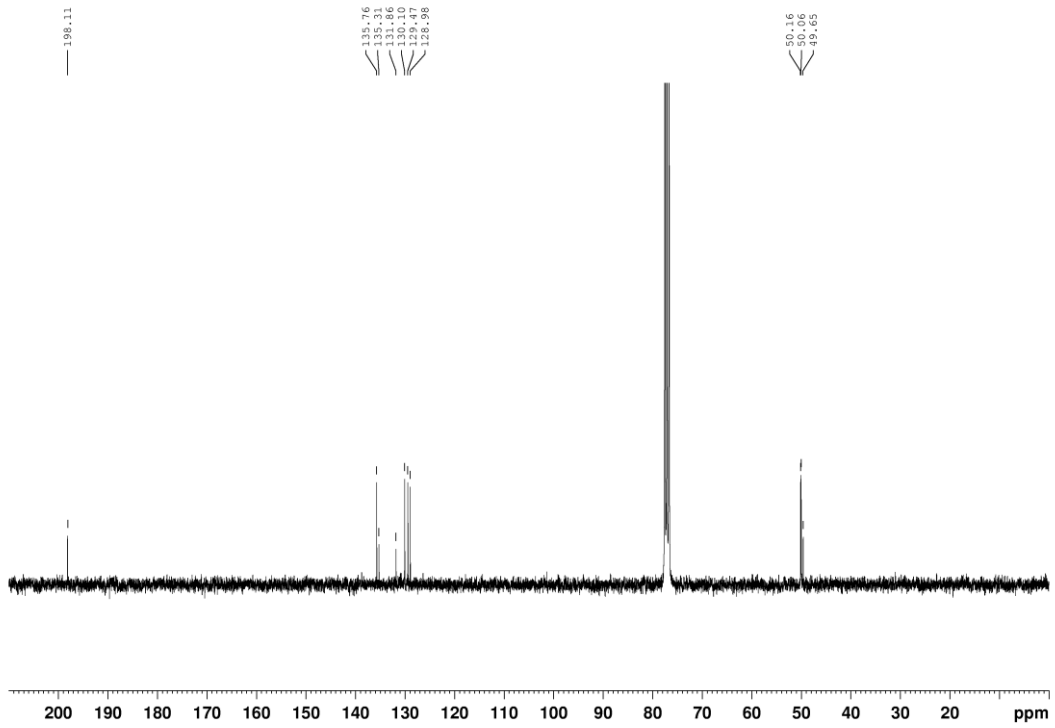

Figure 57 ^{13}C NMR spectrum of **7** in $CDCl_3$

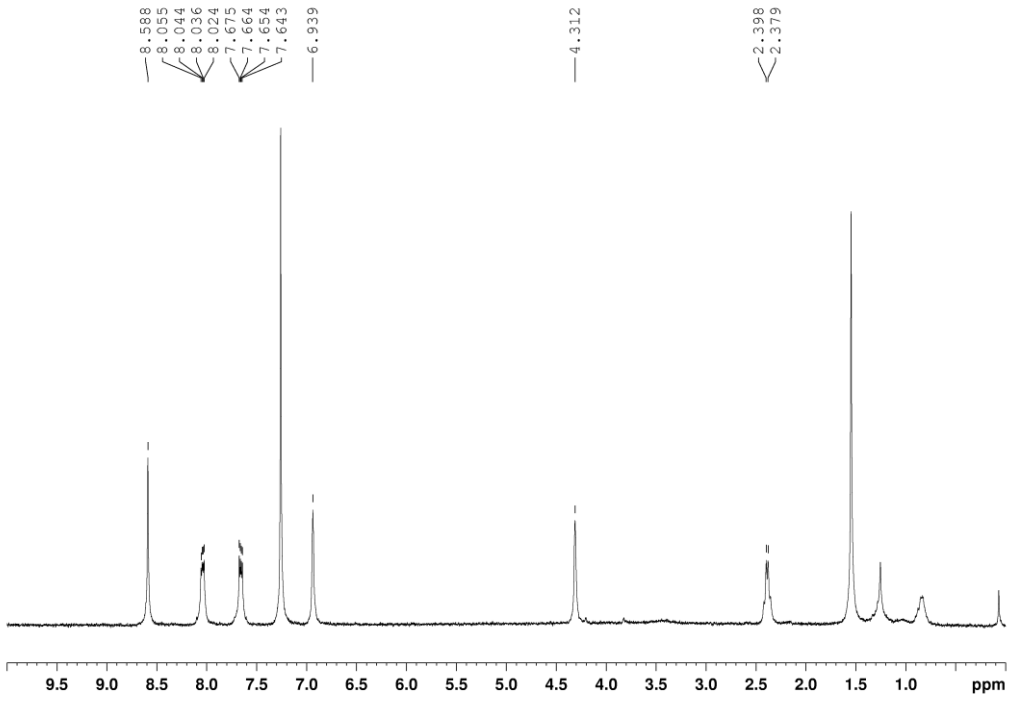

Figure 58 ^{1}H NMR spectrum of **8** in $CDCl_3$

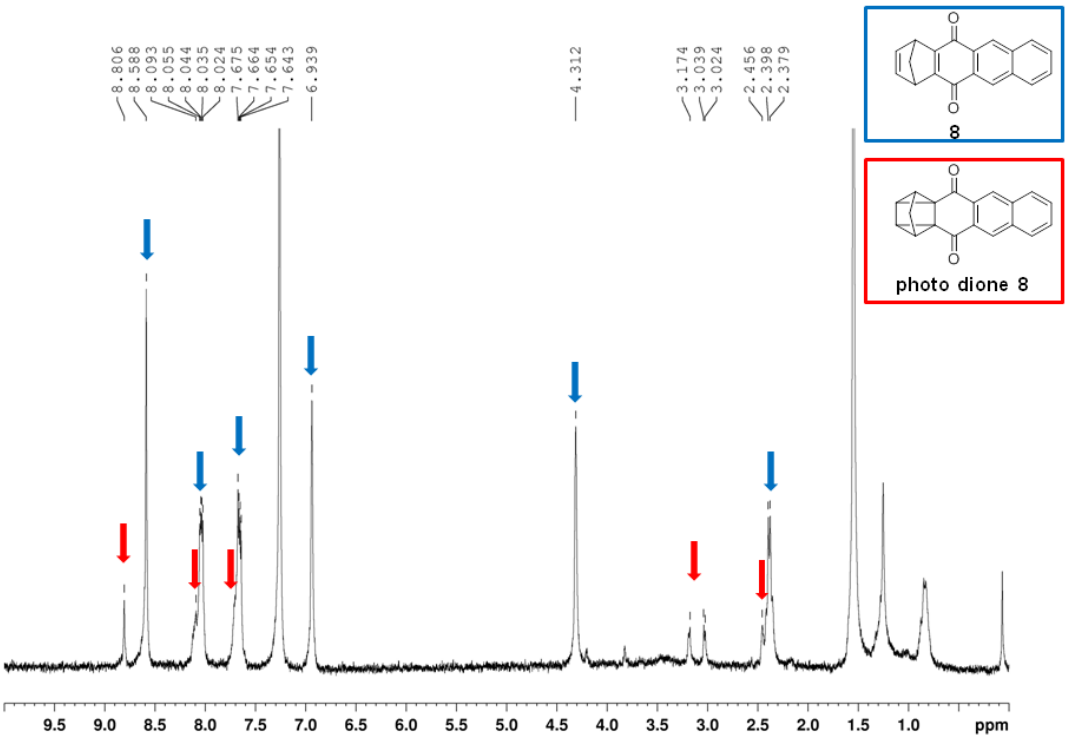

Figure 59 Formation of **photo dione 8** after storage of **8** in $CDCl_3$ at visible light for 3 hours

11.2 Polymers

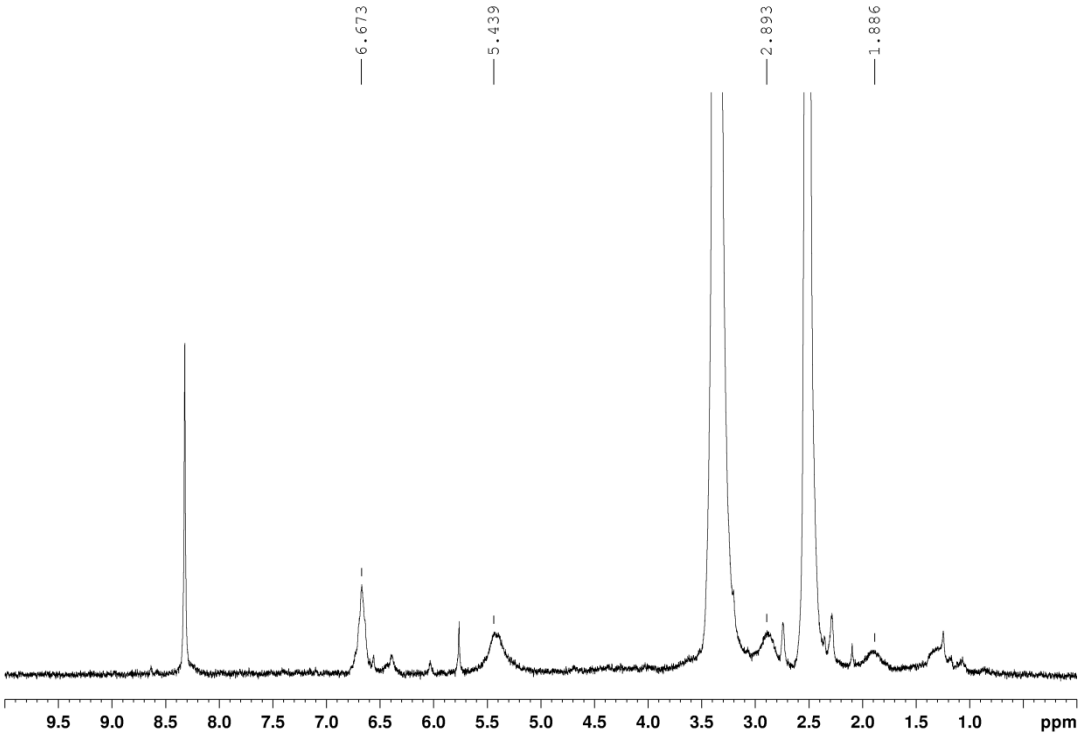

Figure 60 ^{1}H NMR of **poly1** in DMSO-d_6

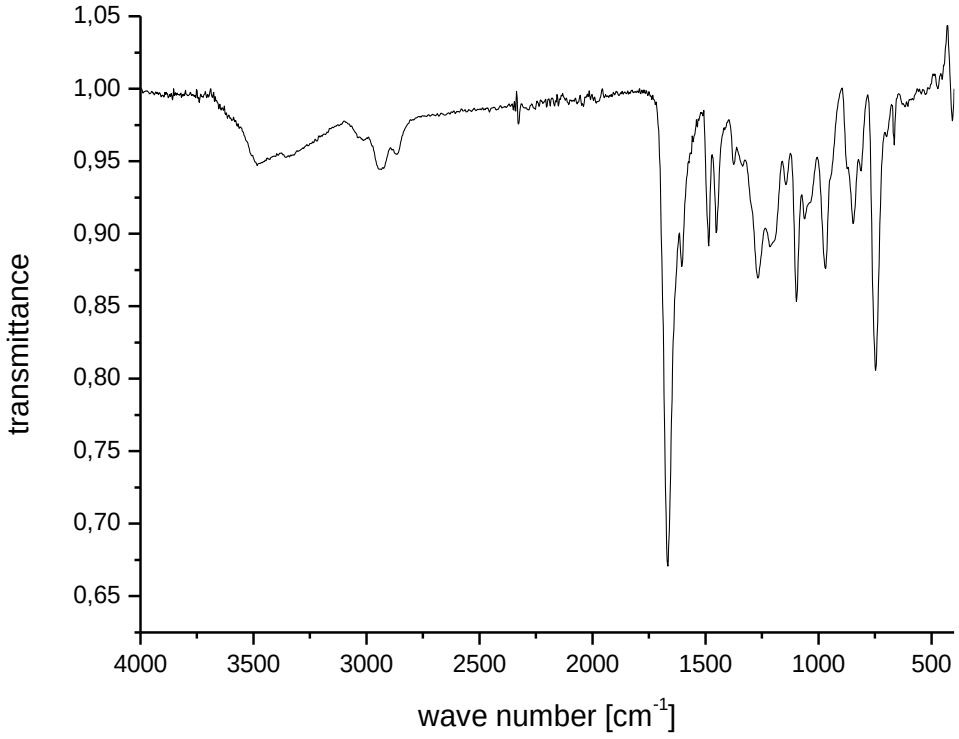

Figure 61 ATR-FTIR spectrum of **poly1**

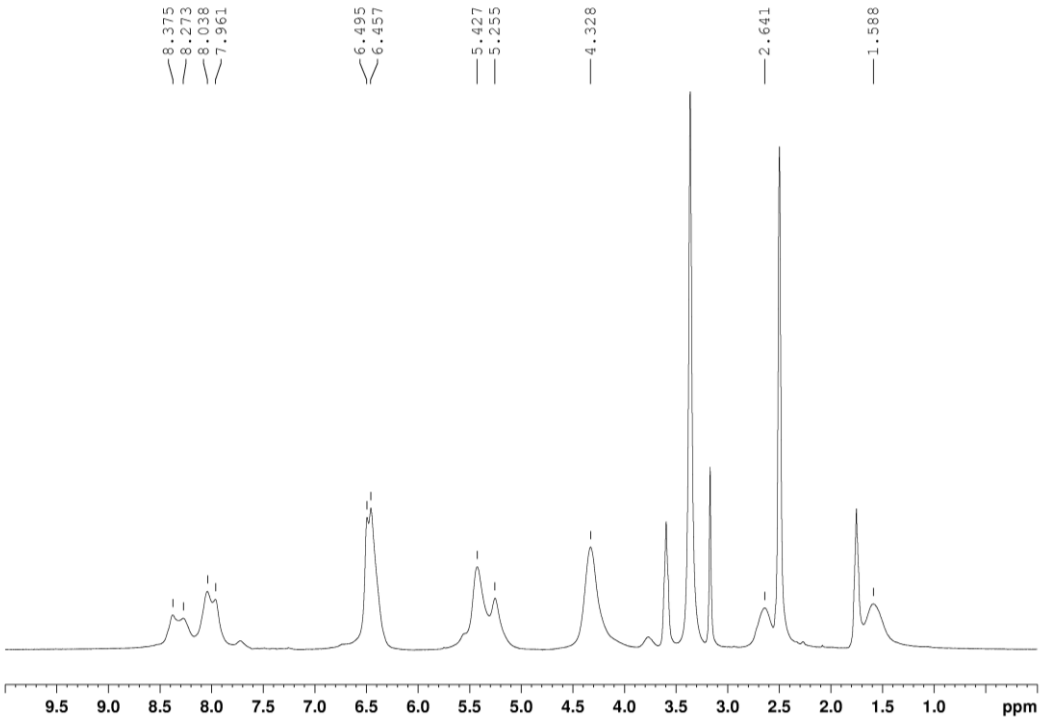

Figure 62 ^{1}H NMR spectrum of **poly2** in DMSO-d_6

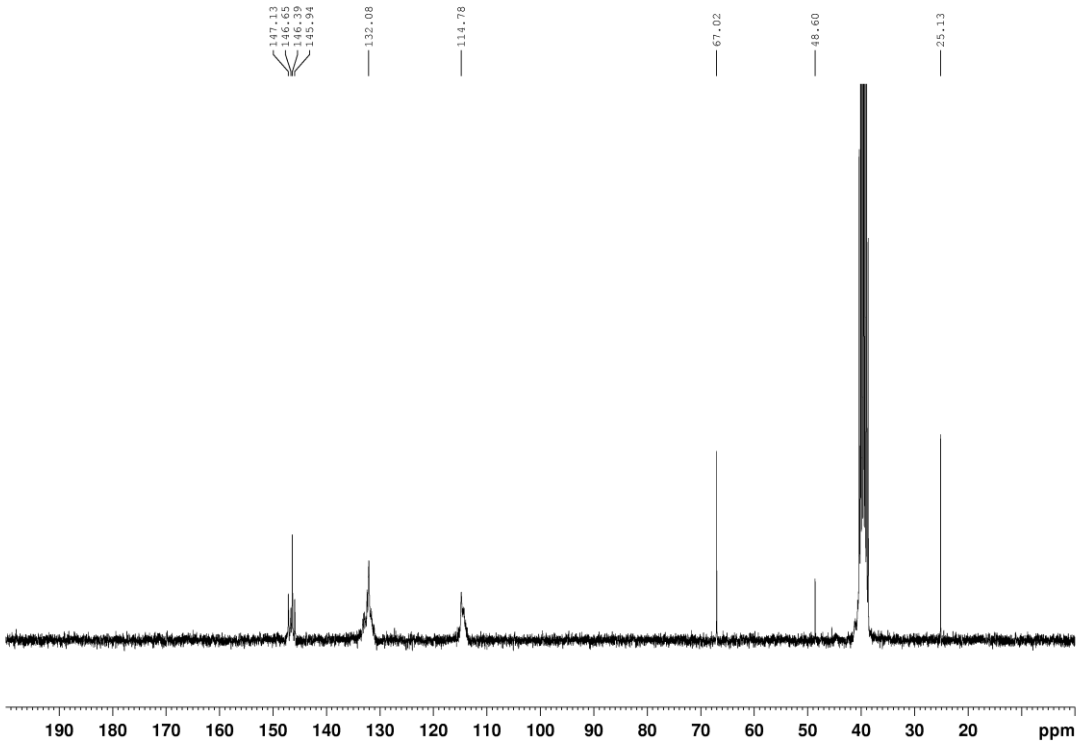

Figure 63 ^{13}C NMR spectrum of **poly2** in DMSO-d_6

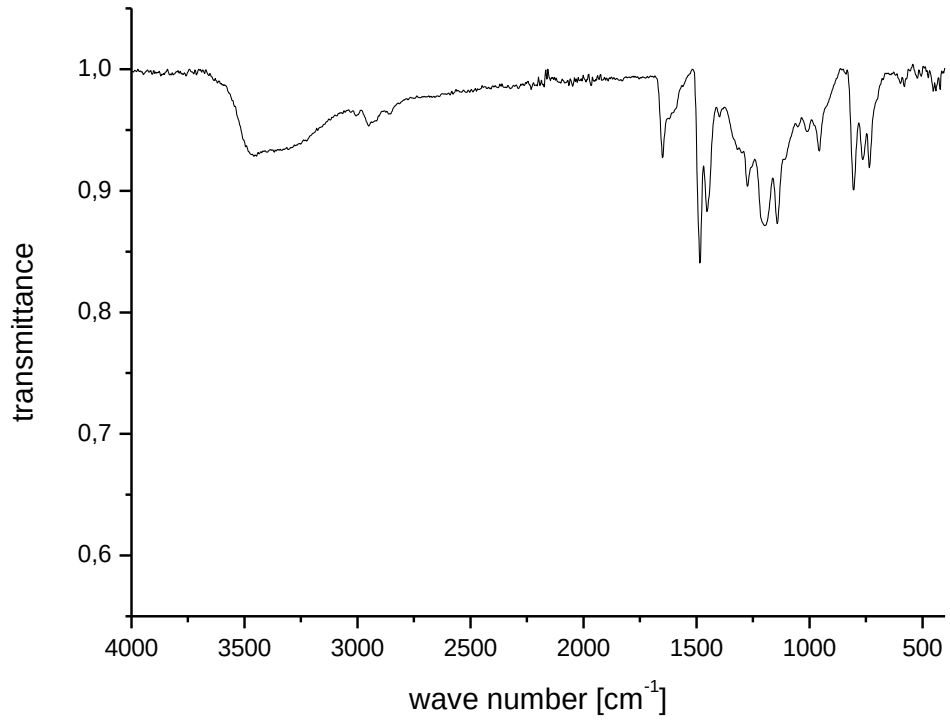

Figure 64 ATR-FTIR spectrum of **poly2**

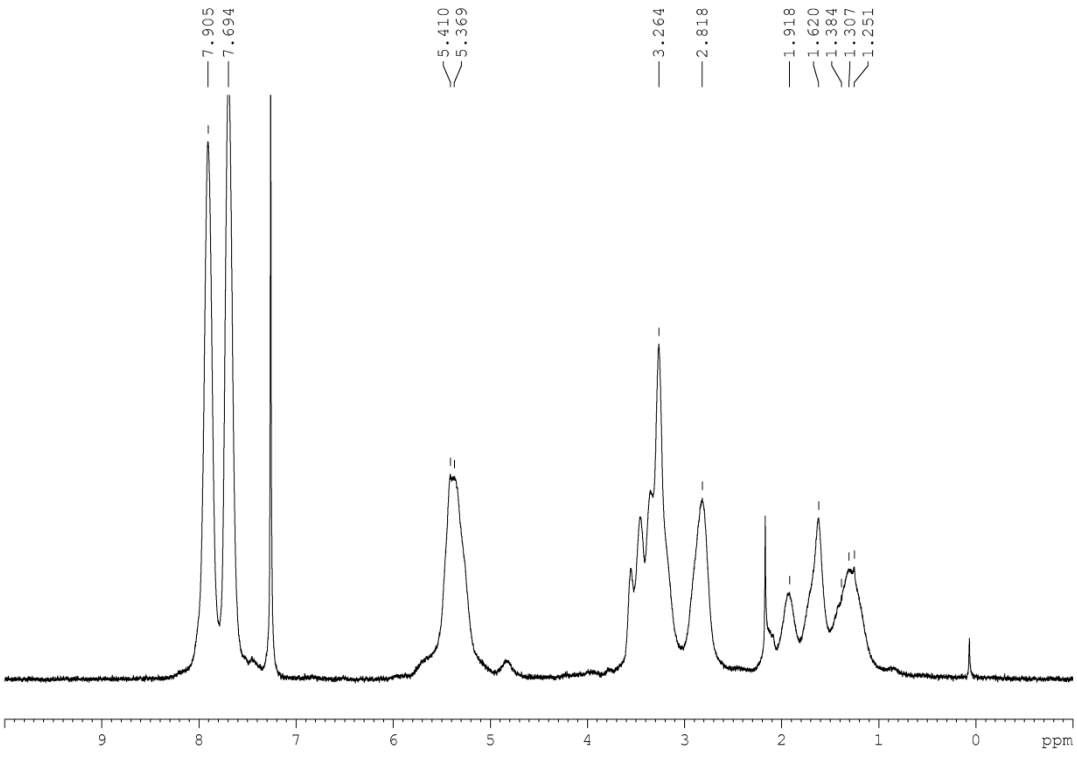

Figure 65 ^{1}H NMR spectrum of **poly4**in $CDCl_3$

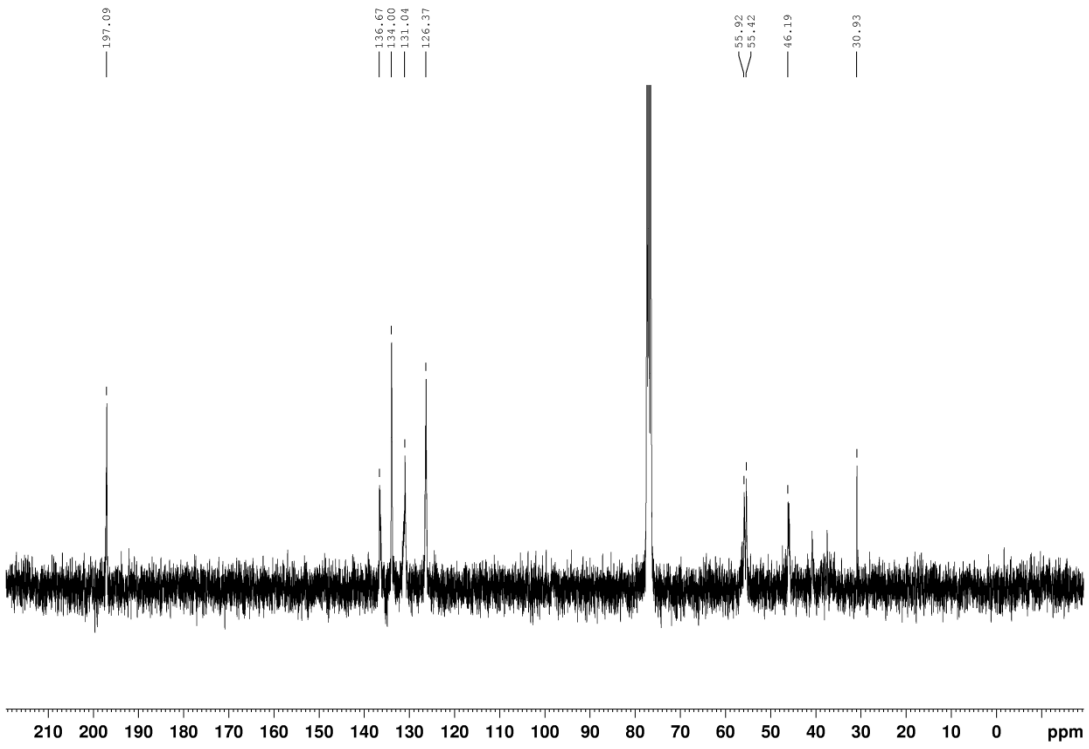

Figure 66 ^{13}C NMR spectrum of **poly4** in $CDCl_3$

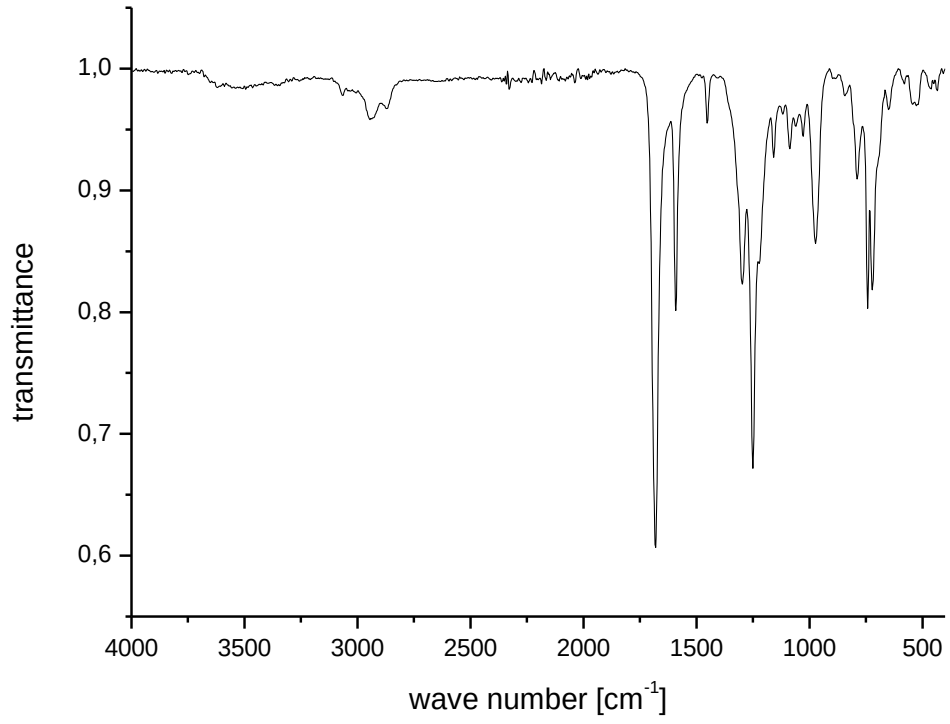

Figure 67 IR spectrum of **poly4**

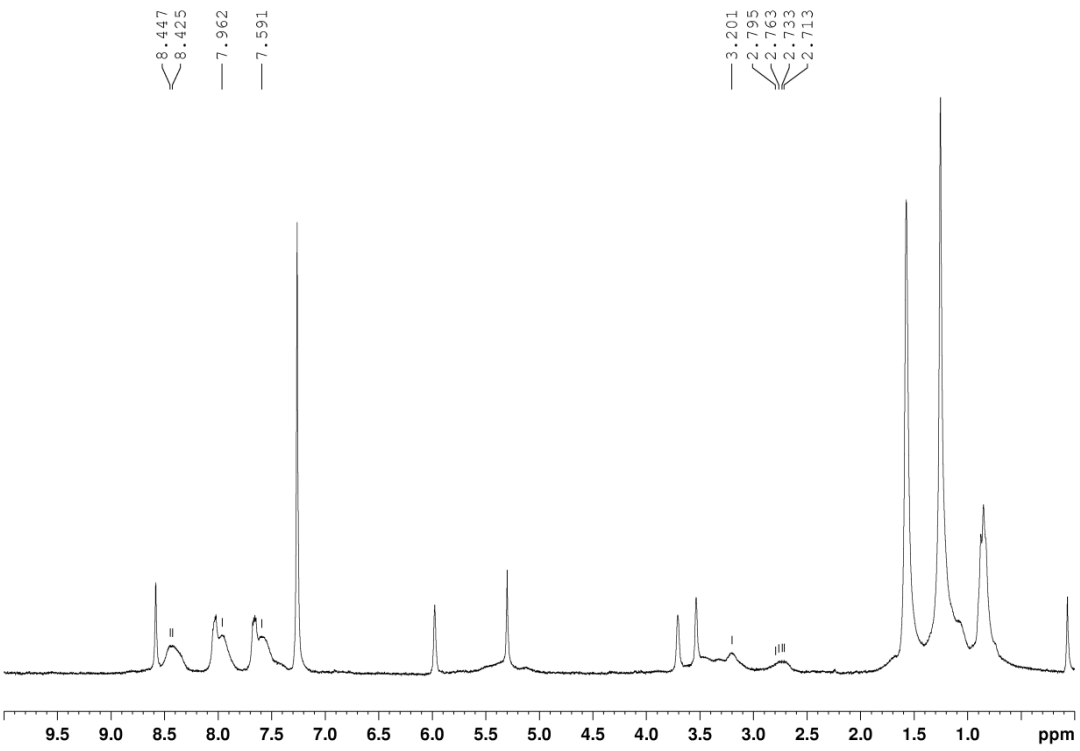

Figure 68 ^{1}H NMR spectrum of **poly7** in $CDCl_3$

11.3 Monomer functionalisation

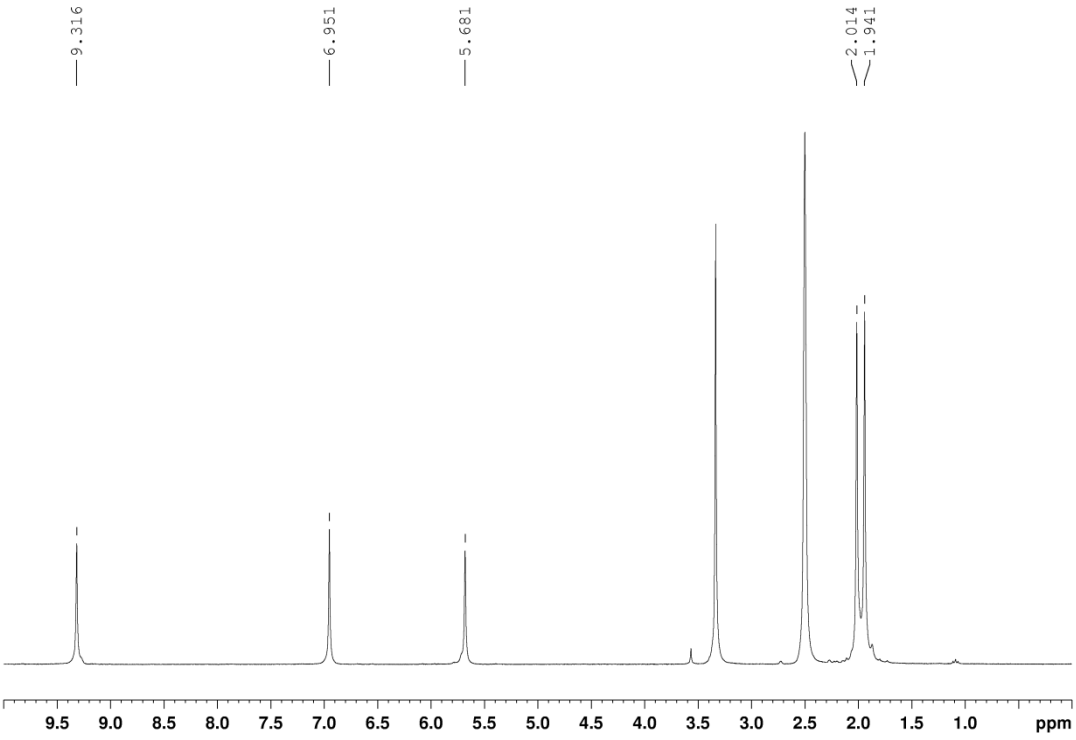

Figure 69 ^{1}H NMR of **9** in DMSO-d_6

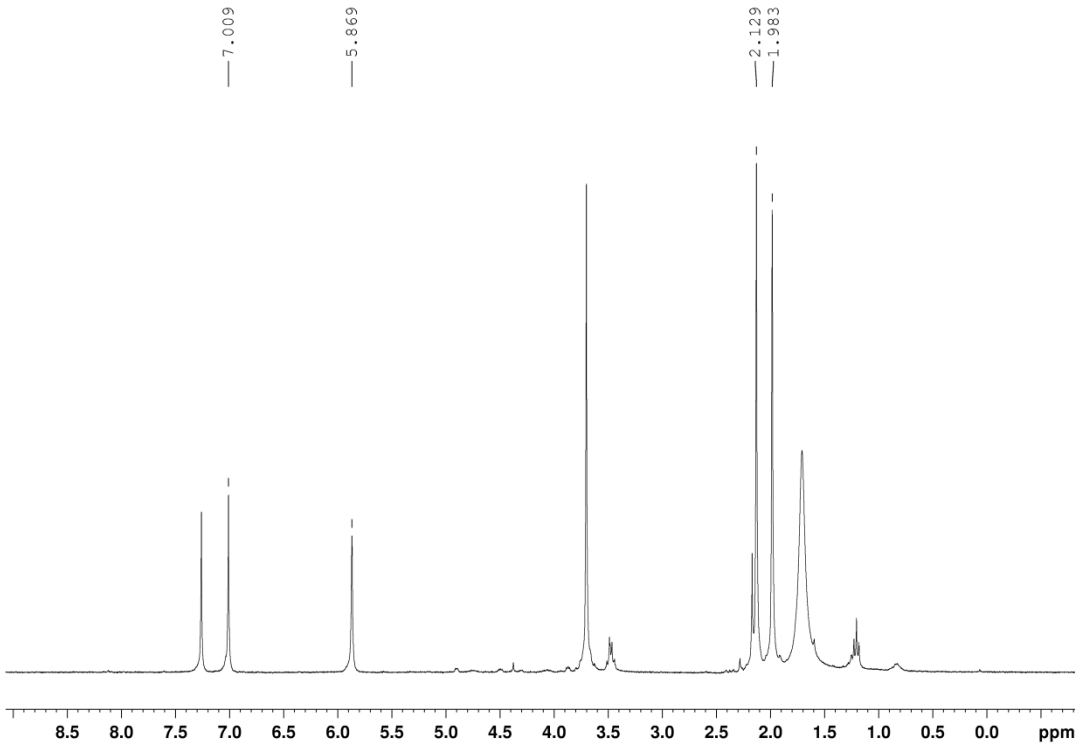

Figure 70 ^{1}H NMR spectrum of **10** in $CDCl_3$

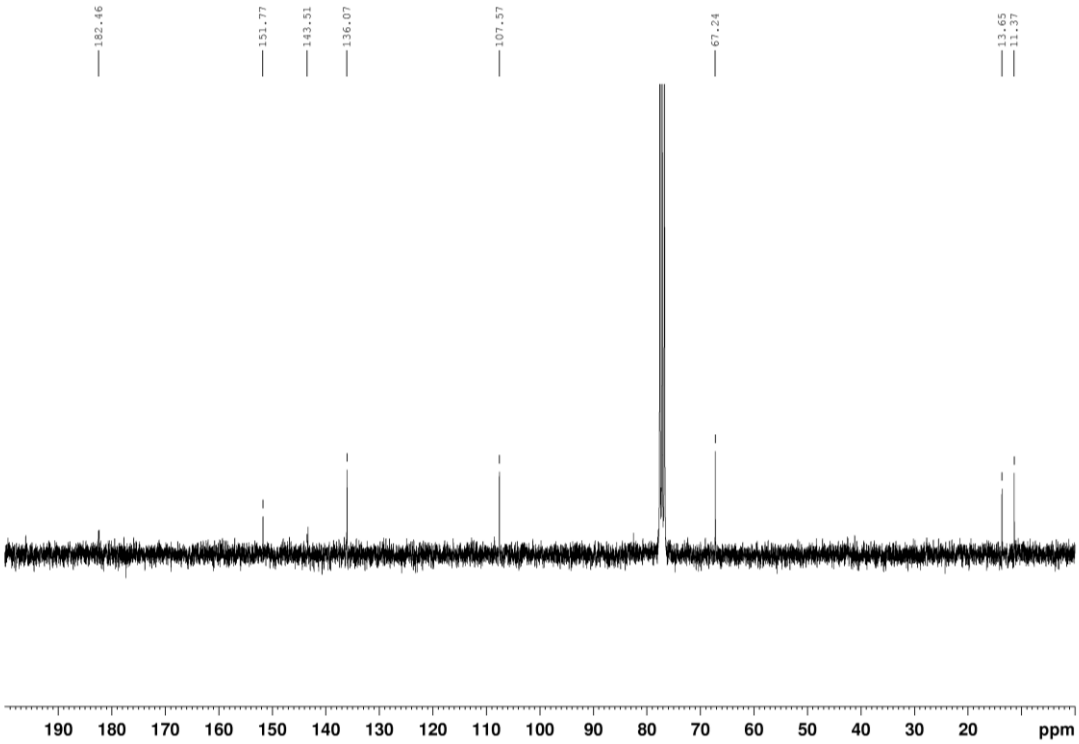

Figure 71 ^{13}C NMR spectrum of **10** in $CDCl_3$

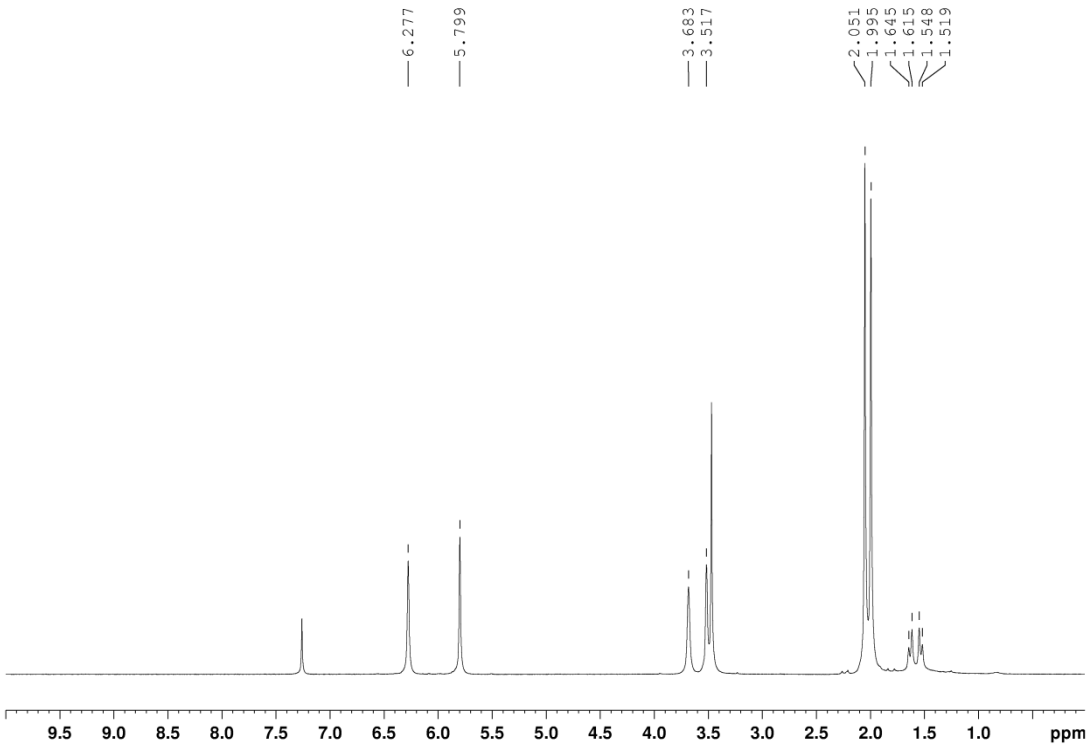

Figure 72 ^{1}H NMR spectrum of **11** in $CDCl_3$

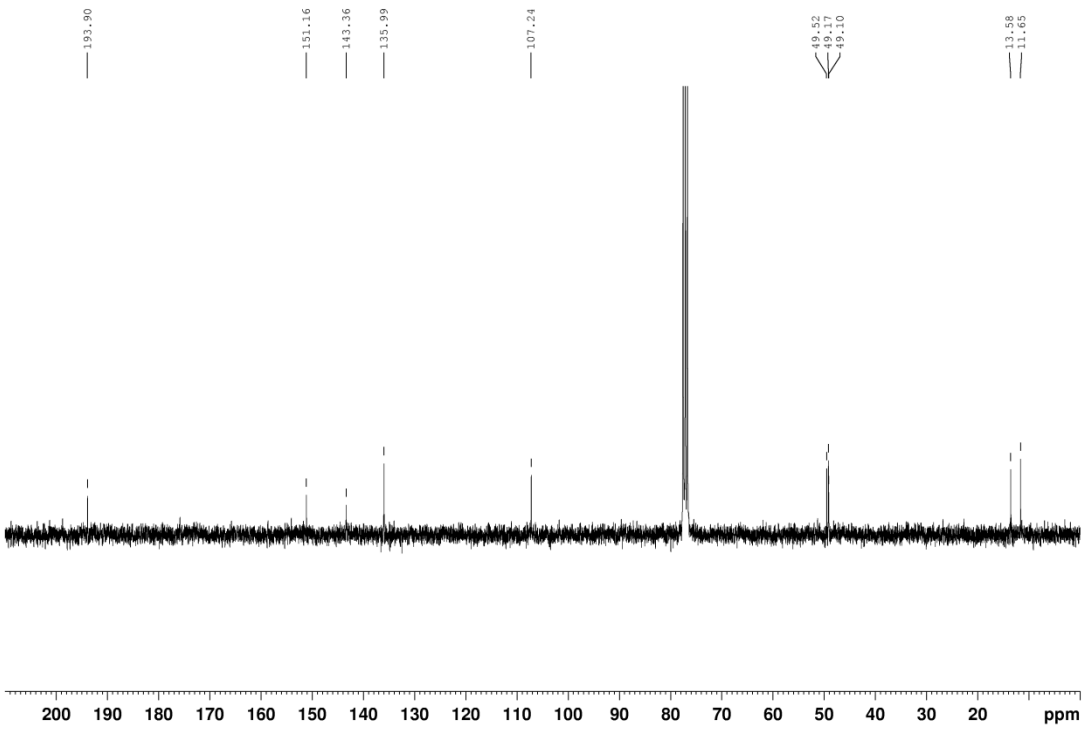

Figure 73 ^{13}C NMR spectrum of **11** in $CDCl_3$

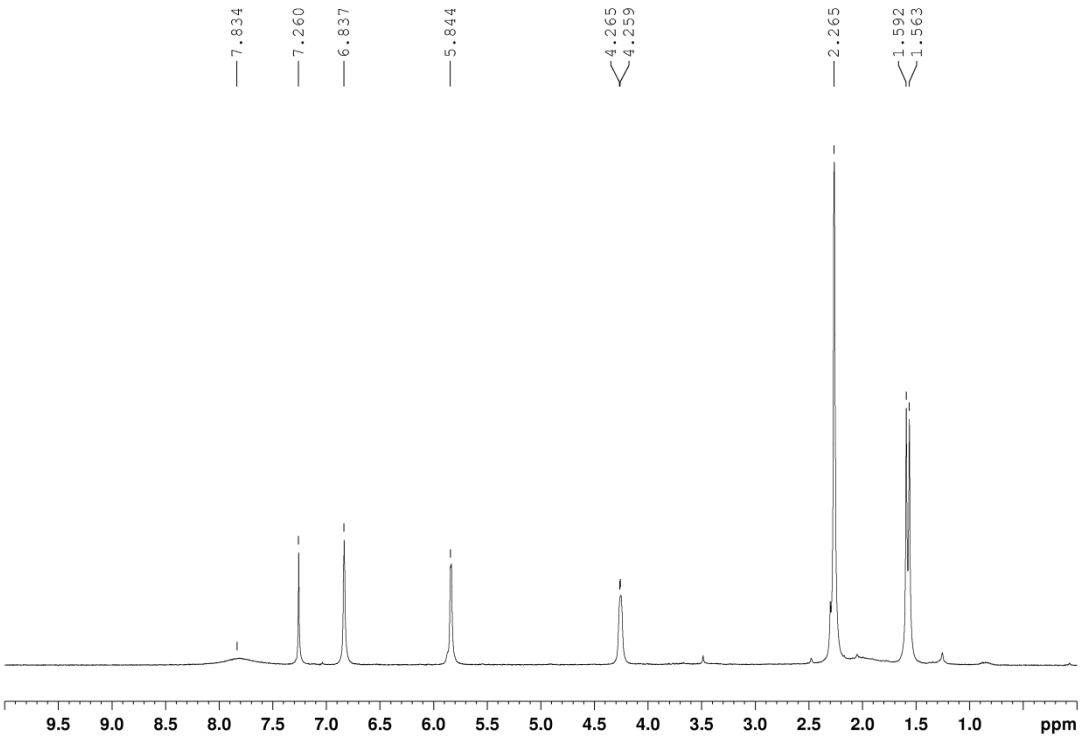

Figure 74 ^{1}H NMR spectrum of **12** in $CDCl_3$

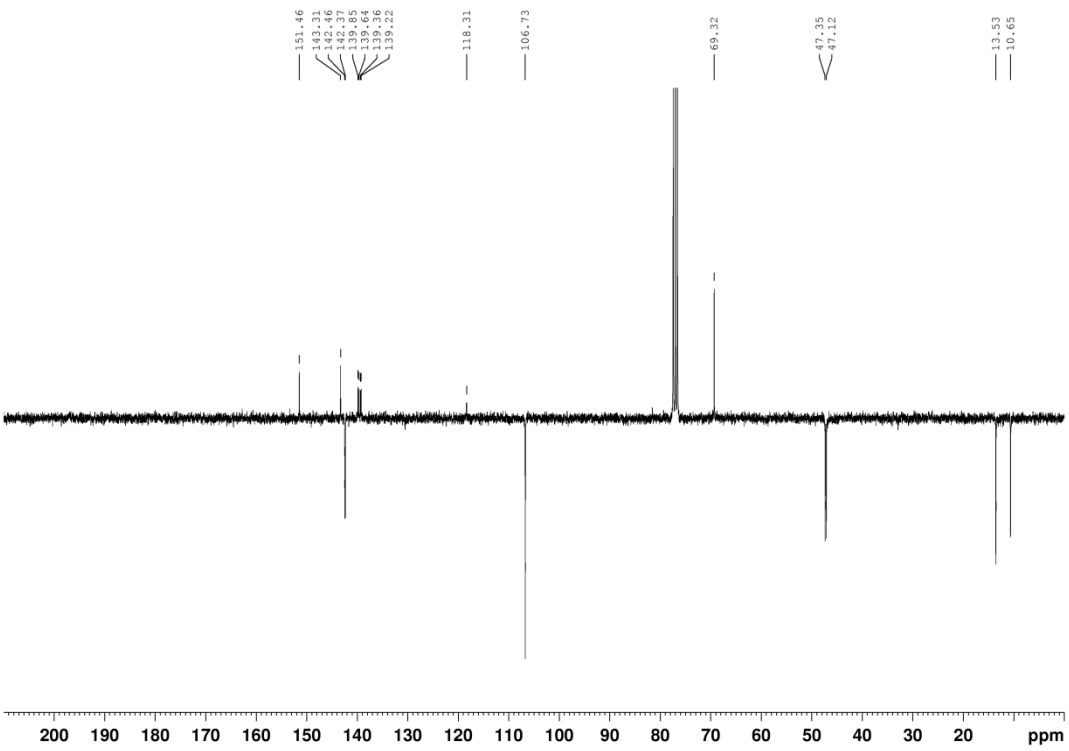

Figure 75 ^{13}C APT spectrum of **12** in $CDCl_3$

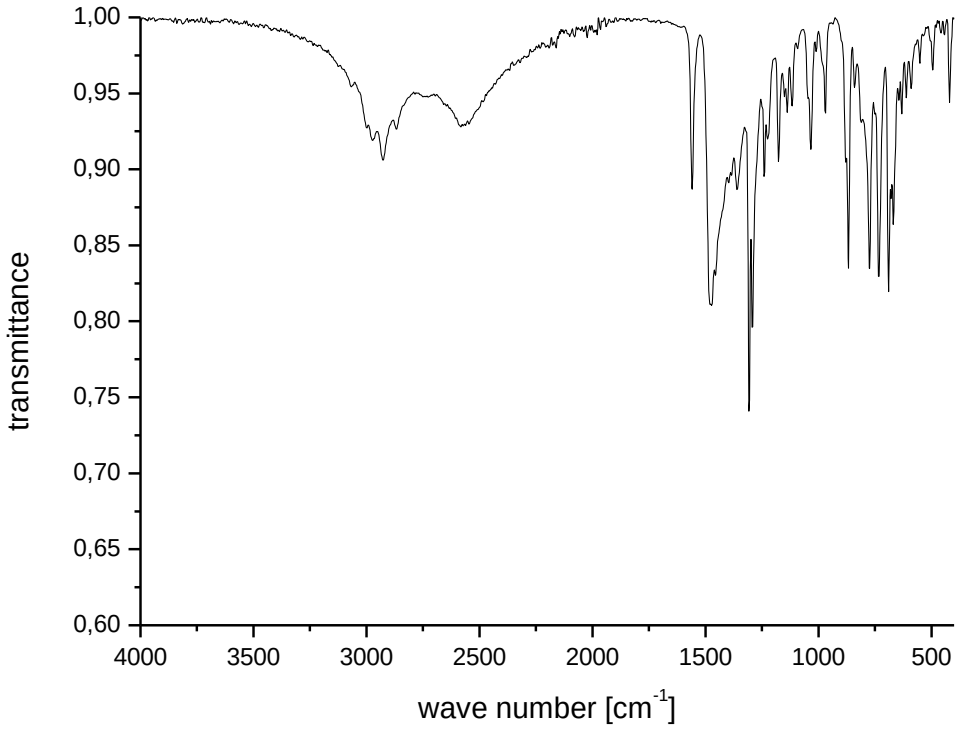

Figure 76 ATR-FTIR spectrum of **12**

11.4 Metal complexes

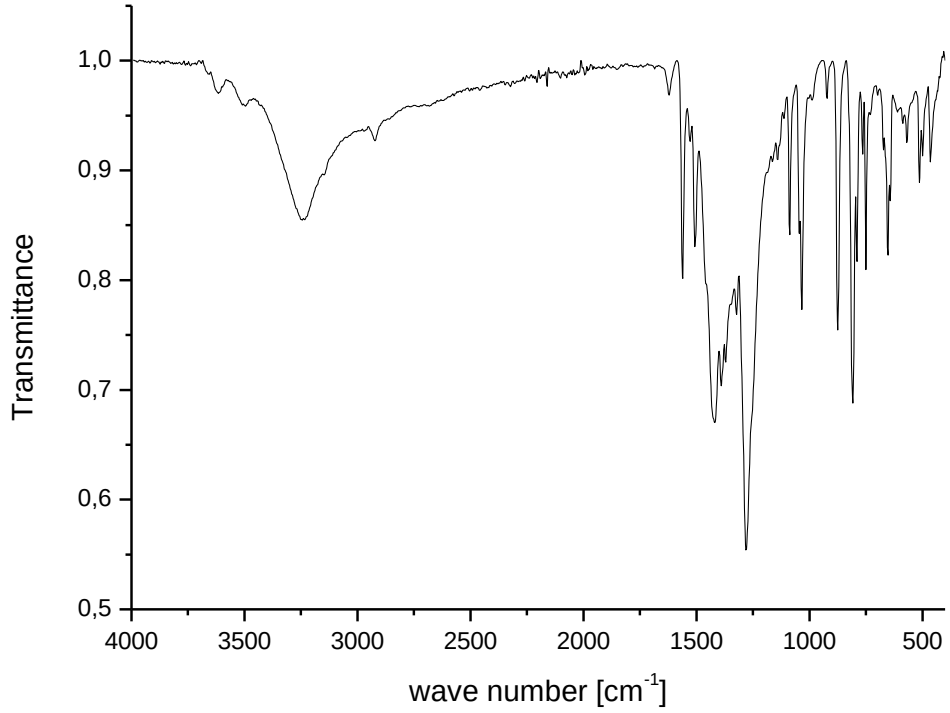

Figure 77 ATR-FTIR spectrum of **13**

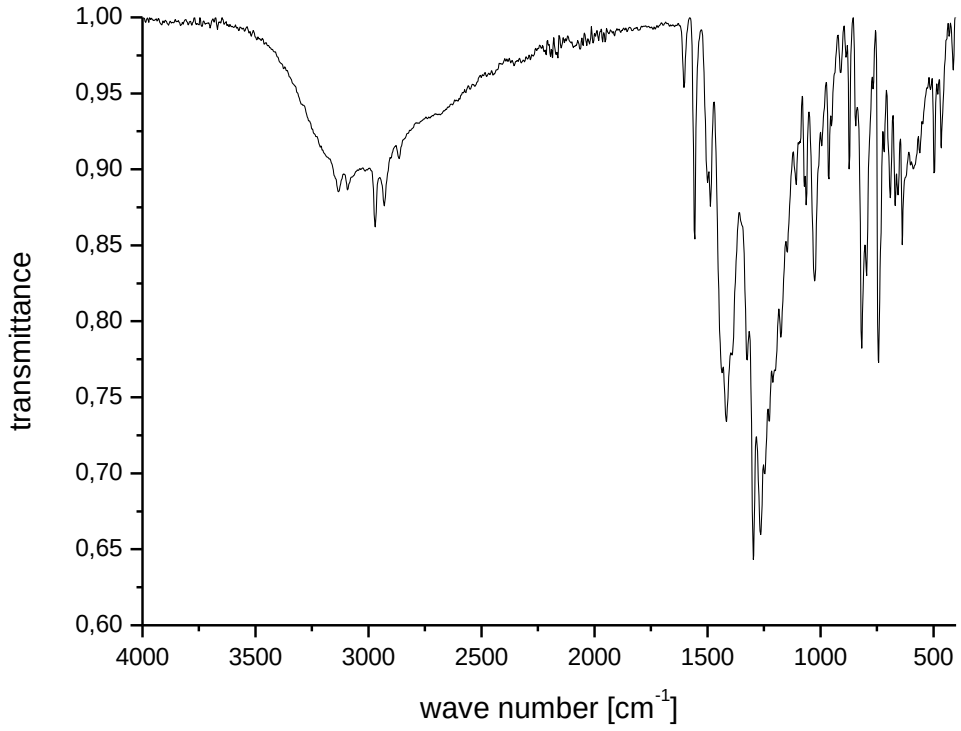

Figure 78 ATR-FTIR spectrum of **14**

11.5 Coordination polymers

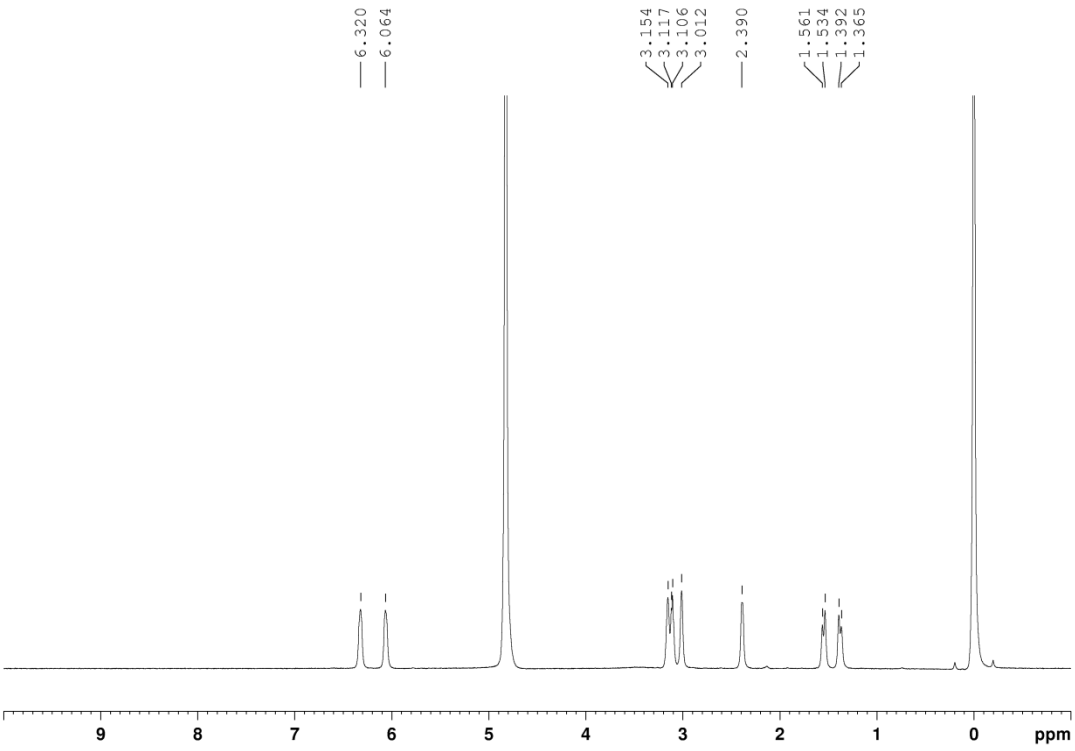

Figure 79 ^{1}H NMR spectrum of NDC-Na in D_2O with TMS as internal standard

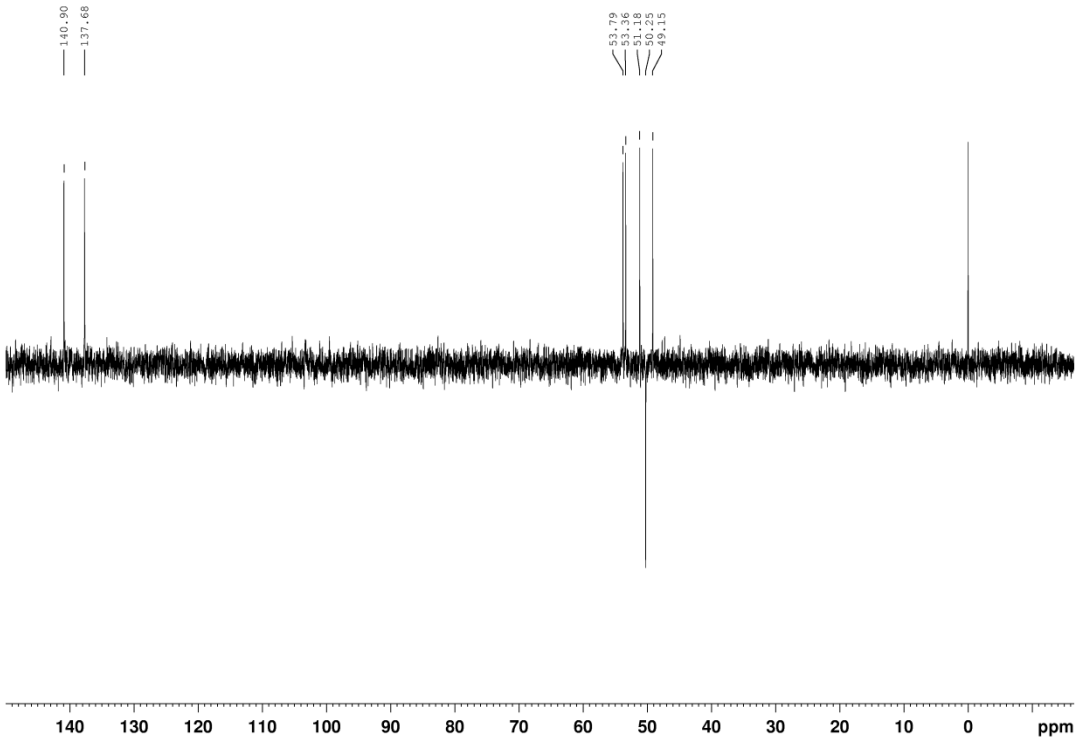

Figure 80 ^{13}C APT spectrum of NDC-Na in D_2O with TMS as internal standard

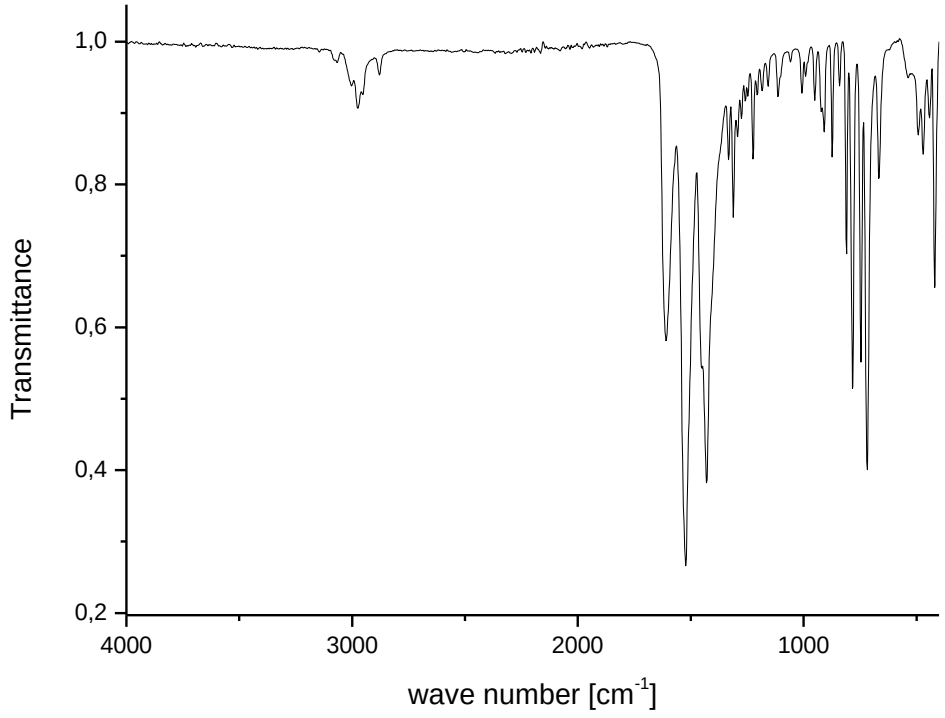

Figure 81 ATR-FTIR spectrum of **15**, synthesized from ZnO and NDC

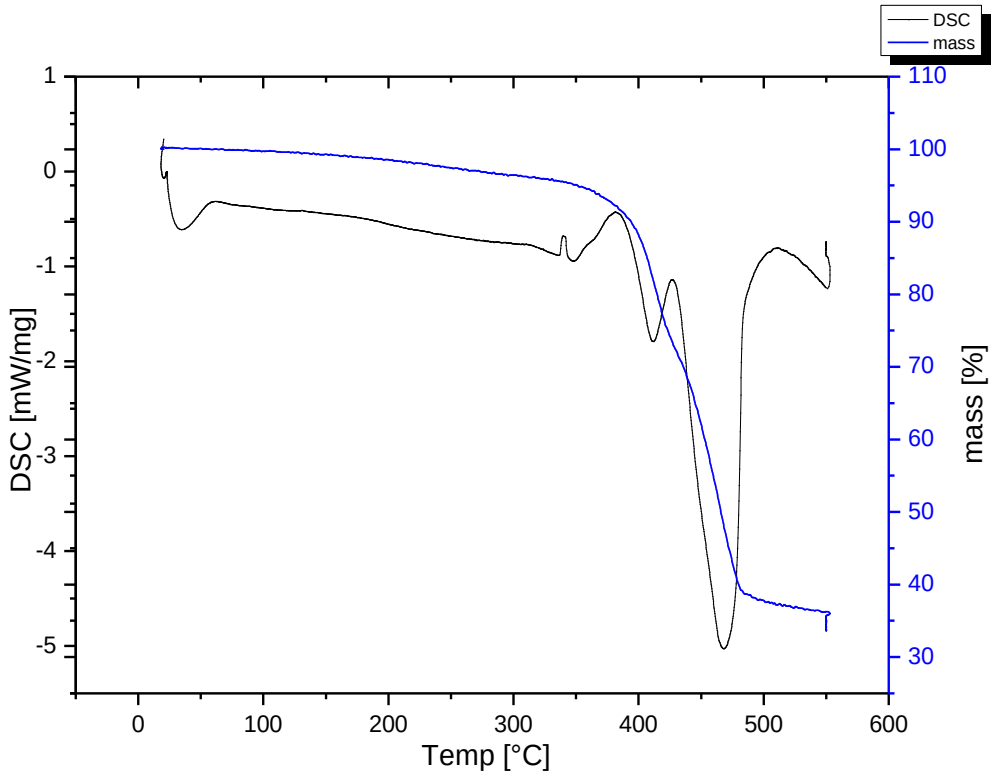

Figure 82 TGA/DSC of **15**, synthesized from ZnO and NDC

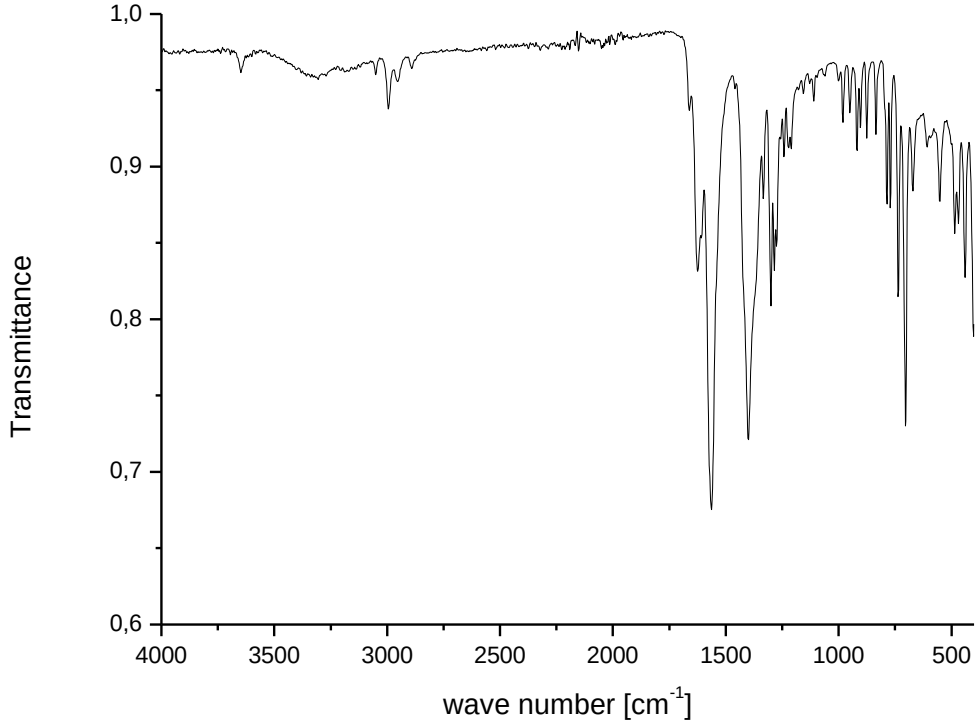

Figure 83 ATR-FTIR spectrum of **16**, synthesized from $MnCO_3$ and NDC

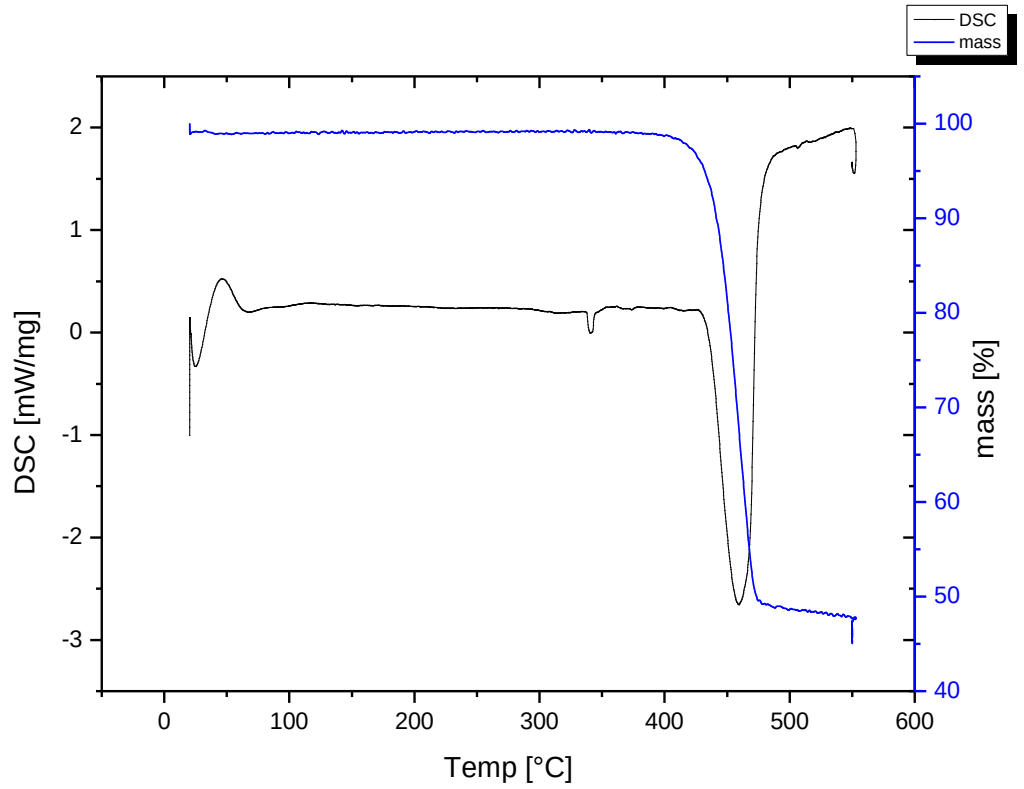

Figure 84 TGA/DSC of **16**, synthesized from $MnCO_3$ and NDC

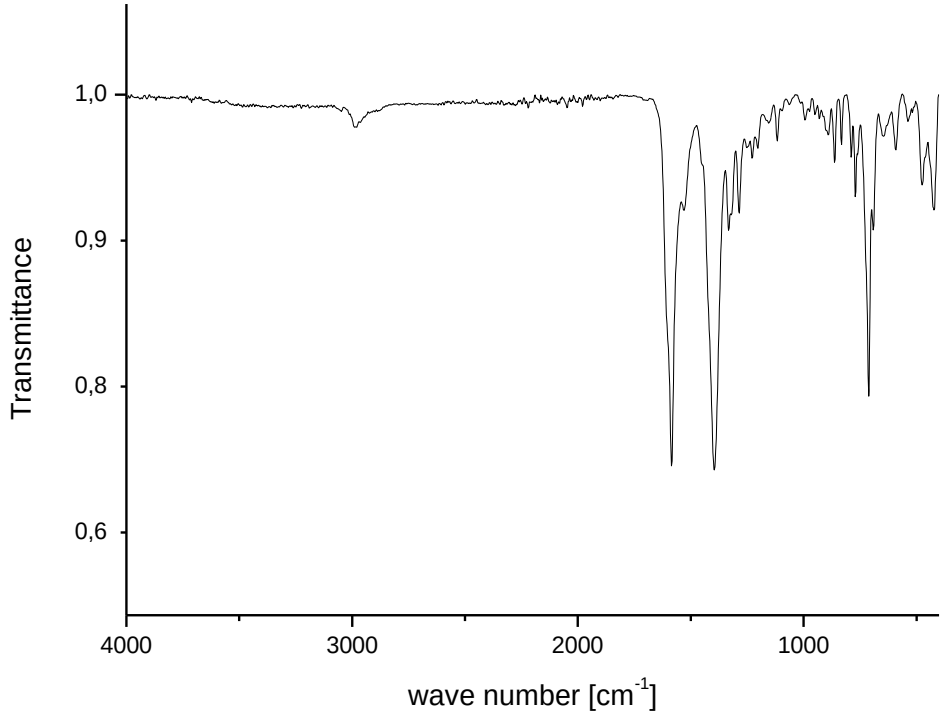

Figure 85 ATR-FTIR spectrum of **17**, synthesized from $CuNO_3$ and NDC-Na

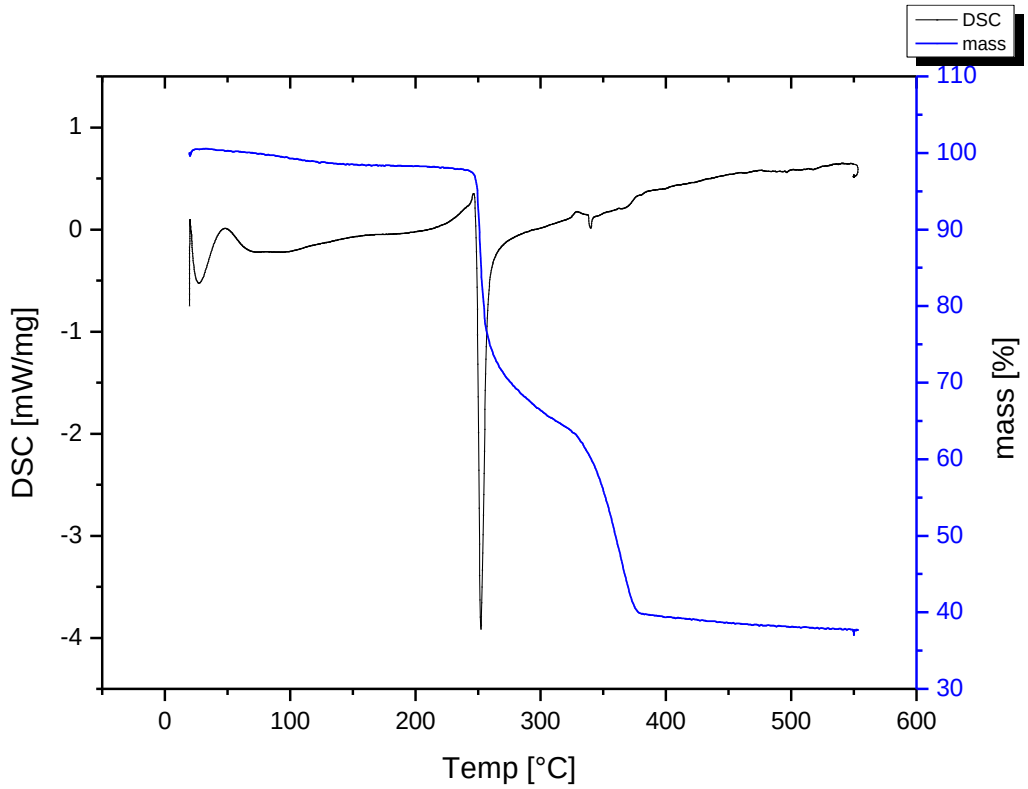

Figure 86 TGA/DSC of dried 17, synthesized from $CuNO_3$ and NDC-Na

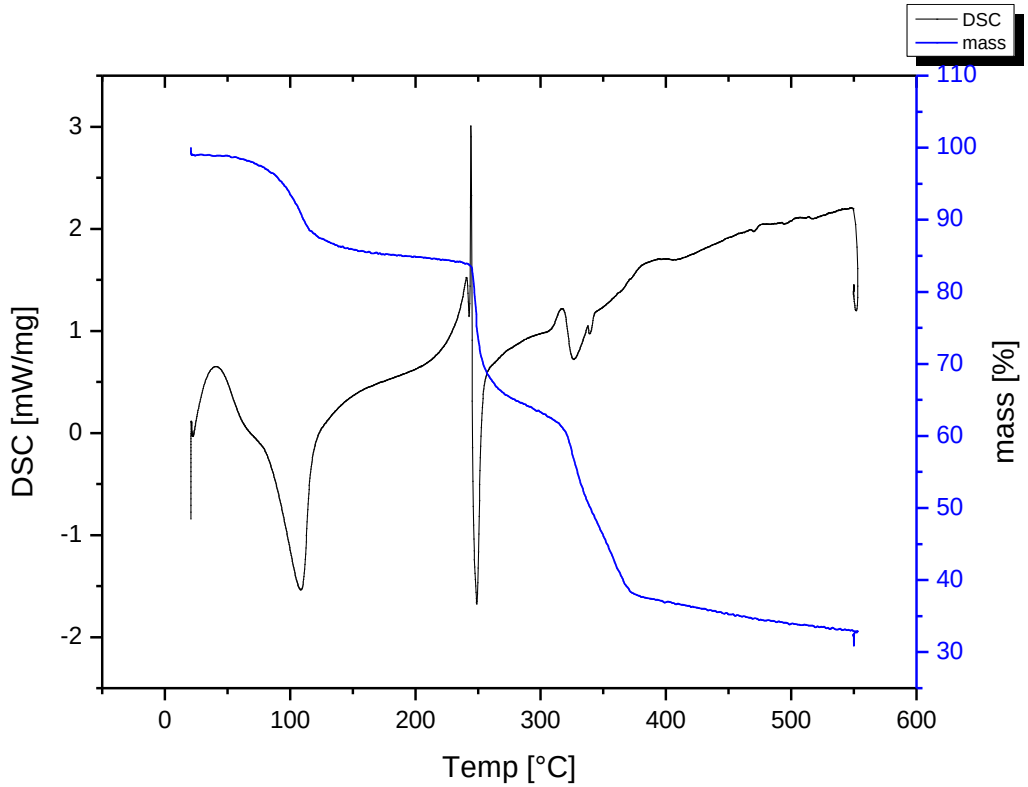

Figure 87 TGA/DSC of wet **17**, synthesized from $CuNO_3$ and NDC-Na

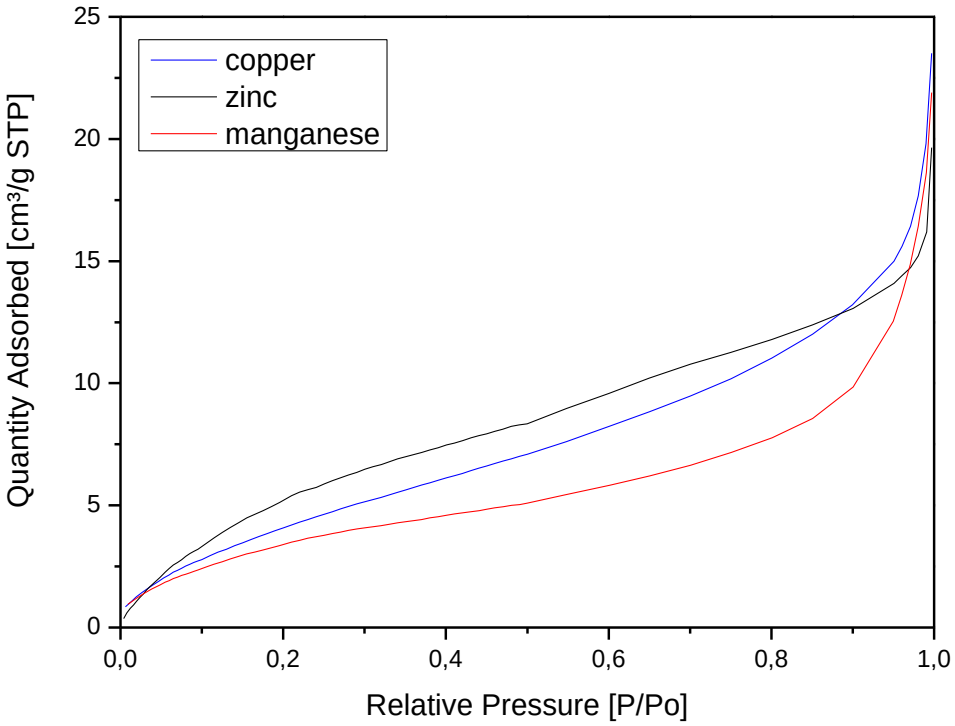

Figure 88 BET surface analysis of coordination polymers **15** (zinc), **16** (manganese) and **17** (copper)